

THERMODYNAMIC MODELING OF METAL ADSORPTION AND MINERAL  
SOLUBILITY IN GEOCHEMICAL SYSTEMS

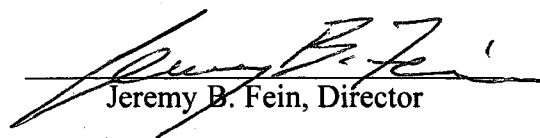
A Dissertation

Submitted to the Graduate School  
of the University of Notre Dame  
in Partial Fulfillment of the Requirements  
for the Degree of

Doctor of Philosophy

by

Daniel Scott Alessi

  
Jeremy B. Fein, Director

Graduate Program in Civil Engineering and Geological Sciences

Notre Dame, Indiana

July 2009

UMI Number: 3364983

### INFORMATION TO USERS

The quality of this reproduction is dependent upon the quality of the copy submitted. Broken or indistinct print, colored or poor quality illustrations and photographs, print bleed-through, substandard margins, and improper alignment can adversely affect reproduction.

In the unlikely event that the author did not send a complete manuscript and there are missing pages, these will be noted. Also, if unauthorized copyright material had to be removed, a note will indicate the deletion.

**UMI<sup>®</sup>**

---

UMI Microform 3364983  
Copyright 2009 by ProQuest LLC  
All rights reserved. This microform edition is protected against  
unauthorized copying under Title 17, United States Code.

---

ProQuest LLC  
789 East Eisenhower Parkway  
P.O. Box 1346  
Ann Arbor, MI 48106-1346

© Copyright 2009

Daniel Scott Alessi

# THERMODYNAMIC MODELING OF METAL ADSORPTION AND MINERAL SOLUBILITY IN GEOCHEMICAL SYSTEMS

Abstract

by

Daniel Scott Alessi

Developing geochemical models that can accurately predict the fate and transport of heavy metals and actinides in soils and aquifers requires detailed information about the quantity and reactivity of each component, across a wide range of environmental conditions. The studies I present in this dissertation provide critical insights into the mechanisms of heavy metal and actinide transport and immobilization by answering questions including: (1) To what extent do monovalent cations adsorb to the cell walls of bacteria? (2) How accurate is the chloroform fumigation-extraction method in determining biomass carbon in naturally occurring soils? (3) Can surface complexation models that are developed for the adsorption of metals on to single sorbents be combined to predict metal distribution in multi-sorbent systems? (4) Does the incorporation of Np(V) into the structure of the uranyl silicate affect its solubility, and therefore thermodynamic stability?

The results of study (1) demonstrate that monovalent cations adsorb to the cell walls of bacteria, albeit weakly. I model the adsorption data invoking discrete surface functional groups on the bacteria, and show how this approach is a simpler alternative to electrostatic models in accounting for the effects of ionic strength on the adsorption of

higher-charged metals. The results of study (2) indicate that the fumigation-extraction method may fail to accurately determine biomass carbon because chloroform vapor adsorbs to clays during fumigation, artificially inflating the organic carbon pool by entering into the subsequent extraction solutions. Because the increase in total organic carbon in the extracts is interpreted as biomass, the method must be corrected for the effects of chloroform contamination to be accurate. Study (3) demonstrates that surface complexation models of metal adsorption to individual soil components can be combined to predict Cd distribution in mixtures of these sorbents in many cases; however, to describe Cd adsorption behavior in the presence of a dissolved organic ligand, models must invoke ternary complexes between the sorbents, Cd, and the organic ligand. Finally, in study (4), it is revealed that a relatively small substitution of Np for U in the structure of soddyite causes a dramatic decrease in its solubility. This result has important implications for geochemical modeling of repositories because Np-incorporated soddyite will release substantially less U into solution than pure soddyite.

**To my family.**

## CONTENTS

FIGURES .....	v
TABLES .....	viii
ACKNOWLEDGMENTS .....	ix
CHAPTER 1: INTRODUCTION .....	1
1.1 Overview and Research Questions .....	1
1.2 Monovalent Cation Adsorption to Bacterial Surfaces .....	3
1.3 Testing the Fumigation-Extraction Method for Soil Microbial Biomass .....	5
1.4 Predicting Metal Adsorption to Mixtures of Geosorbents .....	7
1.5 Solubility of Np-incorporated Soddyite .....	9
CHAPTER 2: EXPERIMENTAL MEASUREMENT OF MONOVALENT CATION ADSORPTION ONTO <i>BACILLUS SUBTILIS</i> CELLS .....	12
2.1 Introduction .....	12
2.2 Methods .....	14
2.2.1 Bacteria growth and preparation .....	14
2.2.2 Li <sup>+</sup> and Rb <sup>+</sup> adsorption experiments .....	15
2.2.3 Cd adsorption experiments .....	17
2.3 Results .....	18
2.4 Discussion .....	21
2.4.1 Thermodynamic modeling .....	21
2.4.2 Modeling of monovalent cation adsorption to <i>B. subtilis</i> .....	25
2.4.3 Monovalent cation competition with Cd .....	28
2.5 Conclusions .....	31
CHAPTER 3: TESTING THE VALIDITY OF THE CHOROFORM FUMIGATION- EXTRACTION METHOD FOR DETERMINING MICROBIAL BIOMASS C IN SOILS .....	33
3.1 Introduction .....	33
3.2 Materials and Methods .....	36
3.3 Results and Discussion .....	40
3.4 Conclusions .....	50

CHAPTER 4: CADMIUM ADSORPTION TO MIXTURES OF SOIL COMPONENTS: TESTING THE COMPONENT ADDITIVITY APPROACH .....	52
4.1 Introduction .....	52
4.2 Methods.....	55
4.2.1 Preparation of bacterial cells.....	55
4.2.2 Preparation of mineral powders.....	56
4.2.3 Cd adsorption experiments .....	57
4.3 Results and Discussion.....	59
4.3.1 Cd adsorption to individual components.....	59
4.3.2 Modeling approach.....	61
4.3.2.1 Calculation of Cd- <i>Bacillus subtilis</i> stability constants .....	63
4.3.2.2 Kaolinite proton and metal adsorption model.....	65
4.3.2.3 HFO proton and metal adsorption model.....	67
4.3.3 Cd adsorption to two-component mixtures.....	69
4.3.4 Cd adsorption to three-component mixtures.....	80
4.4 Conclusions .....	83
 CHAPTER 5: THE EFFECT OF NP(V) INCORPORATION ON THE SOLUBILITY OF SODDYITE .....	 84
5.1 Introduction .....	84
5.2 Materials and Methods.....	86
5.3 Results and Discussion.....	90
5.4 Conclusions .....	96
 CHAPTER 6: CONCLUSIONS.....	 99
 REFERENCES .....	 105

## FIGURES

<p>2.1 (A) Lithium adsorption to <i>B. subtilis</i> as a function of ionic strength and pH. Initial experimental conditions were 20 g l<sup>-1</sup> <i>B. subtilis</i> cells and 2.34 × 10<sup>-5</sup> M Li. The pH 5 model curve represents the best-fit model that accounts for Li adsorption onto Site 2 only. Curves for the pH 7 and pH 9 models show the extent of adsorption that would be predicted using the <math>K_{Na}</math> and <math>K_{Li}</math> values determined from modeling the pH 5 data, and assuming no additional adsorption of Li onto Sites 3 or 4. (B) Best-fit model for Li adsorption to Site 2 of <i>B. subtilis</i> at pH 5 (solid curve). Dashed curves are models resulting from a ± 0.2 variation in the best-fitting log stability constant value of <math>K_{Li}</math>.....</p>	19
<p>2.2 (A) Rubidium adsorption to <i>B. subtilis</i> as a function of ionic strength and pH. Initial experimental conditions were 20 g l<sup>-1</sup> <i>B. subtilis</i> cells and 2.34 × 10<sup>-5</sup> M Rb. The pH 5 model curve represents the best-fit model that accounts for Rb adsorption onto Site 2 only. Curves for the pH 7 and pH 9 models show the extent of adsorption that would be predicted using the <math>K_{Na}</math> and <math>K_{Rb}</math> values determined from modeling the pH 5 data, and assuming no additional adsorption of Rb onto Sites 3 or 4. (B) Best-fit model for Rb adsorption to Site 2 of <i>B. subtilis</i> at pH 5 (solid curve). Dashed curves are models resulting from a ± 0.2 variation in the best-fitting log stability constant value of <math>K_{Rb}</math>.....</p>	20
<p>2.3 (A) Cd adsorption to <i>B. subtilis</i> cells in Na-, K-, and Li-perchlorate electrolytes. Initial experimental conditions were 10 g l<sup>-1</sup> <i>B. subtilis</i> cells and 8.90 × 10<sup>-5</sup> M Cd in a 0.1 M perchlorate solution. Curves indicate the best-fit models for Cd adsorption onto bacterial Site 2 with (solid curve) and without (dashed curve) inclusion of the Na-Site 2 complexation reaction in the model. The speciation of Site 2, with and without Na-Site 2 complexation, is depicted in (B) and (C), respectively .....</p>	22
<p>2.4 Cd adsorption to 10 g l<sup>-1</sup> <i>B. subtilis</i> cells in 0.1 M NaClO<sub>4</sub> electrolyte at pH 5.9±0.2. Adsorption models with and without Na-Site 2 complexation included yield identical best fits (solid curve) to the data. Data are from Mishra et al. (2008) .....</p>	29
<p>3.1 Experimental results from the bacteria-only system, plotted in terms of the concentration of extracted TOC as a function of the initial mass of bacteria present in the sample.....</p>	41

3.2 Fumigation results for humic acid-only samples, plotted in terms of the concentration of extracted TOC as a function of the initial mass of humic acid present in the sample.....	43
3.3 Fumigation results for silica sand-only samples, plotted in terms of the concentration of extracted TOC as a function of the initial mass of sand present in the sample .....	44
3.4 Results for fumigation experiments with a constant 50 g of silica sand and varying amounts of bacteria, plotted in terms of the concentration of extracted TOC as a function of the initial mass of bacteria present in the sample.....	46
3.5 Fumigation results for montmorillonite-only samples (SWy-2), plotted in terms of the concentration of extracted TOC as a function of the initial mass of montmorillonite present in the sample.....	47
3.6 Fumigation results for wet montmorillonite samples (SWy-2), plotted in terms of the concentration of extracted TOC as a function of the initial dry mass of montmorillonite present in the sample.....	48
3.7 Fumigation results for kaolinite-only samples (KGa-1b), plotted in terms of the concentration of extracted TOC as a function of the initial mass of kaolinite present in the sample.....	49
4.1 Adsorption of (A) $8.9 \times 10^{-5}$ M Cd(II) and (B) $8.9 \times 10^{-6}$ M Cd(II) to $1 \text{ g l}^{-1}$ HFO (■), $1 \text{ g l}^{-1}$ <i>B. subtilis</i> cells (◆), and $1 \text{ g l}^{-1}$ kaolinite. Curves represent best-fit models to HFO (grey line), <i>B. subtilis</i> (solid line), and kaolinite (dashed line) Cd adsorption data .....	60
4.2 Adsorption of (A) $8.9 \times 10^{-5}$ M Cd(II) and (B) $8.9 \times 10^{-6}$ M Cd(II) to mixtures of HFO and <i>B. subtilis</i> cells. Dashed lines represent best-fit models to $1 \text{ g l}^{-1}$ HFO and <i>B. subtilis</i> end members from Figure 1. Darkened symbols and lines represent adsorption data and predicted adsorption behavior for two-sorbent mixtures, including $0.75 \text{ g l}^{-1}$ HFO + $0.25 \text{ g l}^{-1}$ <i>B. subtilis</i> cells (▲, thin line), and $0.25 \text{ g l}^{-1}$ HFO + $0.75 \text{ g l}^{-1}$ <i>B. subtilis</i> cells (●, thick line).....	71
4.3 Adsorption of (A) $8.9 \times 10^{-5}$ M Cd(II) and (B) $8.9 \times 10^{-6}$ M Cd(II) to mixtures of kaolinite and <i>B. subtilis</i> cells. Dashed lines represent best-fit models to $1 \text{ g l}^{-1}$ kaolinite and <i>B. subtilis</i> end members from Figure 1. Darkened symbols and lines represent adsorption data and predicted adsorption for two-sorbent mixtures, including $0.75 \text{ g l}^{-1}$ <i>B. subtilis</i> cells + $0.25 \text{ g l}^{-1}$ kaolinite (▲, thin line), and $0.25 \text{ g l}^{-1}$ <i>B. subtilis</i> cells + $0.25 \text{ g l}^{-1}$ kaolinite (●, thick line).....	73
4.4 Adsorption of (A) $8.9 \times 10^{-5}$ M Cd(II) and (B) $8.9 \times 10^{-6}$ M Cd(II) to mixtures of HFO and kaolinite. Dashed lines represent best-fit models to $1 \text{ g l}^{-1}$ HFO and kaolinite end members from Figure 1. Darkened symbols and lines	

represent adsorption data and predicted adsorption for two-sorbent mixtures, including 0.75 g l<sup>-1</sup> HFO + 0.25 g l<sup>-1</sup> kaolinite (▲, thin line), and 0.25 g l<sup>-1</sup> HFO + 0.25 g l<sup>-1</sup> kaolinite (●, thick line)..... 75

4.5 Adsorption of 8.9 × 10<sup>-5</sup> M Cd to 1 g l<sup>-1</sup> A) HFO, C) *B. subtilis*, and E) kaolinite, and 8.9 × 10<sup>-6</sup> M Cd to B) HFO, D) *B. subtilis*, and F) kaolinite. Darkened symbols and lines represent adsorption data and predicted adsorption for mixtures without acetate. Open symbols are adsorption data in the presence of 0.3 M acetate. Dashed line indicates the predicted extent of adsorption in acetate experiments without the adsorption of a Cd-acetate complex, and grey line is the best-fit model including a Cd-acetate ternary surface complex ..... 77

4.6 Adsorption of 8.9 × 10<sup>-6</sup> M Cd to three-component mixtures of HFO, kaolinite, and *B. subtilis*, and in the presence of 0.3 M dissolved acetate. Darkened symbols and lines represent adsorption data and predicted adsorption for mixtures without acetate. Open symbols and dashed lines are adsorption data and predicted adsorption in the presence of 0.3 M acetate, respectively. Sorbent mixtures include A) 0.8 g l<sup>-1</sup> HFO + 0.1 g l<sup>-1</sup> *B. subtilis* + 0.1 g l<sup>-1</sup> kaolinite, B) 0.1 g l<sup>-1</sup> HFO + 0.8 g l<sup>-1</sup> *B. subtilis* + 0.1 g l<sup>-1</sup> kaolinite, C) 0.1 g l<sup>-1</sup> HFO + 0.1 g l<sup>-1</sup> *B. subtilis* + 0.8 g l<sup>-1</sup> kaolinite, D) 0.33 g l<sup>-1</sup> HFO + 0.33 g l<sup>-1</sup> *B. subtilis* + 0.33 g l<sup>-1</sup> kaolinite ..... 81

5.1 Measured aqueous concentrations of Np (A) and U and Si (B) during solubility experiments at pH 3.4. Solid phase Np concentrations are: 24 ppm (◆), 919 ppm (△), 2730 ppm (●), and 6511 ppm (□)..... 91

5.2 The solid phase activity coefficient ( $\Gamma_{soddyite}$ ) as a function of the mole fraction of uranyl soddyite ( $X_{soddyite}$ ) ..... 97

## TABLES

4.1 Proton and Cd reactions at <i>Bacillus subtilis</i> cell walls, kaolinite, and HFO .....	61
4.2 Molal site concentrations of sorbents in two- and three- component mixtures .....	70
4.3 Ternary complexation reactions.....	79
5.1 Properties of Np-incorporated soddyites .....	89
5.2 Equilibrium species concentrations and pH from each solubility experiment used for thermodynamic calculations, reported as log molalities.....	93

## ACKNOWLEDGMENTS

I would like to thank my advisor, Prof. Jeremy Fein, for his mentoring and support during my doctoral studies. His enthusiasm, availability, and patience made all the difference. I would also like to thank the members of my committee, including Profs. Peter Burns, Patricia Maurice, and Robert Nerenberg, for reading my dissertation and for providing advice and assistance throughout my time at Notre Dame. I thank Jennifer Szymanowski for giving invaluable help in completing many of the experiments included here, and Dennis Birdsell and Jon Loftus for frequent help with analytical instruments.

My stipend and tuition were largely subsidized by a University of Notre Dame Presidential Doctoral Fellowship provided by the Arthur J. Schmitt Foundation. Thanks to the trustees and fellows of the Schmitt Foundation for their generous support. I was partially supported by an Environmental Molecular Science Institute grant from the National Science Foundation to the University of Notre Dame.

# CHAPTER 1

## INTRODUCTION

### **1.1 Overview and Research Questions**

The ability to accurately predict the mobility of metal cations and radionuclides in geologic systems depends on accurate characterization of the reactivity of every component in the system with the elements of interest. Adsorption, dissolution, and precipitation reactions at bacterial, organic, and mineral surfaces control the fate of these aqueous species in geologic systems. My dissertation research addresses several important questions that relate to metal or radionuclide mobility, including:

(1) Do monovalent metal cations adsorb to bacterial cell walls? If they do adsorb, can we quantify the stability of the important bacterial surface complexes, and by so doing can we account for the effect of ionic strength on the adsorption of higher charged cations onto bacteria? It is often assumed that monovalent cations exhibit negligible site-specific binding to cell wall functional groups, and therefore only influence the adsorption of higher charged metals through non-specific electrostatic surface charging effects. However, this assumption has not been rigorously tested. If site-specific monovalent metal binding occurs, then accounting for site competition between monovalent and higher valence ions may be a more straightforward approach to quantifying the effect of ionic strength on metal adsorption than the current models of surface electric field effects. In Chapter 2, I report results from experiments that

measured the adsorption of  $\text{Li}^+$  and  $\text{Rb}^+$  onto the Gram-positive soil bacteria *Bacillus subtilis* as a function of pH and electrolyte ionic strength to determine stability constants for these metals and  $\text{Na}^+$ . Using the stability constant determined for the surface complexes between these monovalent cations and the bacteria, we correct previously determined apparent stability constants for metal-bacterial surface complexes involving  $\text{Cd}^{2+}$ .

(2) Is the fumigation-extraction procedure for determining biomass content of geologic samples accurate and/or precise enough to enable calculations of metal speciation in mass transport models? Metal binding to microbial cells can significantly affect the speciation and overall mobility of metals in groundwater and soils, so the biomass content must be precisely and accurately determined in order to model the fate and transport of metals in these systems. The fumigation-extraction procedure is the most commonly-accepted method of determining soil microbial biomass content, but control experiments for the procedure have never been conducted, so its accuracy and precision are not constrained. I performed chloroform fumigation experiments on individual soil components, including silica sand, montmorillonite, kaolinite, a humic acid, and *Bacillus subtilis* bacterial cells, to determine if the method can accurately determine biomass amounts, and if chloroform adsorption to these surfaces during fumigation affects the results of this procedure. Based on the data from these experiments, I discuss the validity of the fumigation-extraction method for various soil types in Chapter 3.

(3) Can we develop models that accurately account for metal binding and distribution among the various components of soils? Although there are many empirical studies of bulk adsorption of metals onto soils, the ability of surface complexation

models (SCM) to model the speciation and distribution of metals in multi-sorbent systems has not been widely tested. In this study (Chapter 4),  $\text{Cd}^{2+}$  adsorption to mixtures of soil components is measured at varying pH and ionic strength conditions to determine the capability of a non-electrostatic SCM to independently account for the distribution of the metal to the surfaces.

(4) How does the incorporation of neptunium into the structure of the uranyl silicate soddyite affect the mineral solubility? Soddyite with neptunium in the structure is likely to form under the oxidizing conditions of some nuclear repositories. If the neptunium has a substantial effect on soddyite solubility, the mobility of neptunium and uranium in a geologic repository setting could be much different than currently predicted. To answer this question, I synthesized soddyite powders with varying trace amounts of Np in the structure. Chapter 5 presents the results of solubility experiments performed with these Np-incorporated soddyites.

## **1.2 Monovalent Cation Adsorption to Bacterial Surfaces**

Water in the subsurface contains a range of metal ions that compete for adsorption sites on soil and aquifer surfaces. Although the binding of various metals onto bacterial cell wall functional groups has been studied extensively (e.g., Beveridge and Murray, 1976; Beveridge, 1989; Ledin et al., 1997; Yee and Fein, 2001; Fein et al., 2002; Borrok and Fein, 2004; Gorman-Lewis et al., 2005; Covelo et al., 2007; Johnson et al., 2007), the binding constants for monovalent cations, which in many systems are the most concentrated cations present, are not known. Laboratory measurements of divalent metal adsorption onto bacterial surfaces are usually conducted in the presence of a concentrated monovalent salt electrolyte to buffer ionic strength, but monovalent cations are assumed to be inert to adsorption onto bacterial surface functional groups.

The decrease in divalent metal adsorption to surfaces with increasing ionic strength is often attributed to a decrease in the strength and extent of the electric field of the adsorbing surface with increasing ionic strength. However, if monovalent metals adsorb onto surface functional groups and thereby compete with divalent metals for available sites, an alternative approach for modeling the ionic strength effect on divalent metal adsorption may be to account for monovalent adsorption explicitly.

In our study, we test this alternative approach to accounting for the ionic strength effect by using a non-electrostatic surface complexation model (NEM). The NEM approach assumes that the functional groups on surfaces behave the same as dissolved ligands, so that the electrostatic terms can be neglected entirely (Davis and Kent, 1990). Instead, ions in solution are assumed to directly and simultaneously compete for surface functional groups, the assumption being that monovalent adsorption is onto specific sites rather than only due to electrostatic attraction from the surface electric field in general. In this regard, NEMs are simpler to apply than electrostatic models. Although electrostatic interactions do occur between ions and surfaces, they are difficult to model due to the difficulty in modeling the nature and extent of the surface electric field, especially in complex realistic systems (Davis et al., 1998). A range of surface electric field models exist, but all are empirical in that they require calibration with a number of adjustable parameters, and typically the models fit experimental adsorption data equally well (Hayes et al., 1991). The NEM approach minimizes the number of required modeling parameters, but without an understanding of site-specific monovalent ion adsorption, the NEM approach cannot account for the effect of ionic strength on cation adsorption. The research presented in Chapter 2 represents an attempt to adapt non-

electrostatic adsorption models to account for these ionic strength effects without having to characterize the nature and extent of the surface electric field.

In the first study of this dissertation (Chapter 2), I conduct experiments to determine the extent of adsorption of monovalent metals to the Gram-positive soil bacteria *Bacillus subtilis* in order to calibrate a non-electrostatic adsorption model that can account for the effect of ionic strength on metal adsorption. The experiments are performed as a function of ionic strength and pH. Because bacterial cells contain high concentrations of  $\text{Na}^+$  and  $\text{K}^+$  that could enter into solution during metal adsorption experiments, the experiments were not conducted with these metals, but instead with  $\text{Li}^+$  and  $\text{Rb}^+$ . A NEM is used to model the monovalent adsorption data and solve for discrete metal-bacteria binding constants for the monovalent cations. These constants are then used to determine the competitive effect of monovalent cations on the adsorption of  $\text{Cd}^{2+}$  onto bacterial surface adsorption sites. This approach may serve as an alternative modeling approach to electrostatic models for accounting for ionic strength effects on cation adsorption onto bacterial surfaces.

### **1.3 Testing the Fumigation-Extraction Method for Soil Microbial Biomass**

Modeling metal speciation, bioavailability, and mobility in systems such as soils and aquifers using a surface complexation approach requires accurate and precise estimates of the type and quantity of each type of binding site in the system, and the binding constants for the cation of interest onto each binding site type. Soils are complex, having a myriad of possible combinations of constituent parts (Gardiner and Miller, 2004). In the most general sense, natural soils consist of inorganic and organic components and soil moisture. The inorganic fraction consists of minerals such as quartz, iron oxides, feldspars, clays, and micas. The organic portion includes humic

substances and microorganisms. In order to develop general models of metal speciation and distribution in soils, not only do we need to know the equilibrium constants for each binding reaction that occurs, but we also need accurate and precise methods to quantify the concentration of each component in a natural soil sample.

Commonly used methods of biomass determination include direct counting of bacteria using a microscope and the use of adsorbent fluorescent dyes for spectrophotometric measurement of cells. These methods yield highly imprecise values for cell concentrations (Poglazova et al., 1996). Jenkinson and Powlson (1976a, b) introduced a biocidal fumigation method for soils to determine the live cell biomass-carbon in soils. This approach is significantly more precise than previous biomass determination methods; it is able to detect microbial biomass differences of 5% to 10% at a 0.05% probability level (Voroney et al., 2008). The work of Jenkinson and Powlson demonstrated that chloroform ( $\text{CHCl}_3$ ) fumigation completely lyses live cells in 24 hours, and the evolved gas is collected. Organisms killed during the fumigation process are readily mineralized to  $\text{CO}_2$ , so that the difference in  $\text{CO}_2$  gas evolution between fumigated and unfumigated samples is a measure of biomass-carbon (Smith et al., 1995). Vance et al. (1987) and Tate et al. (1988) used a similar method, but extracted organic carbon from fumigated and unfumigated samples using a 0.5 M  $\text{K}_2\text{SO}_4$  solution. These solutions were analyzed for total dissolved organic carbon as the measure of biomass-carbon. The Vance et al. (1987) method attributes the enhanced amount of organic carbon extracted from a fumigated sample relative to an unfumigated control exclusively to cell lysis caused by chloroform fumigation. The method would be highly inaccurate if chloroform adsorbed onto any soil components during fumigation and desorbed during the extraction procedure. Under these circumstances, the chloroform would

subsequently enhance the amount of organic carbon extracted from a fumigated sample, and therefore the enhancement of organic carbon could not be attributed exclusively to sample biomass.

Although both the Vance et al. (1987) and the Tate et al. (1988) papers are heavily cited and considered current standard procedures for biomass determination in soils, control experiments using individual soil components have never been performed, and the accuracy of the approach remains untested. Haney et al. (1999) questioned the acceptability of the fumigation-extraction method to determine biomass carbon by showing that the amount of carbon extracted using a 0.5 M  $K_2SO_4$  solution can vary as a function of pH. There is also some evidence that suggests that chloroform can adsorb to soils both from aqueous solution (Dural and Peng, 1995) and from the atmosphere (Chen, 1993). In this study (Chapter 3), I test whether the fumigation-extraction method is valid for different soil types by performing fumigation experiments with individual soil components, including a humic acid, a quartz sand, two types of clays, and a bacterial species. By determining which soil components retain chloroform through the fumigation procedure, this study determines which types of soils are likely to yield inflated biomass carbon readings using the fumigation-extraction method.

#### **1.4 Predicting Metal Adsorption to Mixtures of Geosorbents**

The ultimate goal of this project is to test the accuracy of surface complexation models that predict metal adsorption and distribution in multi-sorbent systems.

Although metal adsorption in multi-component systems has been studied empirically (e.g., Ledin et al., 1997, 1999; Krantz-Rulcker et al., 1996; Fingler et al., 2004), the ability of the SCM approach to predict metal adsorption and distribution in soils has not been tested. Davis et al. (1998) attempted to use a SCM to predict  $Zn^{2+}$  adsorption to

mineral assemblages. They used a component additivity (CA) approach to independently predict adsorption onto assemblages of minerals. Specifically, the authors conducted surface titrations and  $Zn^{2+}$  adsorption experiments on individual minerals and calculated proton- and metal-surface complex stability constants for each mineral surface site type. The adsorption behavior of  $Zn^{2+}$  onto mixtures of these minerals was then measured and compared to independent predictions of the adsorption behavior based on the calculated individual stability constants and the known concentration of each site type in the mixtures. Davis et al. (1998) found that the CA approach could not account for the pH-dependent adsorption behavior, likely due to interactions among the minerals that were not accounted for in the CA surface complexation model.

Davis et al. (1998) also tested a generalized composite (GC) approach to modeling adsorption. The GC is a semi-empirical method that attributes metal adsorption onto mixtures of surfaces to generic functional groups, rather than the specific groups of the CA. Unlike the CA approach, the GC approach cannot be extended to other mixtures of the same surfaces because it is only valid for the surface ratios present in the experiment for which it was calibrated. Because of its added flexibility and increased number of adjustable parameters, Davis et al. (1998) found that the GC approach was more successful in accounting for  $Zn^{2+}$  adsorption to mineral assemblages than was the CA approach. However, Pagnanelli et al. (2006) and Fowle and Fein (1999) demonstrated that a non-electrostatic surface complexation model (NEM) approach combined with the CA approach can be successful in predicting metal adsorption to mixtures of pure minerals and bacteria, respectively. It remains unclear if the CA approach is capable of predicting metal distribution in mixtures containing minerals, microbes, and organic acids.

In Chapter 4, I test whether the CA approach can account for the distribution of  $\text{Cd}^{2+}$ , a toxic metal of environmental interest, between an aqueous phase and mixtures of kaolinite, bacteria, iron oxyhydroxide, and dissolved acetate. In order to obtain internally consistent stability constants for the important Cd surface complexes, I first measure adsorption of  $\text{Cd}^{2+}$  onto the individual components. From these data, the stability constants between  $\text{Cd}^{2+}$  and each individual component are calculated. The distribution of Cd in binary and ternary mixtures of the components is measured in adsorption experiments and the data are compared to independent predictions from the CA approach. The results demonstrate conditions for which the CA approach may be appropriate in predicting  $\text{Cd}^{2+}$  distribution, and those for which more complex models that include interactions between the sorbents are necessary.

### **1.5 Solubility of Np-incorporated Soddyite**

Spent nuclear fuel is likely to alter to uranyl minerals under the moist oxidizing conditions of a geological repository (Finch et al., 1999; Finn et al., 1996; Wronkiewicz et al., 1992, 1996). Radionuclides, such as neptunium, may become incorporated into these secondary uranyl mineral structures (Burns et al., 1997), potentially altering the solubility of the phases and hence the mobilities of U and Np in the repository environment. Soddyite  $((\text{UO}_2)_2(\text{SiO}_4)(\text{H}_2\text{O})_2)$  forms as a common alteration product of spent nuclear fuel in laboratory settings (e.g., Finch et al., 1999), and significant concentrations of Np(V), which is likely to be present in an oxidizing repository, can be incorporated within soddyite (Klingensmith and Burns, 2007). The solubility and thermodynamic properties of pure soddyite have been studied (Gorman-Lewis et al., 2007). It is unclear, however, what effect Np(V) incorporation into the mineral structure of soddyite has on the mineral solubility or on the extent to which Np is released from

the phase.

Gnanapragasam and Lewis (1995) reported that trace levels of radium incorporation exert no effect on the solubility of gypsum and calcite. Curti (1999) reported that the incorporation of rare earth metals and  $\text{Cd}^{2+}$  leads to the formation of insoluble carbonates, but the incorporation of  $\text{Mg}^{2+}$ ,  $\text{K}^+$ ,  $\text{Na}^+$  and  $\text{Li}^+$  forms soluble to very soluble carbonates. The closest analog to this study is that of Rai et al. (2004), who determined the solubility effect of Np(IV) incorporation into uraninite ( $\text{UO}_2(\text{s})$ ). The authors observed ideal solid solution behavior, or a decrease in the aqueous U(IV) concentration in equilibrium with the solid phase that is equal to the decrease in the mole fraction of U(IV) within the solid phase with increasing extents of Np(IV) substitution. The ideal substitution behavior found by Rai et al. (2004) is likely due to similarities in size and charge of U(IV) and Np(IV). However, Np(V) forms the neptunyl cation,  $\text{NpO}_2^+$ , which has different bonding environment and charge than the uranyl cation,  $\text{UO}_2^{2+}$  (Forbes et al., 2008). In order for  $\text{NpO}_2^+$  to substitute for  $\text{UO}_2^{2+}$  in soddyite, it is likely that co-substitution of another ion, such as  $\text{Na}^+$ , must occur, creating a more complex, non-ideal substitution mechanism.

In Chapter 5, I report on experiments that elucidate the effect of  $\text{NpO}_2^+$  incorporation on the solubility of soddyite. I synthesized soddyite samples in the presence of various aqueous Np(V) concentrations and measured the release of U, Np, and Si into solution as a function of time under controlled pH conditions. These data, through the mass action equation for the Np-soddyite dissolution reaction, were used to determine the solid phase activity coefficient for each Np-incorporated phase. The values of these activity coefficients indicate whether Np incorporation follows ideal solid-solution, and the determination of the coefficients as a function of Np content of

the solid phase enables extrapolation of the results to solid phases with more extensive Np incorporation. I also use the data to calculate distribution coefficients that describe the extent of Np release from the Np-bearing soddyite phases. Therefore, the results of this study enable quantitative models of both Np and U mobility under repository conditions.

CHAPTER 2  
EXPERIMENTAL MEASUREMENT OF MONOVALENT CATION ADSORPTION  
TO BACILLUS SUBTILIS CELLS

**2.1. Introduction**

Surface and ground waters typically contain a range of metal ions that compete for adsorption sites on surfaces of soil and aquifer components. Although the binding of environmentally important, divalent and trivalent metals onto soil components has been studied (e.g., Beveridge and Murray 1976; Beveridge 1989; Ledin et al. 1997; Yee and Fein 2001; Covelo et al. 2007), the binding behavior of monovalent cations onto bacterial surface functional groups is not known. Monovalent cations represent a major component of the total dissolved ions in many natural waters. Additionally, concentrated solutions of monovalent salts such as NaCl or NaClO<sub>4</sub> typically are used to buffer ionic strength in metal-bacteria adsorption experiments.

The adsorption of monovalent cations onto mineral and bacterial surfaces has been accounted for indirectly through construction of electric double or triple layer models, which ascribe the association of the cations with the surface to electrostatic interactions with the surface electric field (Stumm et al. 1970; Davis et al. 1978).

Implicit in electrostatic surface complexation models of experimental adsorption data is the assumption that monovalent cations do not compete with higher-charged metals for adsorption onto specific bacterial surface functional groups. Typically, the adsorption of multi-valent cations to minerals and bacteria decreases with increasing ionic strength (e.g., Daughney and Fein 1998; Gu and Evans, 2008). Electrostatic multi-layer models ascribe these ionic strength effects to the contraction of the surface electric field of the sorbent due to non-specific outer-sphere electrostatic attraction of monovalent counter-ions to the electric field of the sorbent (e.g., Davis and Kent 1990; Koretsky 2000). However, electrostatic models require the optimization of a number of parameters from experimental data such as surface electric field capacitance values. Direct model-independent determination of these parameters is impossible, and application of these models to complex real systems is problematic (Davis et al. 1998).

An alternative approach to accounting for ionic strength effects on multi-valent cation adsorption is to ascribe the adsorption behavior to direct competition between the electrolyte monovalent cations and the less abundant multivalent cations for specific surface sites. This approach obviates the need for determining electrostatic modeling parameters by instead including electrostatic effects in the apparent metal-surface equilibrium constants (Davis and Kent 1990). Equilibrium constants determined using this approach have the advantage of being independent of ionic strength and pH. Although the binding between surface functional groups and monovalent cations is likely to be weak, the concentration of the background electrolyte in metal adsorption experiments is often several orders of magnitude greater than that of the metal of interest. Thus, it is possible that monovalent metals significantly reduce the adsorption of higher charged metals via specific adsorption onto sites at the bacterial surface.

In this paper, we report the results of experiments conducted to determine the extent of adsorption of three monovalent cations,  $\text{Li}^+$ ,  $\text{Rb}^+$ , and  $\text{Na}^+$ , to the Gram-positive soil bacterial species *Bacillus subtilis* as a function of ionic strength and pH. Adsorption data are modeled using a non-electrostatic surface complexation model (NEM) approach, and discrete metal-bacteria binding constants are determined for each monovalent cation. These constants are then used to determine the competitive effect of monovalent cations on the adsorption of Cd at bacterial surface sites.

## 2.2 Methods

### 2.2.1 Bacteria growth and preparation

The Gram-positive soil bacterium *Bacillus subtilis* was initially cultured on agar slants made of 0.5% yeast extract and trypticase soy agar. Cells from the slant were transferred to 3 ml of growth medium consisting of trypticase soy broth (TSB) and 0.5% yeast extract and allowed to grow for 24 hours at 32°C. After the growth period, these bacteria were transferred to 2 l of identical broth and allowed to grow for another 24 hours at 32°C, reaching stationary phase. Bacteria were harvested by centrifuging the broth at 9,000 g for 10 minutes to pellet the bacteria. After decanting the broth, the bacteria were washed four times in  $\text{NaClO}_4$  electrolyte solutions of the same ionic strength as the target ionic strength for an individual adsorption experiment, between  $10^{-3}$  and  $10^{-1}$  M. After each wash, the bacteria were centrifuged at 8100 g for 5 minutes to pellet the bacteria and the electrolyte was discarded. The cells were then resuspended in fresh electrolyte using a Vortex and stir rod. The bacteria were transferred to a weighed centrifuge tube after the final wash, and centrifuged two times for 30 minutes at 8100 g, decanting the remaining supernatant each time. The weight of the resulting wet bacterial

pellet has been determined to be 8 times the dry weight (Borrok et al. 2005). The growth and washing procedure renders the bacteria alive, but metabolically inactive (Borrok et al. 2007).

### 2.2.2 $\text{Li}^+$ and $\text{Rb}^+$ adsorption experiments

Batch metal-bacteria adsorption experiments were performed with the monovalent cations  $\text{Li}^+$  and  $\text{Rb}^+$  (separately) in the presence of a  $\text{NaClO}_4$  electrolyte, as a function of  $\text{NaClO}_4$  concentration and pH. A perchlorate electrolyte solution was chosen because this anion does not complex strongly with metal cations. Because Na and K are present in biological cells and leach into solution to some extent, it is impossible to conduct adsorption experiments with these elements due to mass balance difficulties. Instead, we conducted  $\text{Li}^+$  and  $\text{Rb}^+$  adsorption measurements because these elements are not present appreciably in cells, and therefore rigorous constraints on their mass balances could be imposed on the experimental systems.

To verify that  $\text{Li}^+$  or  $\text{Rb}^+$  did not enter into electrolyte solutions from within the cells, control experiments were performed by suspending  $20 \text{ g l}^{-1}$  wet mass *B. subtilis* cells in  $10^{-1}$ ,  $10^{-2}$ , and  $10^{-3}$  molal  $\text{NaClO}_4$  electrolyte solutions. Each ionic strength bacterial suspension was separated into a set of test tubes, and the pH of each tube was adjusted using small volumes of HCl or NaOH to a value between 2 and 10. The tubes were placed on a rotary shaker to equilibrate for 2 h, after which the steady-state pH of each system was measured. The systems were then centrifuged at  $8100 \text{ g}$  for 10 min to separate the bacteria from the solution, and the resulting supernatants filtered through  $0.45 \text{ }\mu\text{m}$  nylon membranes and acidified with  $25 \text{ }\mu\text{L}$  of  $2.0 \text{ M}$  HCl per 10 ml of solution. Metal concentrations in all solutions were immediately analyzed using Inductively

Coupled Plasma – Optical Emission Spectrometry (ICP-OES). In all control experiments, the measured concentrations of  $\text{Li}^+$  and  $\text{Rb}^+$  were below the detection limits of the ICP-OES.

Isotherm  $\text{Li}^+$  and  $\text{Rb}^+$  adsorption experiments were performed as a function of ionic strength at a range of fixed pH values between pH 3 and 9. Each experiment was initiated by suspending 20 g  $\text{l}^{-1}$  wet mass *B. subtilis* in a  $\text{NaClO}_4$  electrolyte solution with a concentration between  $10^{-1}$  and  $10^{-3}$  M. The pH of each suspension was adjusted as needed with small volumes of NaOH or HCl, and the systems were allowed to equilibrate on a rotary shaker for 2 h. This process of pH adjustment was repeated until each system was within  $\pm 0.1$  units of the target pH. The amount of acid or base added was recorded in order to calculate the final experimental ionic strength value. After each suspension reached steady-state pH conditions, 10 ml aliquots of the bacterial suspension were removed from each system, placed into polypropylene test tubes, spiked to a final concentration of  $2.34 \times 10^{-5}$  M  $\text{Li}^+$  or  $\text{Rb}^+$  using 1000 mg  $\text{l}^{-1}$  Li or Rb stock solutions prepared from  $\text{LiClO}_4$  or  $\text{RbClO}_4$  salts, and allowed to react for another 2 h. The preparation of these  $\text{LiClO}_4$  and  $\text{RbClO}_4$  stock solutions and all additions of the solutions to experiments were performed gravimetrically. After reaching steady-state, the pH of experimental systems with  $\text{Li}^+$  and  $\text{Rb}^+$  were measured. The final pH levels for the  $\text{Li}^+$  experiments were  $2.99 \pm 0.03$ ,  $4.99 \pm 0.03$ ,  $6.95 \pm 0.07$ , and  $9.19 \pm 0.09$ , and for the  $\text{Rb}^+$  experiments,  $2.98 \pm 0.03$ ,  $5.18 \pm 0.10$ ,  $6.98 \pm 0.04$ , and  $9.02 \pm 0.04$ . Henceforth, for convenience we refer to these experiments as pH 3, 5, 7, and 9, respectively. The test tubes were centrifuged, filtered, and acidified in the same manner as the control experiments (described above), and metal concentrations in the solutions were immediately analyzed using ICP-OES. We found that the signal strength of the ICP-OES

varied strongly with solution ionic strength and composition (data not shown). To control for this effect, we centrifuged and filtered the extra Li- and Rb-free bacterial suspension that was not used in each Li<sup>+</sup> and Rb<sup>+</sup> adsorption experiment, and made Li or Rb calibration standards for ICP-OES analysis using the resulting supernatants. In this way, each experimental system had its own set of calibration standards made in a background matrix that was identical to that of the experimental samples. Analytical uncertainties associated with the ICP-OES analysis, as determined by repeat analyses of calibration standards, were less than ±3% in all cases. The amount of metal adsorbed in each experimental system was determined by subtracting the measured metal concentration remaining in solution from the initial known metal concentration in each experiment.

### 2.2.3 Cd adsorption experiments

Batch Cd metal adsorption experiments were performed between pH 2.0 and 5.5 in the presence of Li-, Na-, and KClO<sub>4</sub> electrolytes to determine if the type of monovalent cation in the buffering electrolyte affected Cd adsorption behavior. Experiments were initiated by suspending 20 g l<sup>-1</sup> washed *B. subtilis* cells in a 0.1 M Li-, Na-, or KClO<sub>4</sub> solution containing 8.90 × 10<sup>-5</sup> M Cd from a 1000 mg l<sup>-1</sup> Cd stock solution. The Cd stock solution was prepared from a Cd(ClO<sub>4</sub>)<sub>2</sub> salt. The experimental pH adjustments, equilibration time, centrifugation, filtering, and acidification for each system was identical to the procedures used for Li<sup>+</sup> and Rb<sup>+</sup> batch adsorption experiments described previously. Concentrations of Cd remaining in the filtered supernatants were analyzed using ICP-OES. Cd standards were prepared gravimetrically from a 1000 mg l<sup>-1</sup> Cd stock solution made from a Cd(NO<sub>3</sub>)<sub>2</sub> salt, diluted to desired

concentrations using the same perchlorate salt matrix as the experimental systems being analyzed. The Cd signal strength reported by the ICP-OES did not vary significantly with solution ionic strength, and uncertainties were within  $\pm 3\%$  for these experiments.

### 2.3 Results

The measured extents of  $\text{Li}^+$  and  $\text{Rb}^+$  adsorption onto *B. subtilis* are shown as a function of ionic strength at various pH values in Figures 2.1 and 2.2, respectively. The addition of NaOH to achieve the pH 9 conditions, or HCl to achieve pH 3 and 5, substantially increases the ionic strength of the background electrolyte in the experiments that had an initial ionic strength of  $10^{-3}$  M. For this reason, each experiment is plotted using the actual ionic strength of the experiment, which is the sum of the ionic strength contribution from the  $\text{NaClO}_4$  electrolyte and that from the acid or base additions.

In both the  $\text{Li}^+$  and  $\text{Rb}^+$  experiments, no significant adsorption is observed at any ionic strength in experiments conducted at pH 3, whereas significant adsorption is observed in the pH 5, 7, and 9 experiments. The pH 5, 7, and 9 experimental results indicate that the extent of Li and Rb adsorption increases significantly with decreasing ionic strength of the experimental electrolyte. As a function of pH, the amount of metal adsorbed to the bacteria in the pH 5, 7, and 9 experiments does not change significantly at any ionic strength level. This suggests that at pH 5 and above, Li and Rb adsorption behavior is more dependent on ionic strength than pH under our experimental conditions.

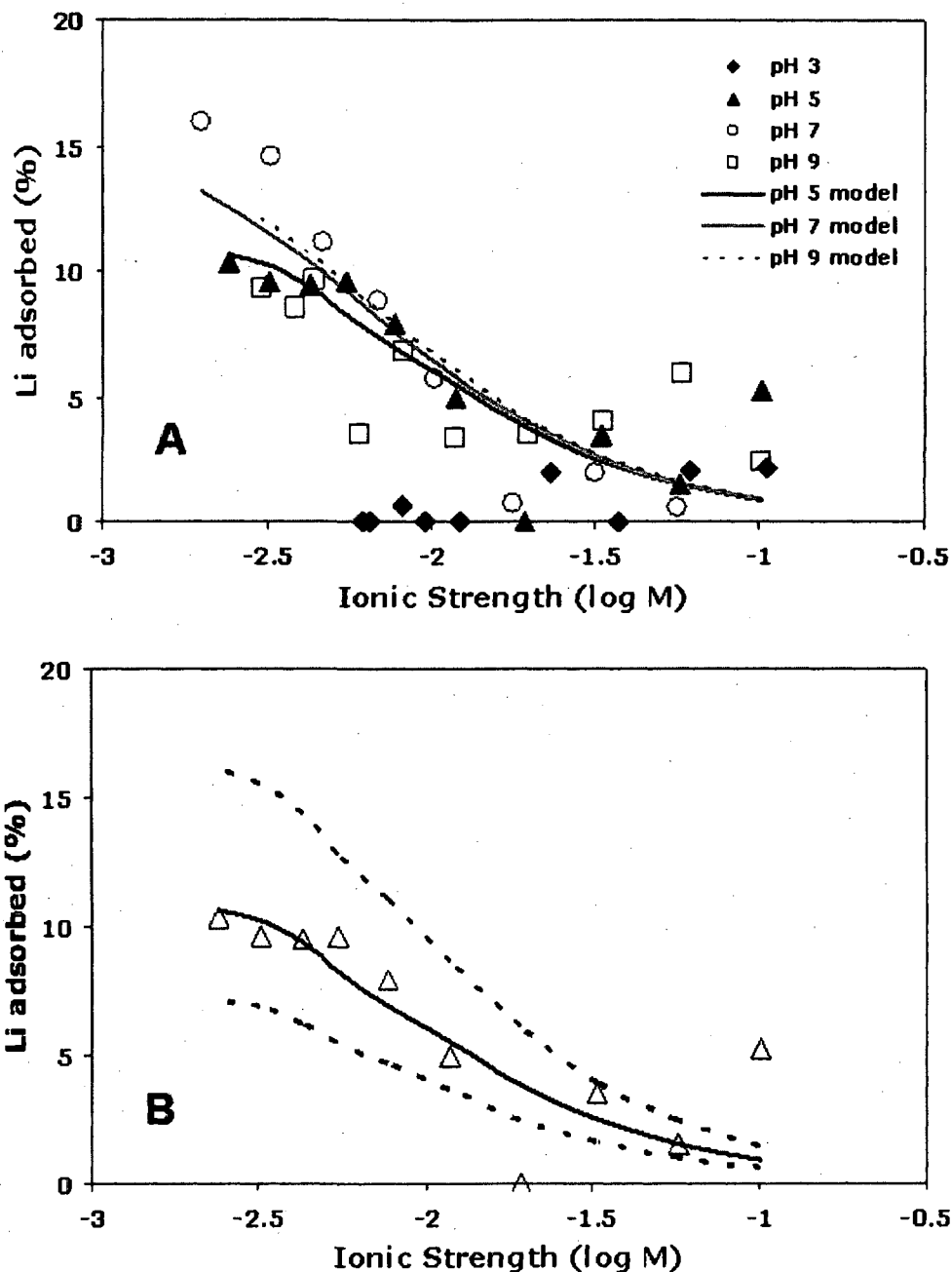


Figure 2.1: (A) Lithium adsorption to *B. subtilis* as a function of ionic strength and pH. Initial experimental conditions were  $20 \text{ g l}^{-1}$  *B. subtilis* cells and  $2.34 \times 10^{-5} \text{ M}$  Li. The pH 5 model curve represents the best-fit model that accounts for Li adsorption onto Site 2 only. Curves for the pH 7 and pH 9 models show the extent of adsorption that would be predicted using the  $K_{Na}$  and  $K_{Li}$  values determined from modeling the pH 5 data, and assuming no additional adsorption of Li onto Sites 3 or 4. (B) Best-fit model for Li adsorption to Site 2 of *B. subtilis* at pH 5 (solid curve). Dashed curves are models resulting from a  $\pm 0.2$  variation in the best-fitting log stability constant value of  $K_{Li}$ .

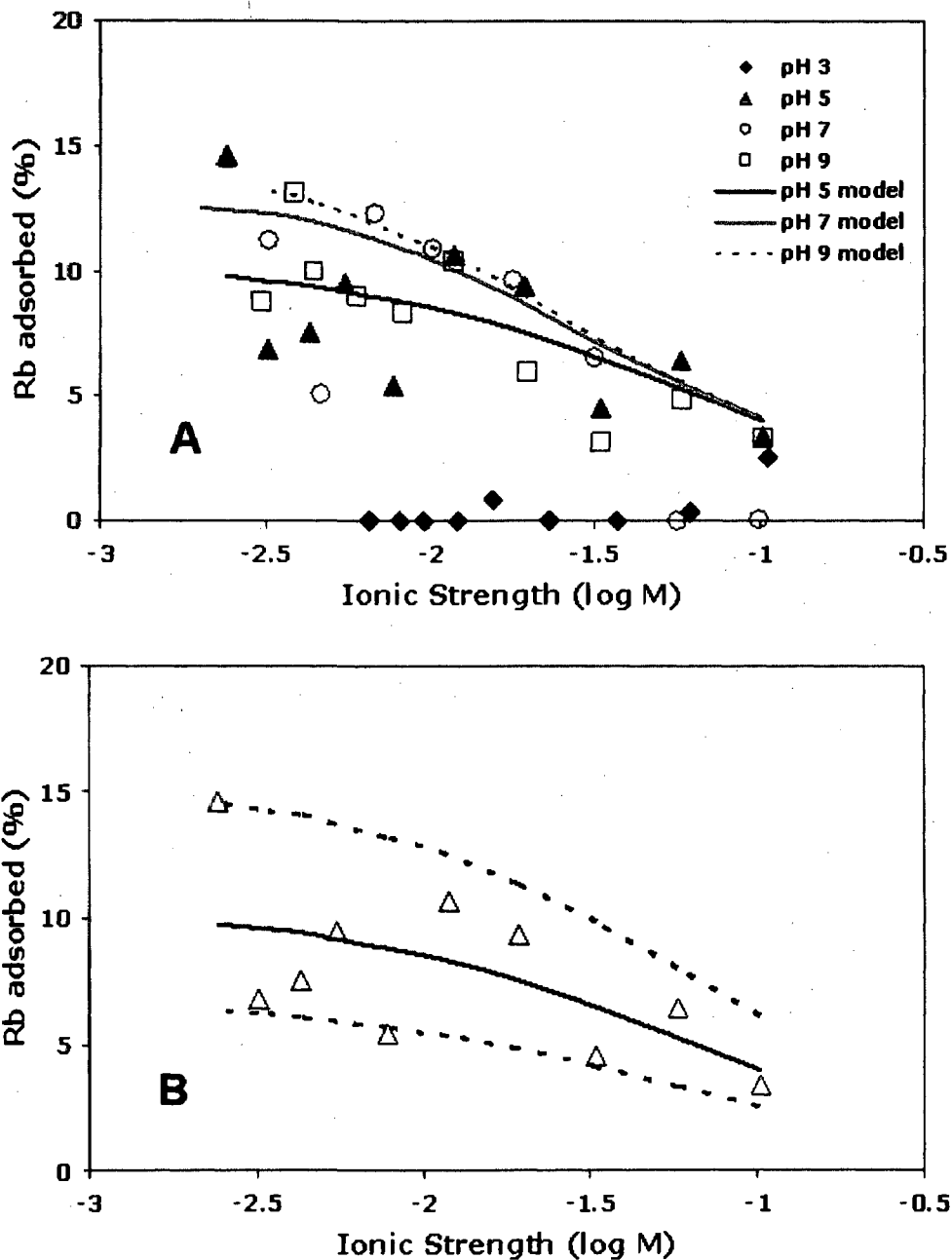


Figure 2.2: (A) Rubidium adsorption to *B. subtilis* as a function of ionic strength and pH. Initial experimental conditions were  $20 \text{ g l}^{-1}$  *B. subtilis* cells and  $2.34 \times 10^{-5} \text{ M}$  Rb. The pH 5 model curve represents the best-fit model that accounts for Rb adsorption onto Site 2 only. Curves for the pH 7 and pH 9 models show the extent of adsorption that would be predicted using the  $K_{Na}$  and  $K_{Rb}$  values determined from modeling the pH 5 data, and assuming no additional adsorption of Rb onto Sites 3 or 4. (B) Best-fit model for Rb adsorption to Site 2 of *B. subtilis* at pH 5 (solid curve). Dashed curves are models resulting from a  $\pm 0.2$  variation in the best-fitting log stability constant value of  $K_{Rb}$ .

Figure 2.3 shows the results of the experiments of Cd adsorption onto *B. subtilis* cells. Cd adsorption increases as a function of increasing pH from approximately 10% at pH 2 to nearly 80% at pH 5.5. The extent of adsorption does not vary significantly as a function of the type of monovalent salt used to buffer the ionic strength of the experimental system, suggesting that the three monovalent cations studied here compete with Cd for adsorption to bacterial surface functional groups to a similar degree.

In general, the extent of adsorption of the monovalent cations studied here was much less than that observed for divalent cations under similar experimental conditions. In the experiments conducted at an ionic strength of  $10^{-1}$  M, adsorption of Li and Rb was approximately 5% or less under the pH conditions studied; in experiments with an ionic strength of  $10^{-2.5}$  M, the maximum extent of Li and Rb adsorption that was observed under any of the pH conditions was 10 – 15%. To compare, the Cd adsorption experiments reported here were conducted at an ionic strength of 0.1 M, using the same bacterial concentration as we used in the Li and Rb experiments. Although the Cd molality in these experiments is nearly four times that of Li or Rb in their adsorption experiments, approximately 75% of the Cd in solution adsorbed onto cell walls at pH 5 (Figure 2.3A), compared to less than 5% adsorption for the Li and Rb.

## **2.4 Discussion**

### *2.4.1 Thermodynamic Modeling*

The objective of the thermodynamic modeling of the experimental data was to determine if a stability constant for the monovalent-bacterial surface complex could account for the adsorption behavior as a function of  $\text{NaClO}_4$  content for each cation studied. We use a non-electrostatic surface complexation model to describe proton and

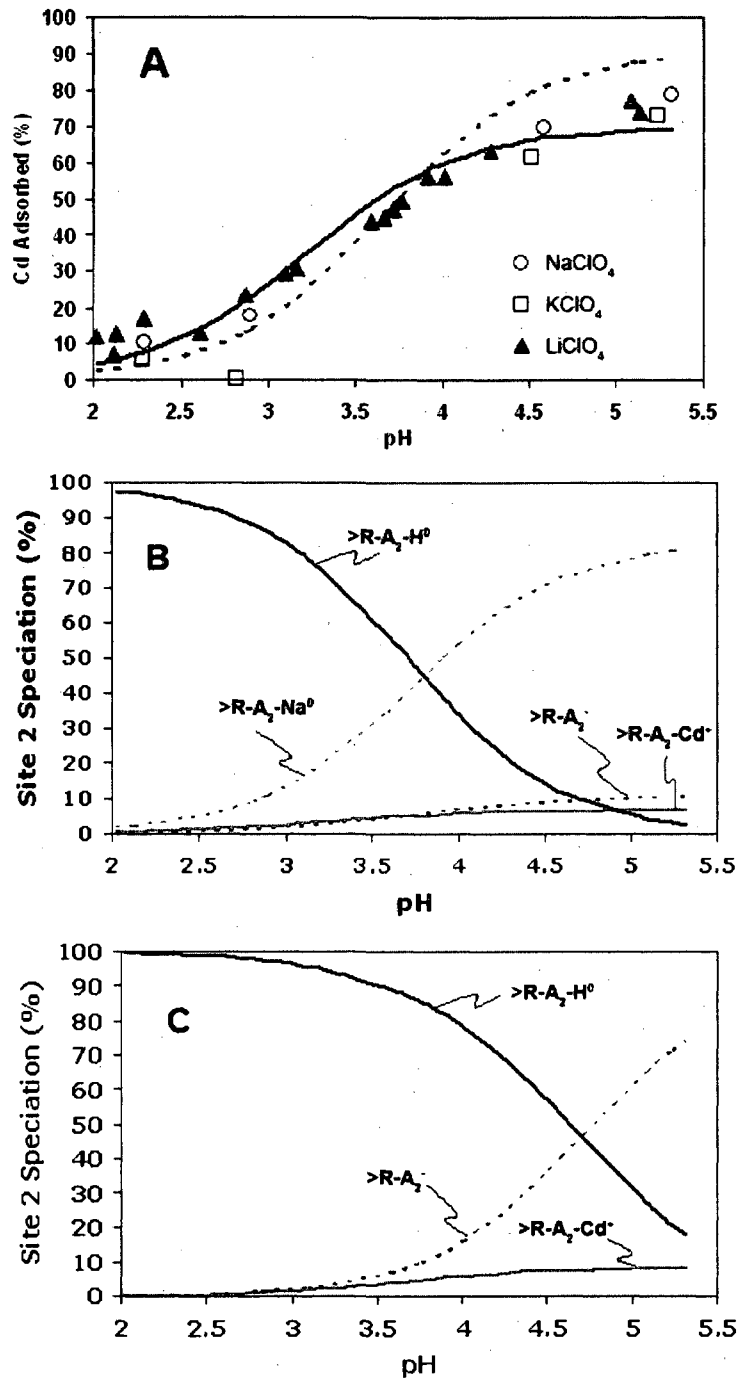


Figure 2.3: A) Cd adsorption to *B. subtilis* cells in Na-, K-, and Li-perchlorate electrolytes. Initial experimental conditions were  $10 \text{ g l}^{-1}$  *B. subtilis* cells and  $8.90 \times 10^{-5} \text{ M}$  Cd in a 0.1 M perchlorate solution. Curves indicate the best-fit models for Cd adsorption onto bacterial Site 2 with (solid curve) and without (dashed curve) inclusion of the Na-Site 2 complexation reaction in the model. The speciation of Site 2, with and without Na-Site 2 complexation, is depicted in (B) and (C), respectively.

metal adsorption onto the cell wall functional groups of *B. subtilis*. A system of mass action equations is used to calculate the distribution of protons and metal cations between the bacterial cell wall functional groups and the solution. In this approach, the proton-activity of the cell wall is ascribed to the deprotonation behavior of cell wall-associated organic acid functional groups:



where  $A_i$  represents a distinct organic acid functional group type, and  $R$  represents the bacterial cell wall macromolecule to which the functional group  $A_i$  is attached. The mass action equation for the deprotonation reaction is:

$$K_a = \frac{[R - A_i^-] a_{H^+}}{[R - A_i(H)^0]}, \quad (2)$$

where  $K_a$  is the equilibrium constant, or acidity constant, for Reaction (1), the brackets represent molar concentrations of the bacterial surface species, and  $a_{H^+}$  is the activity of aqueous protons in the bulk solution. We use a four-site ( $i = 1 - 4$ ) non-electrostatic model (NEM), with protonation constant ( $pK_a$ ) values of 3.3, 4.8, 6.8, and 9.1, to describe proton binding onto the cell wall (Fein et al. 2005). We refer to these sites as Sites 1 – 4, respectively.

Bulk adsorption observations can not be used to distinguish between cation binding to specific bacterial surface sites and non-specific cation binding that results from electrostatic attraction by a surface electric field. Our objective is to model this interaction as binding to specific sites, and therefore as a competition reaction. Experimental measurements of the extent of adsorption as a function of pH in single-metal systems can be used to constrain which sites are involved in the adsorption reactions and to determine the stability constants for the important bacterial surface

complexes (e.g., Fein et al. 1997; Cox et al. 1999; Haas et al. 2001; Ngwenya et al. 2003). However, there are two competing types of monovalent cations present in each of our experimental systems:  $\text{Li}^+$  or  $\text{Rb}^+$  as the adsorbing metal of interest, and  $\text{Na}^+$  from the  $\text{NaClO}_4$  ionic strength buffer. We explicitly account for competition by including metal binding reactions for both cations that are present in each system in our models according to:



where  $M^+$  represents the monovalent metal of interest ( $\text{Li}^+$  or  $\text{Rb}^+$ ) in equation (3). The equilibrium constants ( $K_{eq}$ ) for complexation reactions (3) and (4) are defined by:

$$K_M = \frac{[R-A_i(M)^0]}{[R-A_i^-] a_{M^+}}, \quad (5)$$

$$K_{Na} = \frac{[R-A_i(Na)^0]}{[R-A_i^-] a_{Na^+}}, \quad (6)$$

respectively, where  $[R-A_i^-]$  represents the concentration of deprotonated cell wall functional group  $A_i$ ,  $[R-A_i(M)^0]$  represents the concentration cell wall functional group  $A_i$  that is complexed with metal  $M$ , and  $a_{M^+}$  is the activity of the monovalent metal of interest in solution after equilibrium is attained.

Equations (2), (5), and (6) can be used, together with pH measurements, measurements of the extent of Li or Rb and Na adsorption, and mass balance constraints on Na and Li or Rb, to determine the unknown values of  $K_M$  and  $K_{Na}$ . However, because the extent of Na that adsorbs in each experiment cannot be measured directly, it is not possible to solve for  $K_{Na}$  directly. We can use multiple measurements of Li or Rb adsorption, in experiments conducted with varying total Na concentrations, to constrain

the value of  $K_{Na}$  using an iterative approach to determine simultaneously the best-fitting stability constant values for Na and the adsorbing metal of interest. In this approach, we fix a value for  $K_{Na}$ , and use the data to solve for a value for  $K_M$ . We systematically vary the fixed value for  $K_{Na}$  over a wide range of possible values, determining the value that yields the best overall fit to the data. The fixed value of  $\log K_{Na}$  was initially varied between 0 and 10, in increments of 1. For both the Li and Rb data, the model best fits the data when the  $\log K_{Na}$  value was fixed at 2. To more precisely determine the  $K_{Na}$  value, the value of  $\log K_{Na}$  was then varied between 1.0 and 3.0 in increments of 0.1 to determine the overall best fit for each metal.

We used the computer program FITEQL 2.0 (Westall 1982) to solve for the stability constants for the metal-bacterial surface complexes. This program accounts for the aqueous speciation of each metal, and all metal-surface complexes. Li, Rb, and Na are present almost exclusively as free monovalent cations in solution under our experimental conditions. We include aqueous cation hydrolysis reactions, using the constants reported by Baes and Mesmer (1976). The relative goodness of fit of each model is determined by comparing the overall variance parameter,  $V(Y)$ , calculated by FITEQL.

#### *2.4.2 Modeling of monovalent cation adsorption to *B. subtilis**

Little adsorption of Li or Rb was observed at pH 3, and significant adsorption was observed in the pH 5, 7, and 9 experiments. Thus, we conclude that Site 1 (with a pKa value of 3.3) on the bacterial surface does not significantly contribute to the overall adsorption of monovalent cations. Adsorption of both Li and Rb increases significantly from pH 3 to pH 5, and we ascribe this increase to Li and Rb binding directly onto Site 2

(the site with a pKa value of 4.8). Thus, we determine the binding constants for the bacterial surface complexes that are formed by the binding of the monovalent cations onto Site 2, using the pH 5 data only and assuming that the adsorption under these pH conditions involves binding onto Site 2 only. This approach is reasonable because at pH 5 more than 98% of the Site 3 (with a pKa value of 6.8) functional groups are protonated and, therefore, are unlikely to contribute significantly to Li, Rb, or Na binding.

The best-fitting models to the pH 5 data for  $\text{Li}^+$  and  $\text{Rb}^+$  adsorption are shown as solid curves in Figures 2.1B and 2.2B, respectively. We calculate a  $\log K_{\text{Li}}$  value of 2.0, and a  $\log K_{\text{Na}}$  value of 2.3 using the pH 5  $\text{Li}^+$  adsorption data; and a  $\log K_{\text{Rb}}$  value of 1.9 and a  $\log K_{\text{Na}}$  value of 1.5 using the pH 5  $\text{Rb}^+$  adsorption data. To constrain the error of the  $\log K_{\text{Rb}}$  and  $\log K_{\text{Li}}$  values, we fixed the  $\log K_{\text{Na}}$  values in each model, and systematically varied the  $\log K_{\text{Rb}}$  and  $\log K_{\text{Li}}$  values in increments of  $\pm 0.1$  log units, calculating the extent of adsorption that would be predicted in each case. A variation of  $\pm 0.2$  log units in the Rb and Li  $\log K$  values (plotted as dashed curves in Figures 2.2B and 2.1B, respectively) is sufficient to describe the variation in the data.

In order to test whether the monovalent cations adsorb to Sites 3 or 4 under our experimental conditions, we used the calculated  $K_{\text{Na}}$ ,  $K_{\text{Li}}$ , and  $K_{\text{Rb}}$  stability constants for Site 2 to predict the extent of Li or Rb adsorption that would occur at pH 7 and 9, assuming that only cation-Site 2 binding occurs for each metal. The results of this calculation for pH 7 and 9 appear in Figures 2.1A and 2.2A as grey and dashed curves, respectively. Li and Rb adsorption is predicted to increase somewhat from pH 5 to 7 and to remain essentially unchanged between pH 7 and 9 (Figures 2.1A, 2.2A). The predicted increase from pH 5 to 7 arises due to the higher concentration of deprotonated Site 2 sites at pH 7 relative to pH 5. From pH 7 to 9, there is little change in the

concentration of deprotonated Site 2 sites, so the extent of cation binding onto Site 2 is predicted to remain constant for both Li and Rb. The predicted increase in the extent of Rb adsorption from pH 5 to 7 is larger than that predicted over the same pH interval for Li adsorption because  $K_{Na}$  in the Li model is larger than  $K_{Li}$ , so as sites deprotonate going from pH 5 to 7, Na outcompetes Li for the available sites. The opposite trend occurs in the Rb model, where  $K_{Na}$  is smaller than  $K_{Rb}$  so Rb can better compete with Na than does Li under the same circumstances. The observed extents of Li and Rb adsorption agree within experimental uncertainty with the predicted adsorption behaviors for the pH 7 and 9 conditions, suggesting that there is no significant interaction between the monovalent cations and Sites 3 or 4. Therefore, the only stability constants that we can determine from our data are those for the monovalent cations bound to Site 2.

The similarities in the log  $K$  values calculated for Li, Rb, and Na, and the relatively large uncertainties associated with them lead us to propose that reasonable estimates of the adsorption behavior of monovalent cations can be obtained by using a single averaged value for the stability constant for all monovalent cation-bacterial surface complexes. The average log  $K$  value, and associated  $\pm 1\sigma$  uncertainty for monovalent metal adsorption onto Site 2 of *B. subtilis* is  $1.9 \pm 0.3$ .

The Li- and Rb-Site 2 stability constants are small relative to those of divalent and trivalent metals, consistent with our observations of less extensive monovalent metal adsorption compared with that of higher charged cations. For example, using the same modeling approach applied here and the same reaction stoichiometries, Gorman-Lewis et al. (2005) report a log stability constant value of  $6.2 \pm 0.3$  for the binding of the uranyl cation ( $UO_2^{2+}$ ) to Site 2 of *B. subtilis*. Similarly, Borrok et al. (2007) calculate Site 2 log

stability constant values of 3.3 for  $\text{Ni}^{2+}$  and 4.7 for  $\text{Pb}^{2+}$ . Although these constants are large relative to those we calculate for monovalent cations in this study, monovalent cations are often present in natural systems and in laboratory experiments at concentrations that are orders of magnitude greater than those of the higher-charged cations of interest. Thus, monovalent cations may be able to compete effectively for adsorption onto bacterial surface functional groups in these experiments.

#### *2.4.3 Monovalent cation competition with Cd*

Most experiments that have measured metal adsorption onto bacteria have been conducted using a monovalent electrolyte that is present at concentrations up to several orders of magnitude greater than that of the adsorbing metal of interest. Under these conditions, monovalent cations can compete effectively for surface sites. If metal adsorption in these studies is modeled using a non-electrostatic approach and if the competition by monovalent cations is not accounted for in the thermodynamic calculations, then the calculated stability constants for the metal-bacterial surface complexes would need to be corrected. We determine the magnitude of this correction for Cd-bacterial surface complexes, using Cd-*B. subtilis* adsorption data from pH-dependent adsorption experiments reported in this study (Figure 2.3A) and from isotherm adsorption data reported in Mishra et al. (2008) as examples. The data of Mishra et al. (2008), shown in Figure 2.4, were selected because they are isotherm experiments conducted as a function of Cd concentration at pH 5.9, so all of the Cd adsorption in these experiments can be attributed to Cd-Site 2 binding. The experiments in Mishra et al. (2008) were conducted with  $10 \text{ g l}^{-1}$  bacteria suspended in a 0.1 M  $\text{NaClO}_4$  electrolyte at a fixed pH of  $5.9 \pm 0.2$ . Initial Cd solution concentrations in the

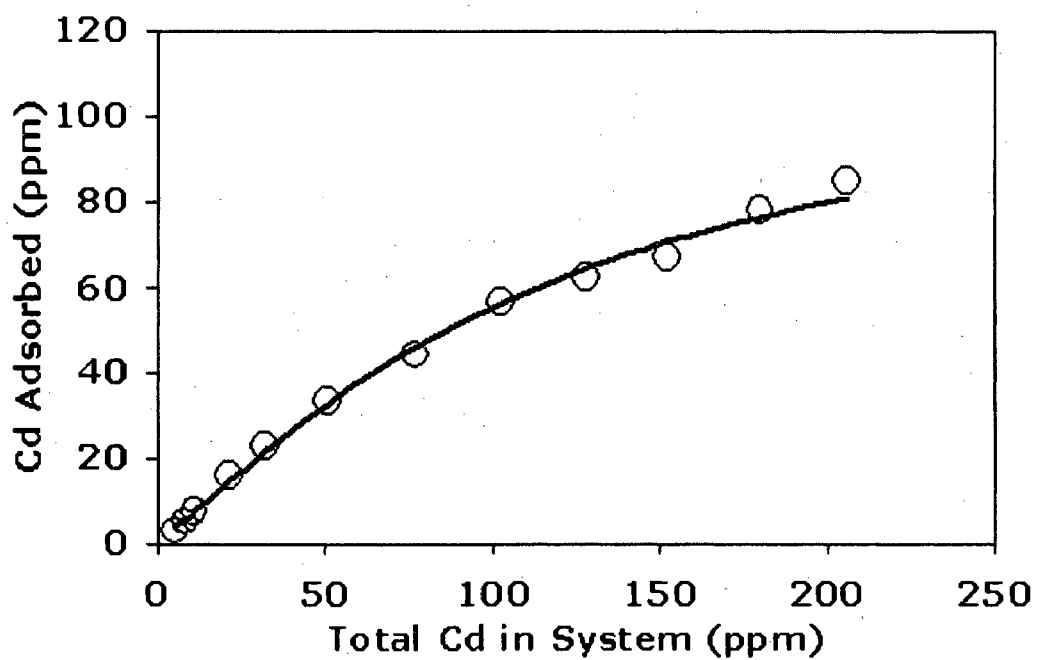


Figure 2.4: Cd adsorption to  $10 \text{ g l}^{-1}$  *B. subtilis* cells in  $0.1 \text{ M NaClO}_4$  electrolyte at  $\text{pH } 5.9 \pm 0.2$ . Adsorption models with and without Na-Site 2 complexation included yield identical best fits (solid curve) to the data. Data are from Mishra et al. (2008).

experiments varied between 5 and 205 ppm. We use the same modeling approach employed by Mishra et al. (2008), but account for  $\text{Na}^+$  binding to Site 2 in order to determine the magnitude of change in the calculated Cd stability constant for this site.

The models with and without  $\text{Na}^+$ -Site 2 binding provide identical fits to the Cd adsorption data (Figure 2.4), but the stability constant calculated for the Cd-Site 2 surface complex increases significantly when the  $\text{Na}^+$  competition reaction is considered. Without considering direct competition of  $\text{Na}^+$  with  $\text{Cd}^{2+}$ , the calculated best-fitting log stability constant value for the Cd-Site 2 complex is 3.4. Including the Na-Site 2 complexation reaction in the model yields an increased calculated best-fitting Cd-Site 2 log stability constant value of 4.4.

We model pH-dependent adsorption data between pH 2 and 5.5 (Figure 2.3A) using the same modeling approach. The calculated log stability constant value for the Cd-Site 2 complex is 3.8 without  $\text{Na}^+$  competition considered (dashed curve), and 4.4 with  $\text{Na}^+$  competition at Site 2 (solid curve). Notably, the model that includes the  $\text{Na}^+$  competition reaction at Site 2 fits the data better than the model without this reaction. Additionally, the magnitude of the correction should be less for cations such as  $\text{UO}_2^{+2}$  that display a higher affinity for the bacterial sites than does  $\text{Cd}^{+2}$ .

The inclusion of  $\text{Na}^+$  competition in the models significantly affects the calculated speciation of the cell wall functional groups. The differences in the speciation of Site 2 in models with and without the Na-Site 2 reaction are depicted in Figures 2.3B and 2.3C, respectively. In models that consider Na-Site 2 complexation, the Na-Site 2 complex represents the dominant surface species with increasing pH as the protonated site deprotonates. In addition, the stability of the Na-Site 2 complex is such that deprotonation occurs at lower pH than would be predicted from the model that does not

consider Na-Site 2 complexation. Under the conditions of these calculations, when Na-Site 2 complexation is included, the model predicts that half of the Site 2 sites are protonated at approximately pH 3.8, whereas in models that neglect the Na-Site 2 complexation this point occurs at pH 4.8. This same shift in speciation of the protonated site would occur if we modeled the reactions using electrostatic surface models. The Na-Site 2 complexes represent the equivalent of  $\text{Na}^+$  counter-ions that would be predicted to accumulate in the diffuse layer of electrostatic models, with the only difference being the location of the  $\text{Na}^+$  cations relative to the cell wall functional group sites. Therefore, the site-specific Na-binding and electrostatic modeling approaches can successfully account for both multivalent cation adsorption caused by changes in ionic strength as well as the speciation of the surface induced by shifts in ionic strength.

## 2.5 Conclusions

Our results demonstrate that monovalent cations adsorb to bacterial cell walls under some conditions, and that the adsorption can be modeled with site-specific adsorption reactions. With this approach, the ionic strength effect on metal adsorption onto bacteria can be modeled as a competition for available binding sites between the metal of interest and the monovalent cations of the background electrolyte. The stability constant values for Li-, Rb-, and Na-bacterial surface complexes are reasonably close to each other, and reasonable estimates of monovalent adsorption behavior can be achieved by assuming a universal stability constant for all monovalent-bacterial surface complexes. Although monovalent cations adsorb much more weakly than do divalent and trivalent cations, in systems where the concentration of monovalent cations is much higher than that of the higher-charged metals that are present, the monovalent cations

can effectively compete with other cations for available sites and diminish the extent of adsorption of those other cations. The approach of accounting for the ionic strength effect on adsorption by modeling it as competition for specific binding sites yields adsorption models that are easier to apply to complex geologic systems.

## CHAPTER 3

# TESTING THE VALIDITY OF THE CHLOROFORM FUMIGATION-EXTRACTION METHOD FOR DETERMINING SOIL BIOMASS C IN SOILS

### 3.1 Introduction

Soils are complex and variable mixtures of inorganic and organic components and free and adsorbed water. The inorganic fraction typically consists of minerals such as silica, feldspars, clays, and micas; the organic portion includes humic substances and microorganisms. These components represent a mixture of polar and nonpolar adsorbents that can strongly affect the distribution, speciation, and bioavailability of metals and organic pollutants in soils (e.g., Steffan and Akgerman, 1998). In order to develop quantitative adsorption models of contaminant distributions in soil systems, the amount of each component must be precisely determined.

Sequential extraction approaches (e.g., Tessier et al., 1979; Li et al., 1995) can be used to estimate the abundances of broad categories of minerals (carbonates, silicates, etc.) relative to organic components in soil. Furthermore, mineral identities and abundances in a soil sample can be reasonably estimated using x-ray diffractometry approaches (e.g., Brindley, 1984; Bish and Post, 1993). However, the approaches that

have been developed to estimate biological cell mass or numbers in soils lack the precision that is necessary for the estimates to be useful in quantitative geochemical speciation and transport models. Commonly used methods of biomass determination include direct counting of bacteria using an optical microscope, and the use of adsorbent fluorescent dyes for spectrophotometric measurement of cell numbers. Bacterial counts based on optical microscopy or spectroscopy typically yield estimates of cell numbers with uncertainties of an order of magnitude or more, and fluorescent dyes can illuminate particles that are not bacteria leading to falsely high counts (Fægri et al., 1977; Pogalazova et al., 1996). Lindahl and Bakken (1995) showed that physical dispersion methods to separate cells from soil, such as ultrasonication, blender, drill-gun, and shaking approaches, can damage cells. The percentage, viability, and purity of bacterial cells separated from soil also depend strongly on the dispersion technique and whether a surfactant is used in the separation procedure (Bakken, 1985).

Jenkinson and Powlson (1976a, b) introduced a biocidal fumigation method to determine the cell biomass-C in soils. Their work demonstrates that chloroform ( $\text{CHCl}_3$ ) fumigation effectively lyses cells in 24 hours. In this procedure, after the fumigation period, the fumigated soil sample and an un-fumigated control soil are placed in an incubator. The C from organisms that were killed and lysed during the fumigation process is readily mineralized to  $\text{CO}_2$ , so that the difference in  $\text{CO}_2$  gas evolution between fumigated and un-fumigated samples is a measure of the biomass-C (Smith et al., 1995). Vance et al. (1987) and Tate et al. (1988) introduced a similar method that involves a fumigation step, but in this procedure organic C is extracted from fumigated and un-fumigated samples using a 0.5 M  $\text{K}_2\text{SO}_4$  solution instead of an incubation approach. The  $\text{K}_2\text{SO}_4$  solutions are then analyzed for total organic carbon (TOC), and

biomass-C is calculated as the difference in TOC in the extracted solutions from the fumigated and the un-fumigated samples. The fumigation method is based on the assumption that the enhanced amount of organic C extracted from a sample relative to a control is due entirely from cell lysis caused by chloroform fumigation. Vance et al. (1987) found an empirical linear relationship between biomass-C and organic C released by fumigation-extraction. Clearly, if chloroform sorbs onto any of the soil components and is extracted using the  $K_2SO_4$  solution, then the subsequent measurements of enhanced TOC would in part be caused by the presence of chloroform and not only by lysis of biological organisms.

Although the fumigation method is commonly used, and is often considered the preferred method for biomass determination in soil (e.g., Franzluebbers, 1999), control experiments for the approach have never been performed, and so the accuracy of the procedure remains untested. Specifically, in applying the fumigation methods, one implicitly assumes that the introduced chloroform can be completely evacuated from the soil after the 24 h fumigation period. Because chloroform itself contains organic C and could add to the extractable C pool, this assumption must be tested with control experiments involving each of the major components of soils. Haney et al. (1999, 2001) questioned the acceptability of the fumigation-extraction method to determine biomass-C by showing that the amount of C extracted using a 0.5 M  $K_2SO_4$  solution can vary significantly as a function of pH.

Chloroform is volatile under the experimental conditions, and volatile organic carbon (VOC) vapors can sorb substantially to clays (e.g., Guo et al., 1998). Generally, montmorillonite, a 2:1 clay mineral, can sorb 200-300 mg VOC per g clay, and the 1:1 kaolinite has a sorption capacity of  $\frac{1}{4}$  to  $\frac{1}{2}$  of that (Thibaud-Erkey et al., 1995). There is

evidence that suggests that chloroform can sorb to soils both from aqueous solution (Dural and Peng, 1995) and from the atmosphere (Farrell and Reinhard, 1994; Thibaud-Erkey et al., 1995; Yeo et al., 1997; Chen and Dural, 2002), and therefore may show up as biomass C upon extraction with  $K_2SO_4$ .

In this paper, we test the validity of the fumigation-extraction method by performing fumigation control experiments with individual soil components, including humic acid, sand, clays, and bacteria. If the fumigation-extraction approach is valid, then we should observe no difference in TOC in the extracted solutions from the fumigated and un-fumigated samples, except for the bacterial samples, where cell lysis should enhance the extracted TOC in the fumigated samples. However, if chloroform sorbs onto any of the surfaces to a significant extent, then we would observe enhanced TOC in extracted solutions relative to the un-fumigated controls even though no biomass is present in those samples. Our control experiments will determine whether chloroform sorbs onto common soil components. If chloroform sorption does occur onto some soil components, then our experiments will constrain the types of soil for which the fumigation-extraction method can yield accurate biomass C analyses.

### **3.2 Materials and Methods**

Two clays, a silica sand, a humic acid, and a pure strain of bacteria were used as control materials for testing the fumigation-extraction method. The average grain diameter, with  $1\sigma$  uncertainties, of the silica sand (Accusand 40/50) was determined using scanning electron microscopy, and was found to be  $469\pm 89 \mu\text{m}$  ( $n = 84$ ). Schroth et al. (1996) analyzed a suite of Accusand grades and found the average diameter of the 40/50 grains to be  $359\pm 10 \mu\text{m}$  ( $n = 4$ ) using sieve analyses. The clays that were used in

this study included a kaolinite (KGa-1b) and a Na-rich montmorillonite (SWy-2), both of which were obtained from the Source Clays Repository and have been characterized extensively. Dogan et al. (2006) found the mean BET surface areas of KGa-1b and SWy-2 to be  $13.1 \text{ m}^2 \text{ g}^{-1}$  and  $22.7 \text{ m}^2 \text{ g}^{-1}$ , respectively. Cerato and Lutenegger (2002) estimated specific surface areas of  $15 \text{ m}^2 \text{ g}^{-1}$  for KGa-1b and  $637 \text{ m}^2 \text{ g}^{-1}$  for SWy-2 using the ethylene glycol monoethyl ether (EGME) method. Also available are chemical analyses (Mermut and Cano, 2001), infrared analyses (Madejová and Komadel, 2001) and powder x-ray diffraction analyses (Chipera and Bish, 2001) of both clays. We conducted fumigation tests using dried forms of both the kaolinite and montmorillonite samples, and we also conducted a test using a wetted montmorillonite powder in order to test whether wetness of the clay affects the results. In this case, the SWy-2 montmorillonite sample was wetted by soaking the clay in excess water for 1 h in 250 mL centrifuge tubes. After soaking, the tubes were centrifuged for 10 min at 7500 rpm three times and the water decanted each time. The amount of water retained by the clay after centrifugation was calculated by determining the weight difference between wet and dry SWy-2 samples, measuring the mass of the wet and dry clay samples before and after drying each in an oven at  $105^\circ\text{C}$  for 24 h. The dry SWy-2 sample contained  $5.0 \pm 0.2\%$  water by weight and the wet SWy-2 sample contained  $82.8 \pm 1.3\%$  water by weight. The humic acid experiments used a commercial humic acid, which has been characterized by Malcolm and MacCarthy (1986), obtained from the Aldrich Chemical Company. The silica sand, humic acid, and clays were used in experiments without washing or other modification. *Bacillus subtilis*, a gram-positive soil bacterial species, was grown from pure culture slants. Cells from the slant were transferred to 3 mL of trypticase soy broth (TSB) with 0.5% yeast extract and allowed to grow for 24 hours at

32°C. These cells were transferred to 1 L of the same media and allowed to grow for 24 hours at the same temperature. Cells were then harvested in early stationary phase by centrifugation and washed three times in test tubes in a 0.1 M NaClO<sub>4</sub> solution.

The fumigation procedure that we used closely followed the methods of Jenkinson and Powlson (1976a, b) and Vance et al. (1987). Experiments were conducted as a function of the mass of a soil component, with six experiments at different masses performed for each component. We used 0-50 g kaolinite, 0-50 g dry montmorillonite, 0-80 g wet montmorillonite, 0-50 g silica sand, 0-200 mg humic acid, and 0-200 mg bacteria. For each soil component separately, a known mass of material was spread evenly into two glass Petri dishes: one dish was fumigated with chloroform gas for 24 hours, and the other was an un-fumigated control. The fumigation samples were placed in a glass dessicator lined with moist filter paper. A small beaker that contained approximately 25 mL of ethanol-free chloroform and a few boiling chips was placed in the center of the dessicator. Once sealed, the dessicator was evacuated for 2 min, causing the chloroform to boil, thereby exposing the samples to chloroform vapor. After 24 hours in the dark, the beaker of chloroform was removed from the dessicator, and the dessicator was evacuated 8 times to remove chloroform vapor from the samples. Evacuations were performed by connecting the dessicator to a vacuum for 3 min, then sealing the dessicator from the vacuum, and finally slowly opening it to the atmosphere to refill with air. No noticeable chloroform odor existed after this procedure. We performed kinetics experiments, measuring the amount of organic C remaining on samples of dry SWy-2 montmorillonite as a function of evacuation time. The samples exhibited extracted organic C concentrations that were independent of evacuation time, so all subsequent experiments were conducted with eight 3 min evacuations.

Organic C extractions of both fumigated and un-fumigated samples were performed using identical procedures. That is, each sample was transferred into a 500 mL glass media bottle, and 200 mL of 0.5 M  $K_2SO_4$  was added. The bottles were then placed on an oscillating shaker for 30 minutes to thoroughly mix the sample with the  $K_2SO_4$  extractant solution. The supernatant was filtered using Whatman No. 42 filters, and collected for C analysis. We used an organic C analyzer (Shimadzu TOC-5000) to analyze for organic C in the extracts. Sets of six calibration standards for the TOC analyzer were made from a 1000 ppm organic C solution as potassium biphthalate (Ricca Chemical Company, Arlington, TX) in the same 0.5 M  $K_2SO_4$  matrix as the samples. The organic C concentrations in each calibration set were designed to be appropriate for the expected C concentrations in the various samples. Samples and standards were acidified with 1.0  $\mu$ L of 1.0 M trace grade HCl per mL of solution to remove dissolved inorganic C. The TOC instrument analyzed the C concentration in each sample 3 times, with a resulting error of less than 5% for all analyzed solutions. Control blanks containing only 0.5 M  $K_2SO_4$  and the HCl acidification were included with every TOC set, and used to correct each dataset for any background C present in the reagents or from the instrument.

A set of two-component experiments was conducted using a constant 50 g of silica sand and between 0 and 200 mg of bacteria. The fumigation and extraction procedures for these experiments were identical to those conducted for the single-component experiments.

### 3.3 Results and Discussion

The results of the bacteria experiment are depicted in Figure 3.1, which relates the biomass initially placed in the Petri dish to the concentration of organic C extracted in the  $K_2SO_4$  solution. Data for the fumigated samples and for the un-fumigated controls are both plotted, and the calculated difference (the concentration of TOC in the extract from the fumigated samples minus the concentration of TOC in the extract from the un-fumigated controls) is also shown. The un-fumigated controls exhibit increasing extracted TOC with increasing initial biomass in the Petri dish, indicating that the extraction wash dissolves some of the organic C from un-treated bacteria, and that the concentration of organic C in the wash is controlled by the amount of biomass exposed to the wash solution. The fumigated bacterial samples exhibit enhanced TOC in the extraction solution relative to that measured in the extraction solutions for the un-fumigated controls for all initial biomasses studied, and the enhancement increases with increasing initial biomass. The enhanced TOC in the fumigated samples indicates that the chloroform treatment exposes the extraction wash solution to higher levels of organic C than in the un-fumigated case, likely due to cell lysis from fumigation. For an ideal application of the fumigation-extraction approach, the un-fumigated control in a bacteria-bearing system would exhibit little or no extracted TOC in the  $K_2SO_4$  wash solution. However, the difference in TOC concentrations between the fumigated samples and the un-fumigated controls also increases with increasing biomass, and this relationship strongly suggests that the fumigation procedure can be calibrated and used successfully in a bacteria-only system to relate extracted TOC to initial biomass in the sample.

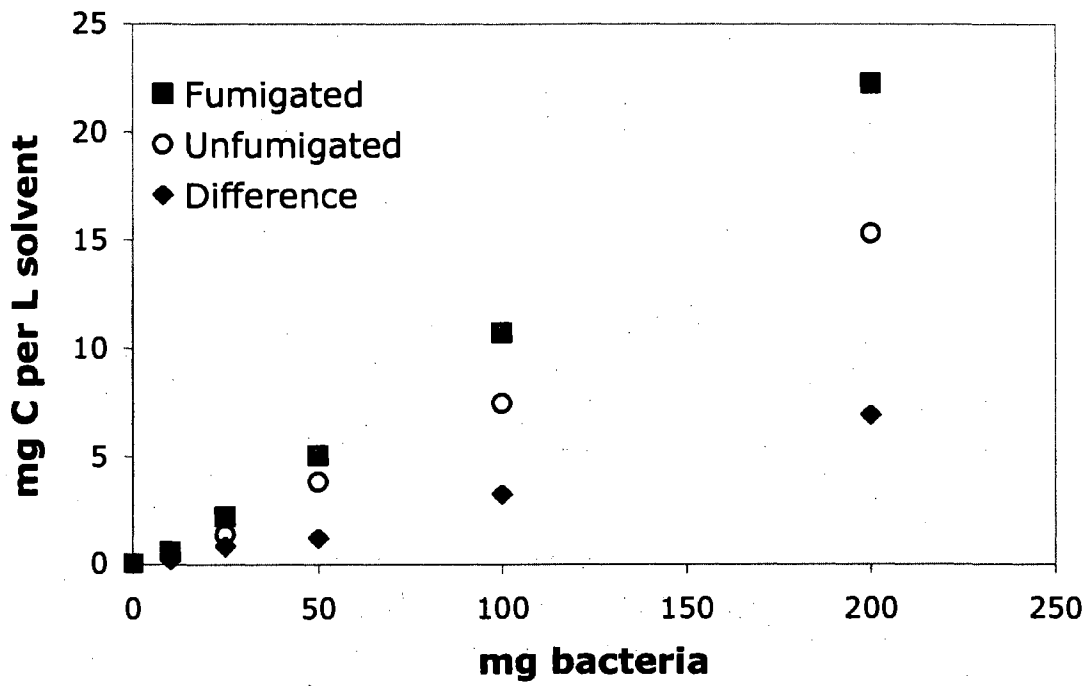


Figure 3.1: Experimental results from the bacteria-only system, plotted in terms of the concentration of extracted TOC as a function of the initial mass of bacteria present in the sample.

For the non-bacterial soil components that we tested, the differences between the organic C concentrations that were extracted from the fumigated samples and the un-fumigated controls should be zero for the fumigation-extraction procedure to be valid. That is, because those single-component systems do not contain any bacterial cells, the fumigation should not lyse any cells and therefore should not introduce additional organic C to the  $K_2SO_4$  wash solution. The humic acid (Figure 3.2) and the silica sand (Figure 3.3) systems show this relationship. In the case of humic acid, we expect the TOC concentration in fumigated and un-fumigated extraction solutions to increase with the amount of humic acid because humic acid is largely composed of organic C. The amount of TOC in the fumigated and un-fumigated extraction solutions from experiments with the same initial mass of humic acid is essentially the same, and is close to being equal to the entire mass of humic acid in each experiment, suggesting that almost all of the humic acid dissolves into the  $K_2SO_4$  wash solution in each extraction. The difference between the two concentrations is close to zero for all humic concentrations tested. This result suggests that the presence of humic acid in a soil does not affect the amount of C attributed to biomass using the fumigation-extraction method.

The results from the silica sand-only systems (Figure 3.3) demonstrate that virtually no TOC is extracted from each sample, and that this result is independent of initial sand mass and is independent of whether the sample was exposed to chloroform. As is the case for the humic acid system, the difference between extractable TOC concentrations in the solutions from fumigated and un-fumigated samples is essentially zero and does not increase with increasing sand mass, indicating that the chloroform fumigation procedure does not add to the extractable C pool. The two-component

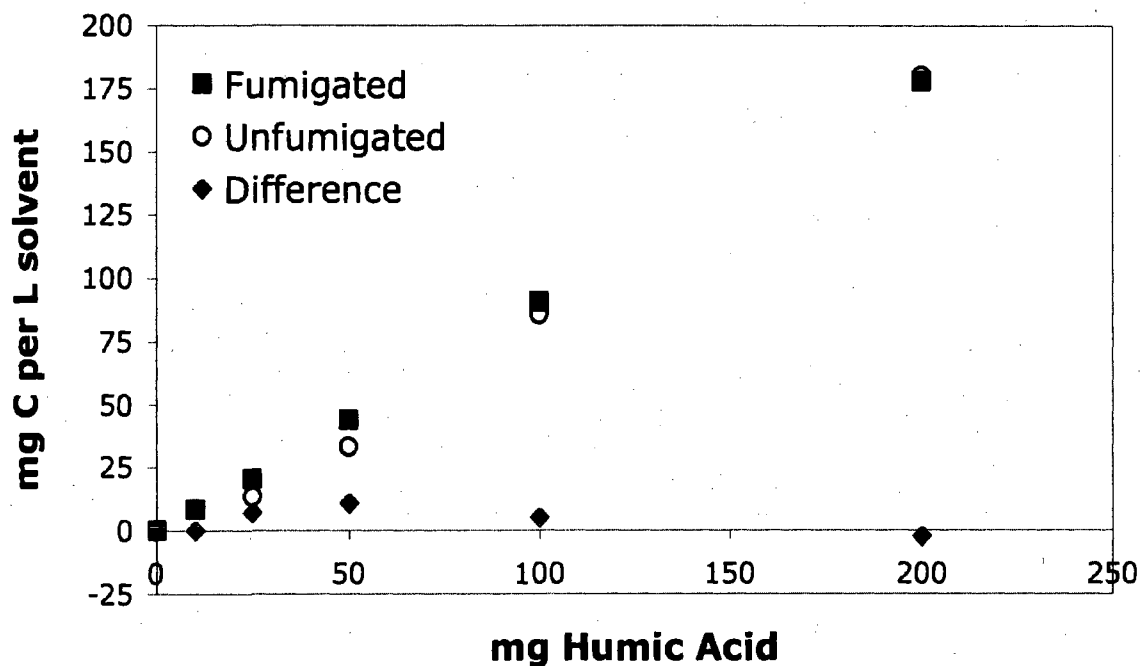


Figure 3.2: Fumigation results for humic acid-only samples, plotted in terms of the concentration of extracted TOC as a function of the initial mass of humic acid present in the sample.

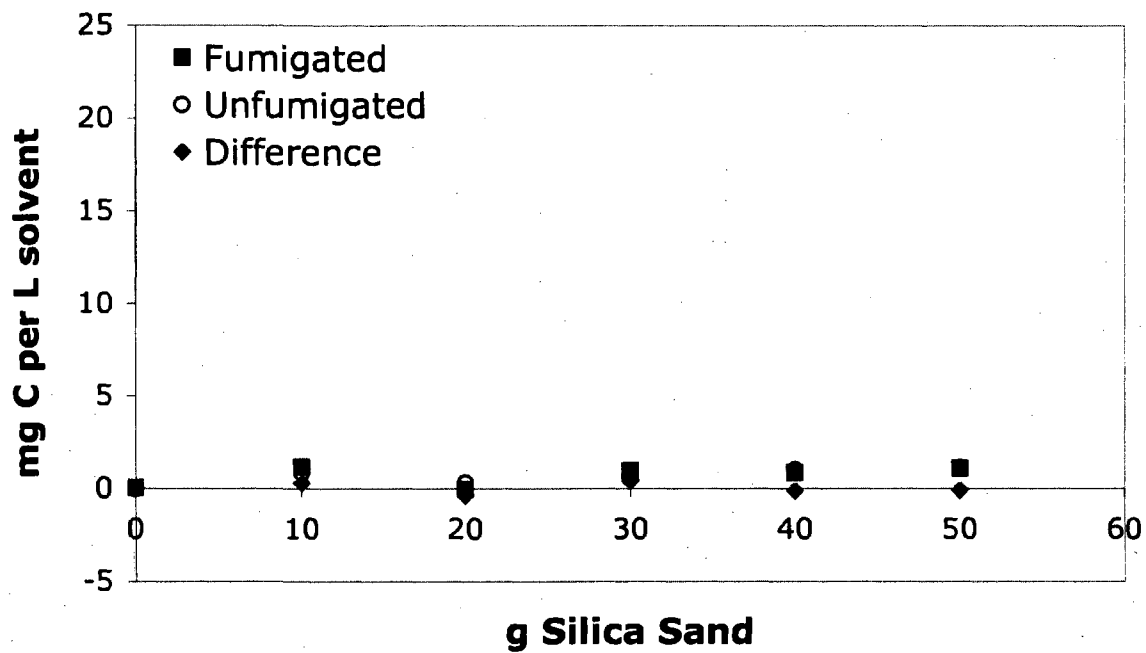


Figure 3.3: Fumigation results for silica sand-only samples, plotted in terms of the concentration of extracted TOC as a function of the initial mass of sand present in the sample.

experiment that involved a constant 50 g of the silica sand and varying amounts of bacteria demonstrates that the method may be difficult to apply to a sand-rich soil or aquifer material (Figure 3.4). The results from the sand and bacteria system indicate that the presence of the silica sand reduces the efficiency of the fumigation-extraction procedure in extracting biomass C from the bacteria that are present in the sample. The silica sand does not sorb chloroform and its presence does not totally block cell lysis due to fumigation. However, for a given mass of bacteria, the concentrations of extracted C from both the fumigated and unfumigated samples are lower when the silica sand is present than it is for the corresponding bacteria-only experiments. The dependence of the extraction efficiency on silica sand content of the sample suggests that the fumigation extraction technique would need to be calibrated for a particular biomass:sand ratio, making it impractical for the determination of biomass in a sample where the ratio of biomass to mass of sand is unknown. However, Figure 3.3 also shows that the values of the difference between fumigated and unfumigated samples in the bacteria-only and in the bacteria and sand experiments are similar for a given biomass,. This result may indicate that the method could be used successfully for determining biomass C in a sandy soil, but more tests would be required to determine if the difference values are independent of silica sand content.

The clays that we studied exhibit markedly different behavior than the other soil components. If chloroform does not sorb onto mineral surfaces, then the model clays, like the silica sand, would show little or no total organic C upon extraction, and no difference between fumigated samples and un-fumigated controls. Unlike the results for silica sand and humic acid, our experiments with wet and dry montmorillonite (Figures 3.5 and 3.6) and kaolinite (Figure 3.7) strongly suggest that chloroform vapor sorbs

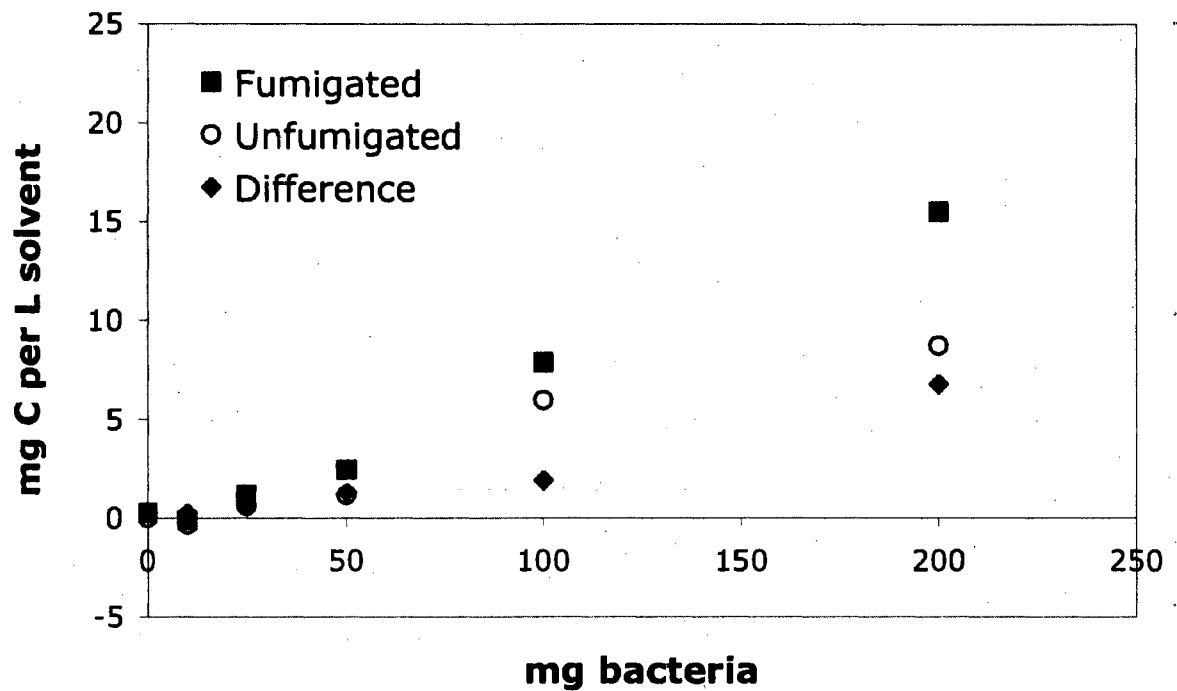


Figure 3.4: Results for fumigation experiments with a constant 50 g of silica sand and varying amounts of bacteria, plotted in terms of the concentration of extracted TOC as a function of the initial mass of bacteria present in the sample.

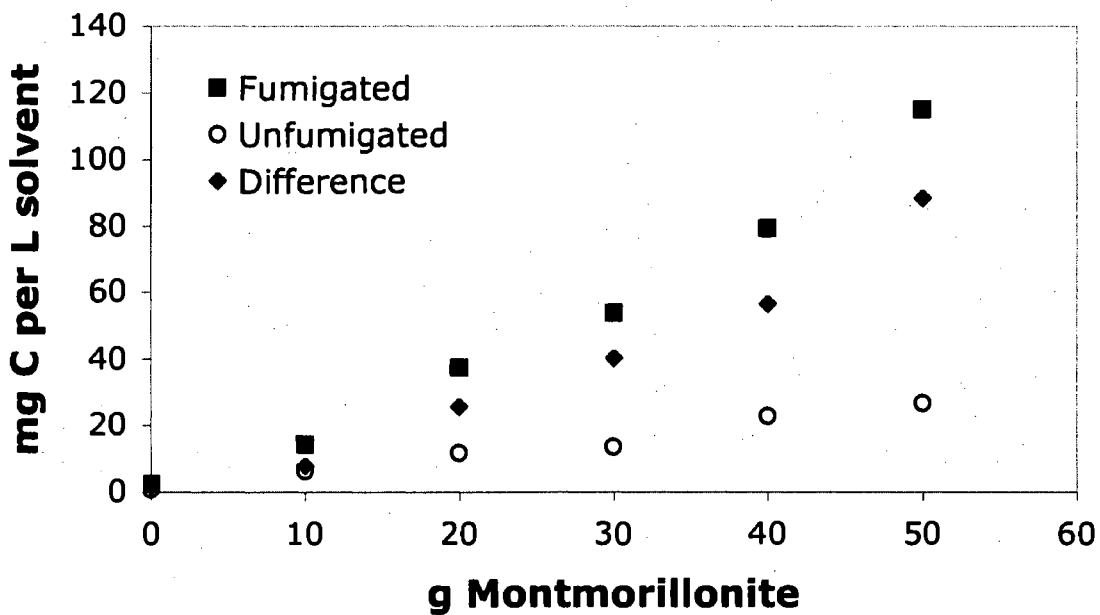


Figure 3.5: Fumigation results for montmorillonite-only samples (SWy-2), plotted in terms of the concentration of extracted TOC as a function of the initial mass of montmorillonite present in the sample.

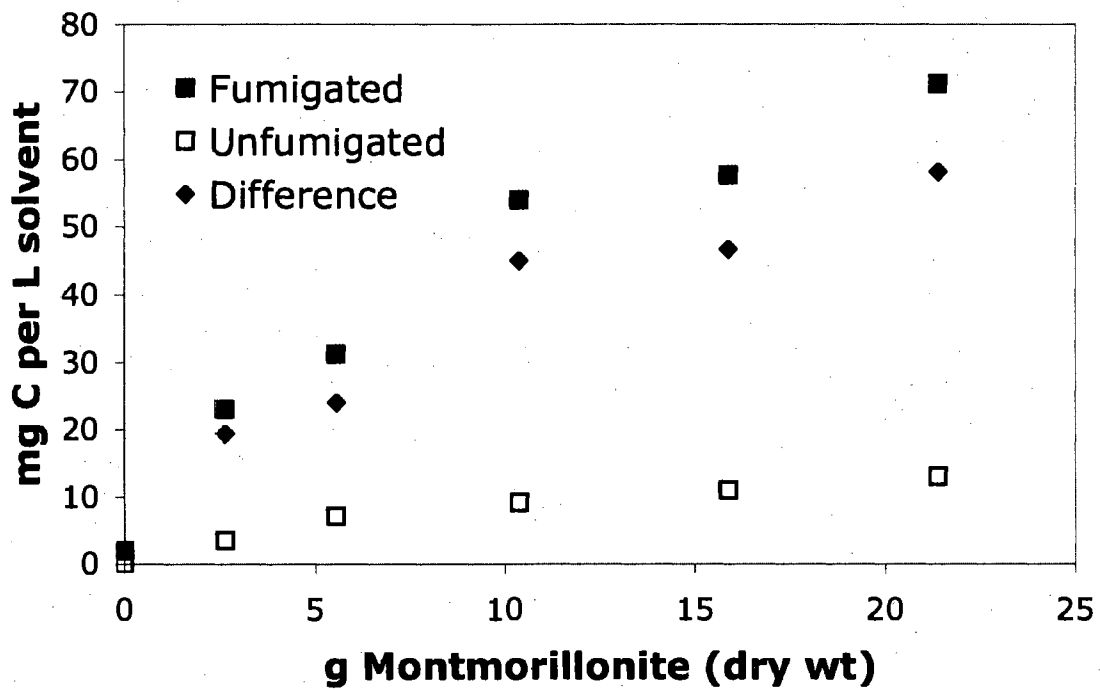


Figure 3.6: Fumigation results for wet montmorillonite samples (SWy-2), plotted in terms of the concentration of extracted TOC as a function of the initial dry mass of montmorillonite present in the sample.

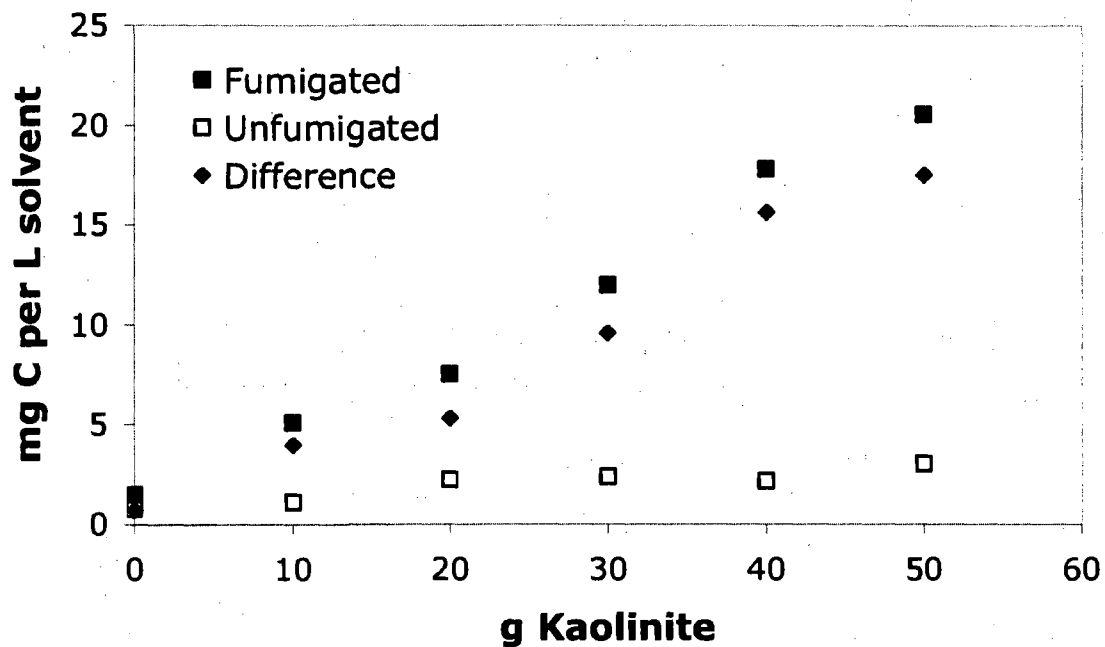


Figure 3.7: Fumigation results for kaolinite-only samples (KGa-1b), plotted in terms of the concentration of extracted TOC as a function of the initial mass of kaolinite present in the sample.

substantially to the clays during the 24 hours of fumigation. That is, the difference between the fumigated clay samples and the un-fumigated controls is not zero, but increases with the mass of clay that is fumigated. Different surface chemistries and a lower surface area for the silica sand relative to the clay samples likely explain why chloroform sorption onto silica sand was negligible in our experiments while we observed extensive chloroform sorption onto both types of clay. The wet montmorillonite experiments demonstrate that natural soil samples that contain hydrated clays also sorb chloroform during the fumigation-extraction method, adding to the organic C pool in the extraction solution. The wetted montmorillonite sorbs significantly less chloroform than the dry montmorillonite samples, but there is still a significant extent of chloroform sorption. The dry and wetted montmorillonite samples contain 5 and 83% water by mass, respectively. Natural soil samples typically contain clays in this hydration range, so our results indicate that these clays sorb significant concentrations of chloroform and that the fumigation-extraction approach can not be accurately used to determine biomass for these types of samples.

### **3.4 Conclusions**

The amount of chloroform sorbed in our experiments adds an average of 1540  $\mu\text{g}$  C per g montmorillonite and 350  $\mu\text{g}$  C per g kaolinite into the extraction solution. The fumigation-extraction method, applied to ten different naturally occurring soils by Vance et al. (1987), yielded between 60 and 1220  $\mu\text{g}$  biomass C per g soil. The concentration of sorbed chloroform in our clay experiments is comparable to this range, and our results indicate that sorbed chloroform could contribute substantially to the C pools of these soil samples. In soil samples that contain significant quantities of clay mineral surfaces,

exposure of the sample to chloroform leads to chloroform sorption onto the clays. The subsequent  $K_2SO_4$  wash desorbs the chloroform into the wash solution, and because chloroform contains organic C, its presence on the clays and in the wash solution contributes to the organic C concentration that is determined for the sample. Clearly, for soil samples with significant concentrations of clay minerals, the fumigation-extraction procedure yields results for biomass C that are artificially high due to the sorption artifacts.

Our results show that chloroform fumigation-extraction is not valid for soils containing substantial amounts of clay. It may be possible to use the fumigation-extraction method to find estimates of biomass C concentrations for materials that are poor in clay, such as a silica sand groundwater aquifer that also contains humic acid and/or bacteria. However, because most soils contain substantial clay mineral fractions, our results indicate that the fumigation-extraction method is not accurate for determination of the biomass C in soils.

## CHAPTER 4

### CADMIUM ADSORPTION TO MIXTURES OF SOIL COMPONENTS: TESTING THE COMPONENT ADDITIVITY APPROACH

#### 4.1 Introduction

The fate of heavy metals in soils and aquifers can be controlled by their adsorption to solid components (e.g., Meng and Letterman, 1996; Ledin et al., 1997, 1999; Covelo, 2007; Lund et al., 2008), aqueous complexation with dissolved organic ligands (e.g., Liu and Gonzales, 1999; Buerge-Weirich et al., 2003), and the formation of ternary surface complexes (e.g., Zachara et al., 1994, Ali and Dzombak, 1996; Fein, 2002). Although metal adsorption in multi-sorbent systems has been studied (e.g., Krantz-Rulcker et al., 1996; Ledin et al., 1997, 1999; Fingler et al., 2004, Covelo et al., 2007), the application of a quantitative surface complexation model (SCM) approach to predict metal distribution among mixtures of geosorbents is complex and difficult (Davis et al., 1998). However, the SCM approach has distinct advantages to empirical models in that the models can be extrapolated to systems of different ionic strength, pH, and component composition (Bethke and Brady, 2000; Koretsky, 2000).

Two approaches can be used when applying SCMs to describe metal distribution in multi-sorbent systems: the component additivity (CA) approach and the general composite (GC) approach. The CA approach predicts the extent of adsorption in mixed systems based on the adsorption affinities of each solute-sorbent combination measured in isolated binary experiments, and the relative concentrations of sorption sites of each sorbent. Success of the CA approach requires that sorbents do not interact with each other, that all solutes in the system have access to all surfaces, and that the only surface complexes that form are those that form in single sorbent, single component systems as well. Previous applications of the CA approach have met with varying degrees of success. For example, Davis et al. (1998) attempted to use a SCM to predict Zn(II) adsorption onto a natural, well-characterized sedimentary mineral assemblage. The CA approach under-predicted Zn(II) uptake, likely due to difficulties in determining absolute site concentrations for each site type within the complex sediment studied. Davis et al. (1998) also applied the generalized composite (GC) approach, a semi-empirical method that assigns generic functional groups to the mineral mixture. The GC approach was more successful in modeling Zn adsorption behavior onto the sediment, but this approach is not predictive, and can only be applied to systems for which laboratory calibration exist. Kulczycki et al. (2005) found that the Pb and Cd adsorption onto two-component systems comprised of ferrihydrite and either *Bacillus subtilis* or *Escherichia coli* bacterial cells was less than what would be expected by summing the metal adsorption to each component determined in one-component experiments. The authors speculated that adhesion between the ferrihydrite and the bacteria masked some of the surface sites on these sorbents, decreasing the adsorption capacity of the mixture.

Several authors have successfully applied SCM models to mixtures of minerals or bacteria, in some cases with dissolved organic ligands present in the systems. For example, Pagnanelli et al. (2006) measured the adsorption of protons and Pb to quartz, muscovite, clinocllore, goethite, and hematite, individually, using a non-electrostatic SCM. They found that a component additivity SCM, using the acidity and equilibrium constants determined for each pure mineral phase, could successfully predict Pb distribution in mixtures of these solids. Fowle and Fein (1999) demonstrated that the CA approach can be successful in predicting metal adsorption to mixtures of *Bacillus licheniformis* and *Bacillus subtilis* bacterial cells. Additionally, Yee and Fein (2003) showed that Cd, Co, Sr, and Zn adsorption onto complex mixtures of 10 species of Gram-negative and Gram-positive bacteria can be predicted with the CA approach. Lund et al. (2008) used a component additivity approach, with a diffuse layer model (DLM) to account for electric field effects, to predict the adsorption of Cu onto mixtures of hydrous ferric oxide (HFO) and kaolinite. The goodness-of-fits of the models to the experimental data were dependent on the model fits to the HFO and kaolinite individually. For mixtures of HFO and kaolinite, the authors postulated that interactions between these solids did not significantly impact Pb adsorption.

Although some tests of the CA approach have been conducted, few have tested its ability to account for metal distributions in systems containing both bacteria and minerals. Applying the CA approach to mixtures of minerals and bacteria may be problematic because bacteria can adhere to mineral surfaces, blocking reactive sites on the bacteria and the mineral (Lower et al., 2001; Ams et al., 2004). In this study, we test the ability of the CA approach to predict metal adsorption behavior in systems that contain mixtures of common soil components: kaolinite, hydrous ferric oxide (HFO),

*Bacillus subtilis* bacterial cells, and acetate as a representative simple dissolved organic acid. We use literature values to describe the proton reactivity and site concentrations for each sorbent, and we calibrate the model by measuring Cd adsorption onto each sorbent separately, using the results to calculate stability constants for the Cd-surface complexes. Our objective in this study is not to determine stability constants that can describe Cd adsorption over a wide range of Cd and sorbent concentrations. Rather, the emphasis is on testing if the CA approach can account for sorbent competition for Cd at a few specific experimental conditions. For this reason, we use the Cd-sorbent stability constants that we calculate for a given Cd:sorbent concentration ratio in single-sorbent systems in order to construct CA models that predict the distribution of Cd in multi-sorbent systems that have the same Cd:total sorbent concentration ratio. We vary the ratios of the sorbents, keeping the total sorbent concentrations constant, and we test systems that both include and exclude the effects of acetate complexation. We compare the CA predictions to the observed extents of adsorption for these systems to test the validity of the CA approach and to determine its strengths and limitations.

## **4.2 Methods**

### *4.2.1 Preparation of bacterial cells*

*Bacillus subtilis*, a Gram-positive soil bacterium, was selected as the biosorbent. The cell wall of this species is well-characterized (e.g., Beveridge, 1989) and the acidity constants and site concentrations of surface functional groups are well-constrained (Fein et al., 1997; 2005). The bacteria were grown and harvested in a manner similar to that described by Borrok et al. (2004). The bacteria were initially grown on agar slants made of 0.5% yeast extract and trypticase soy agar. Cells from the slant were transferred to a

3 ml test tube containing trypticase soy broth (TSB) and 0.5% yeast extract, and allowed to grow for 24 hours at 32°C. After the growth period, bacteria were transferred to 1 l solutions of the same composition, and allowed to grow for another 24 hours at 32°C. Bacteria were harvested in the stationary phase by centrifuging the broth at 9,000 g for 10 minutes to pellet the bacteria. After decanting the broth, the bacteria were washed four times in a 0.1 M NaClO<sub>4</sub> solutions. Between each wash, the bacteria were centrifuged at 8,100 g for 5 minutes to pellet the bacteria, the supernatant was decanted, and the cells were suspended in a fresh 0.1 M NaClO<sub>4</sub> electrolyte. After the washing cycles, the bacteria were transferred to a weighed centrifuge tube after the final wash, and centrifuged one time for 4 min and two times for 30 min at 8100 g, decanting the remaining supernatant each time. The resulting wet weight of the *B. subtilis* bacterial pellet is approximately 5 times the dry weight (Borrok et al., 2004). The method of preparation described here removes excess growth media and adsorbed cations from the bacterial surface, and renders the bacteria alive, but metabolically inactive (Wightman and Fein, 2005).

#### *4.2.2 Preparation of mineral powders*

High-defect kaolinite, KGa-2, from the Source Clay Repository, was used as the clay sorbent in our systems. Following a procedure similar to that used by Schroth and Sposito (1997), the kaolinite was washed repeatedly in a 1 M NaClO<sub>4</sub> solution that was previously adjusted to pH 3.0 with concentrated HCl. After each wash, the supernatant pH was measured, the clay suspension was centrifuged at 8100 g for 5 minutes to pellet the clay, and the supernatant was discarded. This process was repeated until the supernatant pH stabilized at 3.0. The clay was then washed in non-acidified solutions of

NaClO<sub>4</sub>, gradually decreasing in ionic strength from 1 M to 0.1 M. Three final washes in 0.1 M NaClO<sub>4</sub>, the electrolyte and ionic strength of the adsorption experiments, were conducted, and the pH stabilized at 4.5. The clay was then dried at 25°C, ground to a fine powder, and stored in a sealed centrifuge tube.

HFO was produced by titrating a 1.0 l solution of 0.05 M Fe(NO<sub>3</sub>)<sub>3</sub>•9H<sub>2</sub>O with small volumes of concentrated NaOH to increase the solution pH to 6.0. The solution was stirred for 24 h to allow the HFO to precipitate fully, after which the solution was decanted and the HFO powder was washed three times with 18 MΩ ultrapure water. The powder was dried and stored in a sealed polycarbonate test tube.

#### 4.2.3 Cd adsorption experiments

Batch Cd adsorption experiments were performed at initial Cd concentrations of  $8.9 \times 10^{-5}$  M and  $8.9 \times 10^{-6}$  M, referred to hereafter as '10 ppm' and '1 ppm' experiments for simplicity. To determine the stability constants for each important Cd-surface complex, we measured the adsorption of Cd onto each sorbent separately as a function of pH. 1 g l<sup>-1</sup> of kaolinite, *B. subtilis*, or HFO was suspended in a 0.1 M NaClO<sub>4</sub> solution. A small volume of a 1000 mg l<sup>-1</sup> Cd stock solution was added to each bacterial suspension, with the amount determined gravimetrically, to achieve the desired Cd concentration. The Cd stock solution was prepared from a Cd(ClO<sub>4</sub>)<sub>2</sub> salt. While stirring, the bulk suspension then was divided into 8 ml aliquots in polycarbonate test tubes, and small volumes of concentrated HNO<sub>3</sub> or NaOH were used to adjust the pH of each experiment so that a set covered a pH range between approximately 2 and 8. This pH range was selected to avoid the precipitation of Cd-hydroxides that occurs at the experimental Cd concentrations under higher pH conditions. The test tubes were then placed on a rotary shaker for 2 h, after which the final pH of each solution was

measured. The experimental systems were then centrifuged at 8,100 g for 10 min to pellet the solid sorbent, and the supernatant was decanted and filtered through 0.45  $\mu\text{m}$  Nylon membranes. The resulting filtered supernatants were acidified with 15  $\mu\text{l}$  of 15.8 N  $\text{HNO}_3$ .

All filtered experimental supernatants were analyzed for Cd concentrations on the same day that they were collected, using inductively coupled plasma – optical emission spectroscopy (ICP-OES). The amount of Cd adsorbed in each experimental system was determined by difference between the initial known Cd concentration in each experiment and the measured Cd concentration remaining in solution after equilibration with each sorbent. Aqueous Cd standards for ICP-OES calibration were prepared gravimetrically from a 1000  $\text{mg l}^{-1}$  Cd stock solution made from a  $\text{Cd}(\text{NO}_3)_2$  salt, diluted to desired concentrations using the same 0.1 M  $\text{NaClO}_4$  matrix as was used in the experimental systems. The Cd signal strength reported by the ICP-OES did not vary significantly with solution ionic strength, and analytical uncertainty as determined by repeat analysis of standards was  $\pm 3\%$ .

Parent suspensions, consisting of 1  $\text{g l}^{-1}$  of each sorbent in 0.1 M  $\text{NaClO}_4$ , were mixed to generate systems containing two or three sorbents. In this way, the total sorbent concentration in one, two, and three component systems was a constant 1  $\text{g l}^{-1}$ , while the ratio of one sorbent to another could be varied. After mixing, a small aliquot of the Cd stock solution described above was added to the mixture. The solutions were divided into polycarbonate test tubes and the pH adjusted with small volumes of concentrated  $\text{NaOH}$  or  $\text{HNO}_3$ . The test tubes were then placed on a rotary shaker for 2 h, after which the equilibrium pH was measured. Centrifugation, filtration, and

acidification sampling procedures were the same as those described above for the one-component systems.

In the experiments that involved acetate,  $1 \text{ g l}^{-1}$  of sorbent was initially suspended in a  $0.1 \text{ M NaClO}_4$  solution that contained  $0.3 \text{ M}$  acetate as sodium acetate. The suspension was then spiked with Cd to the desired concentration, and the experiments were conducted using the same procedure as is described above. Experiments in the presence of dissolved acetate were conducted with one-sorbent kaolinite, *B. subtilis*, or HFO systems, and in the presence of all three sorbents simultaneously.

## 4.3 Results and Discussion

### 4.3.1 Cd adsorption onto individual sorbents

The extents of Cd adsorption onto  $1 \text{ g l}^{-1}$  HFO,  $1 \text{ g l}^{-1}$  *Bacillus subtilis* cells, and  $1 \text{ g l}^{-1}$  kaolinite are depicted as a function of pH for the 10 ppm (Figure 4.1A) and 1 ppm Cd (Figure 4.1B) experiments. For each of the sorbents, Cd adsorption generally increases with increasing pH from 2 to 8. At both Cd concentrations, HFO adsorbs less than 20% of the total Cd in the systems below pH 5, and the extent of adsorption increases most significantly between pH 6 and 7 to nearly 100% in the 1 ppm Cd experiments and to nearly 80% in the 10 ppm Cd experiments. *Bacillus subtilis* cells exhibit a more shallow pH adsorption edge than does the HFO. The cells adsorb Cd to a similar extent to that of HFO below pH 6, but at higher pH, the extent of adsorption does not increase as much for the bacterial systems as it does for HFO, with the maximum extent of adsorption being 75% at pH 7.9 for the 1 ppm Cd experiments, and 40% at pH 7.7 for the 10 ppm Cd experiments. The kaolinite clay adsorbs Cd more weakly on a per

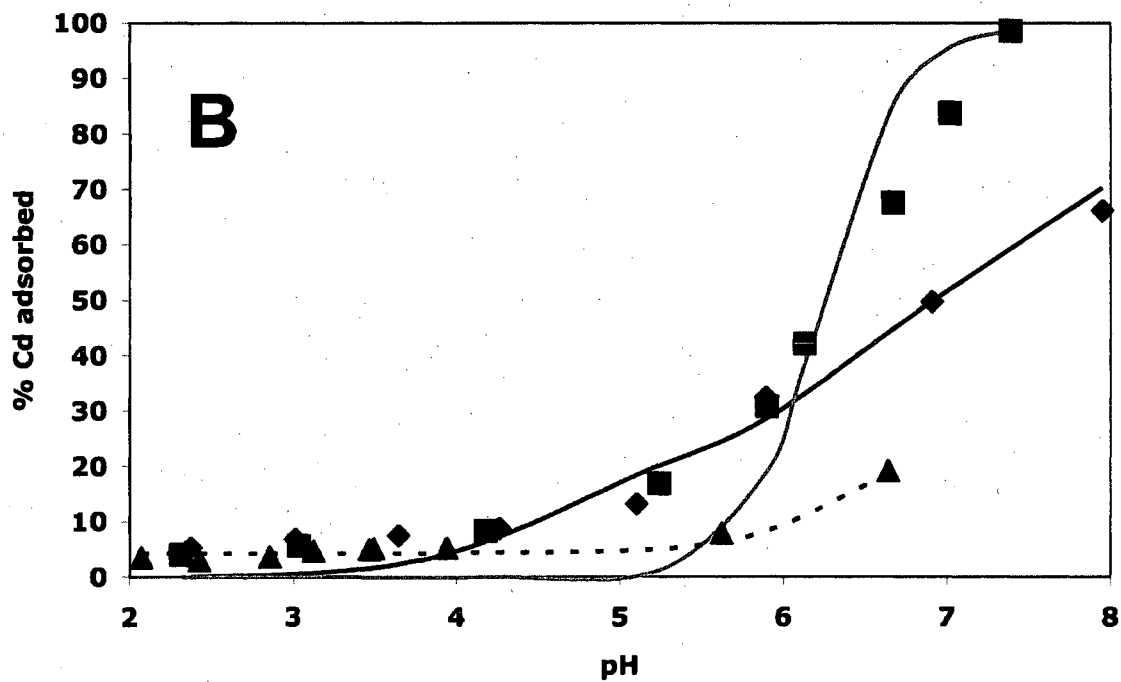
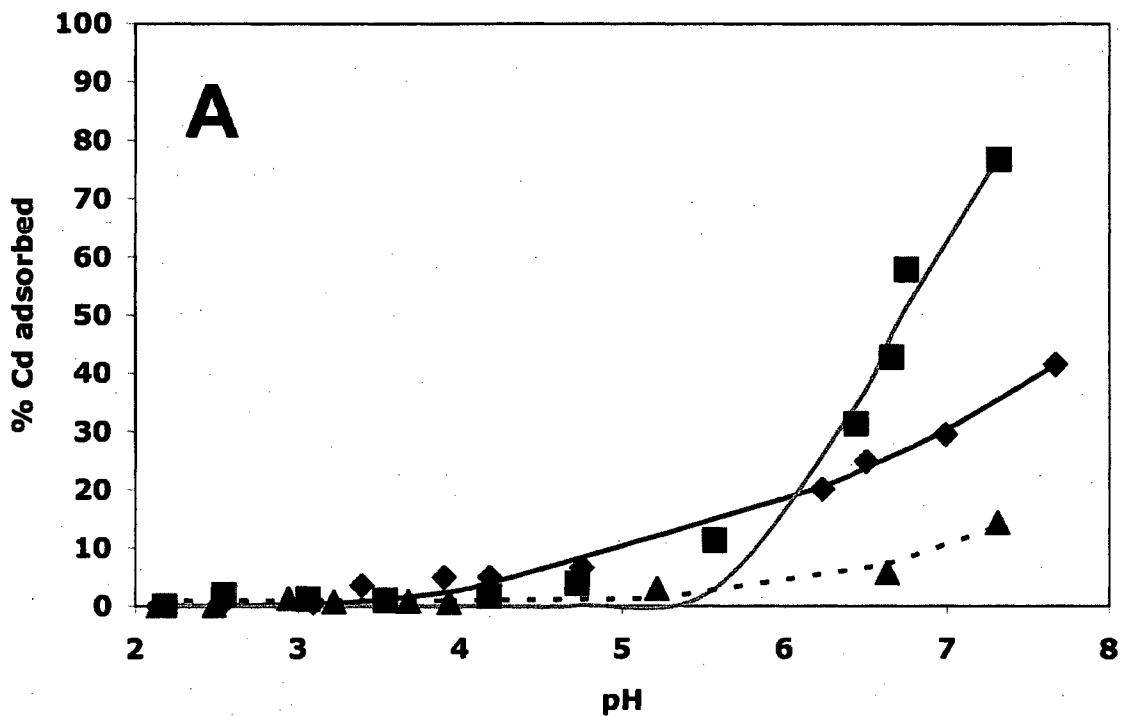


Figure 4.1: Adsorption of (A)  $8.9 \times 10^{-5}$  M Cd(II) and (B)  $8.9 \times 10^{-6}$  M Cd(II) to  $1 \text{ g l}^{-1}$  HFO (■),  $1 \text{ g l}^{-1}$  *B. subtilis* cells (◆), and  $1 \text{ g l}^{-1}$  kaolinite. Curves represent best-fit models to HFO (grey line), *B. subtilis* (solid line), and kaolinite (dashed line) Cd adsorption data.

gram basis than the HFO or the *B. subtilis* cells, never exceeding 20% of the total Cd concentration in the experiments.

#### 4.3.2 Modeling approach

We employ a non-electrostatic model (NEM) surface complexation approach to model the Cd adsorption behavior to *Bacillus subtilis* cells and to kaolinite, and we use a diffuse double layer model (DLM) to describe Cd adsorption to the HFO surface. Fein et al. (2005) performed potentiometric titrations of *Bacillus subtilis* cells and demonstrated that both electrostatic and non-electrostatic models can fit potentiometric titration data for bacteria equally well, but that surface electric field effects are small for bacteria. For our modeling, we employ the Fein et al. (2005) four-site NEM to describe the surface protonation and site concentrations on the bacterial cell wall. The NEM approach may be preferable for complex geologic applications because it requires fewer fitting parameters than do electrostatic models of surface electric field effects. Schroth and Sposito (1997, 1998) conducted potentiometric titrations and metal adsorption experiments on the KGa-2 kaolinite clay used here, and employed two amphoteric, proton-active surface sites and a permanent, pH independent structural charge site to describe protonation and metal adsorption onto the clay surface. The permanent structural charge sites account for the adsorption effects of isomorphic substitutions in the mineral lattice; the amphoteric sites likely represent surface silica and alumina functional groups. The surface reactivity of HFO is described by the DLM of Dzombak and Morel (1990) that employs strong and weak amphoteric surface sites to explain surface protonation and metal adsorption at  $\equiv\text{FeOH}$  sites. The protonation and cadmium adsorption reactions, and related stability constants for each sorbent are listed in Table 4.1.

TABLE 4.1

PROTON AND CD REACTIONS AT *BACILLUS SUBTILIS* CELL WALLS,  
KAOLINITE, AND HFO

<b><i>Bacillus subtilis</i> bacterial cells<sup>1</sup></b>		
Reaction	[Site] <sup>a</sup>	pK <sub>a</sub> <sup>b</sup>
$R-A_1(H)^o \leftrightarrow H^+ + R-A_1^-$	75	3.3
$R-A_2(H)^o \leftrightarrow H^+ + R-A_2^-$	96	4.7
$R-A_3(H)^o \leftrightarrow H^+ + R-A_3^-$	31	6.8
$R-A_4(H)^o \leftrightarrow H^+ + R-A_4^-$	75	8.9
	log K <sub>Cd, 1 ppm</sub>	log K <sub>Cd, 10 ppm</sub>
$Cd^{2+} + R-A_2^- \leftrightarrow R-A_2(Cd)^+$	3.4	3.3
$Cd^{2+} + R-A_3^- \leftrightarrow R-A_3(Cd)^+$	4.7	4.3
$Cd^{2+} + R-A_4^- \leftrightarrow R-A_4(Cd)^+$	4.8	4.9
<b>Kaolinite KGa-2</b>		
Reaction	[Site] <sup>a</sup>	log K <sup>c</sup>
$XOH + H^+ \leftrightarrow XOH_2^+$	35.9	3.5
$XOH \leftrightarrow XO^- + H^+$		-7.2
$YO^-$	13.6	
	log K <sub>Cd, 1 ppm</sub>	log K <sub>Cd, 10 ppm</sub>
$XOH + Cd^{2+} \leftrightarrow XO-Cd^+ + H^+$	-2.8	-2.4
$YO^- + Cd^{2+} \leftrightarrow YO-Cd^+$	3.9	3.9
<b>HFO</b>		
Reaction	[Site] <sup>a</sup>	log K <sup>d</sup>
$\equiv Fe^s OH^0 + H^+ \leftrightarrow \equiv FeOH_2^+$	56	7.29
$\equiv Fe^s OH^0 \leftrightarrow \equiv FeO^- + H^+$		-8.93
$\equiv Fe^w OH^0 + H^+ \leftrightarrow \equiv FeOH_2^+$	2247	7.29
$\equiv Fe^w OH^0 \leftrightarrow \equiv FeO^- + H^+$		-8.93
	log K <sub>Cd, 1 ppm</sub>	log K <sub>Cd, 10 ppm</sub>
$\equiv Fe^s OH^0 + Cd^{2+} \leftrightarrow \equiv FeO-Cd^+ + H^+$	0.4	-0.3
$\equiv Fe^w OH^0 + Cd^{2+} \leftrightarrow \equiv FeO-Cd^+ + H^+$	N/A	-3.6

a. concentration of sites, in  $\mu\text{mol g}^{-1}$

b. values from Fein et al. (2005)

c. values from Schroth and Sposito (1998)

d. values from Dzombak and Morel (1990)

e. log K<sub>Cd</sub> values for each sorbent are calculated from best-fit models to one-component Cd adsorption data collected in this study

#### 4.3.2.1 Calculation of Cd-Bacillus subtilis stability constants

The basis of the Cd adsorption model is the non-electrostatic protonation model of Fein et al. (2005). In this model, deprotonation of cell wall organic acid functional groups is described by the generic reaction:



where  $A_i$  represents one of the four organic acid functional group types needed to account for the protonation behavior of the cell wall ( $i = 1 - 4$ ), and  $R$  represents the cell wall macromolecule to which the functional group  $A_i$  is attached. The mass action equation for the deprotonation reaction is:

$$K_a = \frac{[R - A_i^-] a_{H^+}}{[R - A_i(H)^0]}, \quad (2)$$

where  $K_a$  is the acidity constant for Reaction (1), the brackets represent molar concentrations of the bacterial surface species, and  $a_{H^+}$  is the activity of aqueous protons in the bulk solution. The four protonation constant ( $pK_a$ ) values used to describe proton binding onto the cell wall in the Fein et al. (2005) model are 3.3, 4.7, 6.8, and 8.9.

We describe Cd adsorption onto deprotonated functional groups on the bacterial surface according to:



The equilibrium constant ( $K_{i-Cd}$ ) for complexation reaction (3) involving Site  $i$  is defined by:

$$K_{i-Cd} = \frac{[R - A_i(Cd)^+]}{[R - A_i^-] a_{Cd^{2+}}}, \quad (4)$$

where  $[R-A_i^-]$  represents the concentration of deprotonated cell wall functional group  $A_i$ ,  $[R-A_i(Cd)^+]$  represents the concentration of cell wall functional group  $A_i$  that is complexed with  $Cd^{2+}$ , and  $a_{Cd^{2+}}$  is the activity of  $Cd^{2+}$  in solution after equilibrium is attained.

The objective of the Cd-bacteria experiments is to constrain values of  $K_{i-Cd}$  that can be used to model Cd-bacterial adsorption in the more complex systems. In systems with low metal:sorbent concentration ratios, Cd binding onto only one cell wall functional group is required to describe Cd adsorption (e.g., Fein et al., 1997, Yee and Fein, 2001, Fein et al., 2001). However, systems having higher metal:sorbent ratios may involve more than one Cd-binding site to obtain the best-fit (Yee and Fein, 2001; Borrok and Fein, 2004).

We use the computer program FITEQL 2.0 (Westall 1982) to solve for the stability constants for all metal-sorbent surface complexes. This program accounts for the aqueous speciation of Cd, and all Cd-surface complexes. We include aqueous cation hydrolysis reactions, using the constants reported by Baes and Mesmer (1976). We test a range of models that invoke Cd binding onto between one and four bacterial sites. The relative goodness of fit of each model is determined by comparing the overall variance parameter,  $V(Y)$ , calculated by FITEQL. In both the 10 and 1 ppm bacteria-only systems (Figure 4.1), a model involving Cd adsorption onto bacterial Sites 2, 3, and 4 yields the lowest  $V(Y)$  value. For the 10 ppm Cd experiments (Figure 4.1A), the calculated stability constants  $\log K_{2-Cd}$ ,  $\log K_{3-Cd}$  and  $\log K_{4-Cd}$  are 3.3, 4.3, and 4.9, respectively. The log stability constant values calculated using the 1 ppm Cd experimental data (Figure 4.1B) are similar: 3.4, 4.7, and 4.8. Borrok et al. (2004) invoked Sites 2 and 3 to describe the adsorption of 10 ppm Cd onto  $1 \text{ g l}^{-1}$  of *B. subtilis*,

yielding similar calculated values for  $\log K_{2-Cd}$  and  $\log K_{3-Cd}$  of 3.4 and 4.6, respectively, despite the different Cd: bacterial site ratio of their experiment. We use the equilibrium constants calculated from our data to describe Cd adsorption to *B. subtilis* in systems containing two- and three-sorbent mixtures.

#### 4.3.2.2 Kaolinite proton and metal adsorption model

Schroth and Sposito (1997; 1998) described the surface charge properties of KGa-2, and developed a NEM to describe proton and metal adsorption to the surface of the kaolinite. This model accounts for proton activity with a single amphoteric surface site,  $XOH$ , according to the reactions:



The log equilibrium constant values for reactions 5 and 6 are 3.5 and -7.2, respectively (Schroth and Sposito, 1998). In this approach, Cd adsorption is described by complexation both with the amphoteric site and an additional permanent negatively charged surface site,  $YO^-$ , according to:



We use values for the equilibrium constants for reactions (5) and (6) and for site concentrations from Schroth and Sposito (1998), and we use the measured Cd adsorption behavior of kaolinite as a function of pH to solve for the equilibrium constants for reactions (7) and (8). We calculate  $\log K_7$  and  $\log K_8$  values of -2.8 and 3.9 from the 10 ppm Cd adsorption data, and -2.4 and 3.9 from the 1 ppm Cd experimental data, respectively. The best-fit model for the 10 ppm data is depicted in Figure 4.1A, and that

for the 1 ppm data in Figure 4.1B. Our 10 ppm data sets can be adequately described by Cd adsorption at the *XOH* site only (Equation 7), where a low percentage of free Cd is adsorbed below pH 5. However, it is necessary to invoke the  $YO^-$  site to describe the significant adsorption observed below pH 5 in 1 ppm experiments. The best-fit, as quantified by the  $V(Y)$  parameter, is achieved when both *XOH* and  $YO^-$  sites are invoked for both the 10 ppm and 1 ppm data sets, so both models utilize these two sites.

Schroth and Sposito (1998) calculated  $\log K_7$  and  $\log K_8$  values of -1.45 and 3.65, respectively. Our equilibrium constant values, particularly that of  $K_7$ , are significantly different. Were we to use the  $\log K_7$  value given by Schroth and Sposito (1998) to model our 10 ppm and 1 ppm data, the models would predict significantly more Cd adsorption than we observe below pH 5, where the structural  $YO^-$  site dominates adsorption. For example, in the 10 ppm experiments we never observe more than 15% of the Cd adsorbed to the kaolinite surface at any pH. Using the Schroth and Sposito (1998) constants to model our data yields predictions of more than 30% adsorption between pH 5 and 7. Schroth and Sposito (1998) conducted their experiments with 10 g  $l^{-1}$  kaolinite and  $8.9 \times 10^{-7}$  M Cd (0.1 ppm), and observed a range of 30% to 90% Cd removal from solution across the pH range 2 to 8. Our systems contain 10 or 100 times the initial Cd concentration, and only 1 g  $l^{-1}$  kaolinite. Because their data describe a greater range of adsorption behavior, the equilibrium constants calculated by Schroth and Sposito (1998) are likely applicable to a wider range of conditions than ours. Differences in the calculated  $\log K_7$  value could be attributed to differences in equilibration time between our study and that of Schroth and Sposito (1998), or the large difference in Cd:kaolinite ratios. However, because the other adsorption measurements in our study are conducted under the same conditions as these, and the constants are

reasonably similar, we use our Cd-kaolinite stability constants calculated from 1 ppm and 10 ppm adsorption data (Table 4.1) in the multi-sorbent predictive models of the same Cd concentrations.

#### 4.3.2.3 HFO proton and metal adsorption model

Dzombak and Morel (1990) described the reactive sites on the surface of HFO using two types of amphoteric sites with the same acidity constants, but with different site concentrations. The strong site,  $\equiv Fe^sOH$ , represents a subset of low concentration sites with a high affinity to adsorb metal cations. The weak site,  $\equiv Fe^wOH$ , is a high concentration site with lower cation affinity, useful for describing cation adsorption behavior in systems with higher sorbent-sorbate ratios. Both sites react with protons according to:

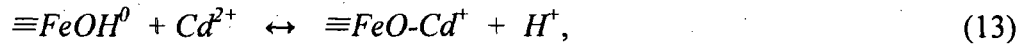


The mass action equations in the DLM include the Boltzmann factor,  $\exp\left(-\frac{\Delta z \psi F}{RT_K}\right)$ , to account for the electrostatic effects on surface free energies (Bethke, 2007), where  $\Delta z$  is the change in surface charge due to cation adsorption,  $\Psi$  is the surface potential,  $F$  is Faraday's constant,  $R$  is the ideal gas constant, and  $T_K$  is the temperature, in Kelvin. Incorporating this factor into the mass law equations for the reactions in (9) and (10) yields:

$$K_{11} \cdot e^{\left(-\frac{\psi F}{RT_K}\right)} = \frac{[\equiv FeOH_2^+]}{[\equiv FeOH^0] a_{H^+}} \quad (11)$$

$$K_{12} \cdot e^{\left(-\frac{\Psi_F}{RT_k}\right)} = \frac{[\equiv FeO^-] a_{H^+}}{[\equiv FeOH^0]} \quad (12)$$

Log  $K_{11}$  and log  $K_{12}$  values are given as 7.29 and -8.93, respectively (Dzombak and Morel, 1990). Adsorption of aqueous  $Cd^{2+}$  onto both the strong and weak HFO surface sites can be represented as:



and the equilibrium constant,  $K_{HFO-Cd}$  is described by:

$$K_{HFO-Cd} \cdot e^{\left(-\frac{\Psi_F}{RT_k}\right)} = \frac{[\equiv FeOH^0] a_{Cd^{2+}}}{[\equiv FeO-Cd^+] a_{H^+}} \quad (14)$$

At low sorbate:sorbent concentrations, where there are abundant surface sites available, metal adsorption can be described by adsorption to the strong site,  $\equiv Fe^sOH$ , only. By modeling 24 sets of pH-dependent Cd adsorption data, Dzombak and Morel (1990) calculated an average stability constant, log  $K_{HFO-Cd}$ , of 0.47 for the strong site. Using one set of pH dependent adsorption data in which the sorbate:sorbent ratio is high, they calculated a log  $K_{HFO-Cd}$  value of -2.90 for the weak site. In this same data set, Dzombak and Morel (1990) calculated the log  $K_{HFO-Cd}$  of the strong adsorption site to be -0.51, significantly below the value of 0.5 calculated from the low sorbate:sorbent ratio data. Our 10 ppm Cd experiments have a high sorbate:sorbent ratio, and it is necessary to invoke binding onto both the strong and the weak sites to fit our data. For these data, we calculate values for the strong and weak sites to be -0.3 and -3.6, respectively. To describe adsorption of 1 ppm Cd to 1 g l<sup>-1</sup> HFO, a lower sorbate:sorbent ratio, it is only necessary to invoke the strong site, consistent with similar datasets in Dzombak and

Morel (1990). The log  $K_{HFO-Cd}$  value that we calculate for the strong site from the 1 ppm Cd data is 0.4. The best-fit to the 10 ppm Cd experiments closely match the observed adsorption behavior (Figure 4.1A). However, the best-fit model of the 1 ppm Cd data exhibits a steeper adsorption edge than is observed in the experimental data, so that the model fails to account for significant adsorption observed below pH 5.5. Several best-fit models to sets of Cd adsorption data in Dzombak and Morel (1990) exhibit a similar trend. To account for Cd adsorption at lower pH, a model would need to incorporate a site that deprotonates at lower pH.

#### 4.3.3 Cd adsorption to two-component mixtures

Figures 4.2, 4.3, and 4.4 compare the measured extents of Cd adsorption onto 2-component sorbent mixtures to the CA model predictions of the Cd adsorption behaviors. The graphs also depict the same model fits to the 1 component end-member systems that are shown in Figure 1 for reference. Models of the two-sorbent mixtures use the acidity and equilibrium constants calculated in the SCMs described in Section 4.3.2 and compiled in Table 4.1 to independently predict the extent of Cd adsorption in each two-sorbent system. Molal ratios of site concentrations for each mixture are listed in Table 4.2.

The Cd adsorption behaviors for mixtures of HFO and *B. subtilis* cells are depicted in Figure 4.2. Experiments containing 75% HFO and 25% *B. subtilis* (by mass) exhibit Cd adsorption behavior similar to that of the corresponding 100% HFO systems. In this system, *B. subtilis* cells contribute 54% of the potential Cd adsorption sites on a molal basis, and HFO the remaining 46%. Clearly, Cd preferably binds to the HFO surface relative to the sites on the *B. subtilis* cell walls. Mixtures of 25% HFO and 75%

TABLE 4.2

## MOLAL SITE CONCENTRATIONS OF SORBENTS IN TWO- AND THREE-COMPONENT MIXTURES

Mixture <sup>a</sup>	HFO <sup>b</sup>	<i>B. subtilis</i> <sup>b</sup>	Kaolinite <sup>b</sup>
75% HFO + 25% <i>B. subtilis</i>	42.2	50.5	
25% HFO + 75% <i>B. subtilis</i>	14.0	151.5	
75% HFO + 25% kaolinite	42.2		12.4
25% HFO + 75% kaolinite	14.0		37.1
75% <i>B. subtilis</i> + 25% kaolinite		151.5	12.4
25% <i>B. subtilis</i> + 75% kaolinite		50.5	37.1
80% HFO + 10% <i>B. subtilis</i> + 10% kaolinite	45.0	161.6	5.0
10% HFO + 80% <i>B. subtilis</i> + 10% kaolinite	5.6	20.2	5.0
10% HFO + 10% <i>B. subtilis</i> + 80% kaolinite	5.6	20.2	39.6
33% HFO + 33% <i>B. subtilis</i> + 33% kaolinite	18.7	67.3	16.5

a. All mixtures add to 1 g l<sup>-1</sup> sorbent.

b. Site concentrations given in μmol g<sup>-1</sup>.

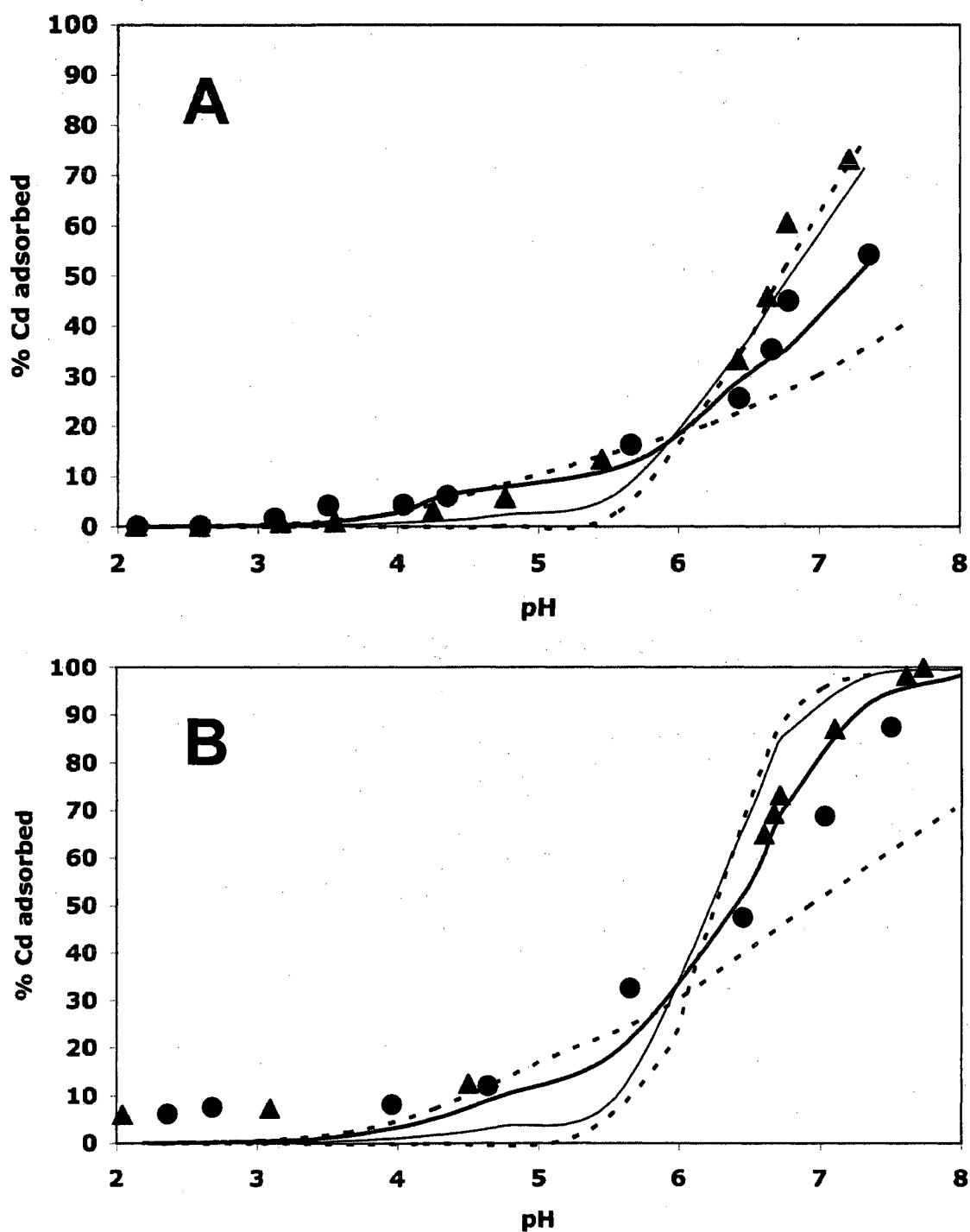


Figure 4.2: Adsorption of (A)  $8.9 \times 10^{-5}$  M Cd(II) and (B)  $8.9 \times 10^{-6}$  M Cd(II) to mixtures of HFO and *B. subtilis* cells. Dashed lines represent best-fit models to  $1 \text{ g l}^{-1}$  HFO and *B. subtilis* end members from Figure 1. Darkened symbols and lines represent adsorption data and predicted adsorption behavior for two-sorbent mixtures, including  $0.75 \text{ g l}^{-1}$  HFO +  $0.25 \text{ g l}^{-1}$  *B. subtilis* cells ( $\blacktriangle$ , thin line), and  $0.25 \text{ g l}^{-1}$  HFO +  $0.75 \text{ g l}^{-1}$  *B. subtilis* cells ( $\bullet$ , thick line).

*B. subtilis* adsorb significantly less Cd than the 100% HFO experiments, but more than was observed in systems containing 100% *B. subtilis* cells. HFO has significantly lower site concentrations compared to *B. subtilis*, contributing less than 46% of the surface sites when it is 75% of the mass of the mixture, and approximately 8% of the sites when it is 25% of the mixture by mass. The predictive models (solid lines) describe the 10 ppm data reasonably well, but exhibit similar misfits to the 1 ppm data to those observed between the model and the 100% HFO data. Lund et al. (2008) observed that discrepancies in fitting metal adsorption to the pure phases caused discrepancies in the predicted fits of multi-component systems using the CA approach, and we observe the same phenomenon. Thus, the difference between the model predictions and experimental data in the two-component 1 ppm experiments is likely caused by the relatively poor fit of the one-component 1 ppm Cd + HFO model.

Figure 4.3 illustrates Cd adsorption behavior onto mixtures of *B. subtilis* and kaolinite. These data show Cd adsorption decreasing systematically with increasing kaolinite in the mixture; 100% *B. subtilis* adsorbs the greatest portion of free Cd, followed by the 75% *B. subtilis* + 25% kaolinite mixture, the 25% *B. subtilis* + 75% kaolinite mixture, and the 100% kaolinite adsorption experiments. In experiments containing 75% *B. subtilis* and 25% kaolinite by mass, the bacteria represent more than 92% of the surface sites on a molal basis, and in mixtures of 25% *B. subtilis* and 75% kaolinite by mass, *B. subtilis* contributes nearly 58% of the reactive sites. However, the majority of Cd adsorption below pH 4 is predicted to occur onto the permanent structural site,  $YO^-$ , of kaolinite. In both the 10 ppm and 1 ppm Cd experiments, the predictive models provide excellent fits to the measured extents of adsorption in the *B. subtilis*-kaolinite systems.

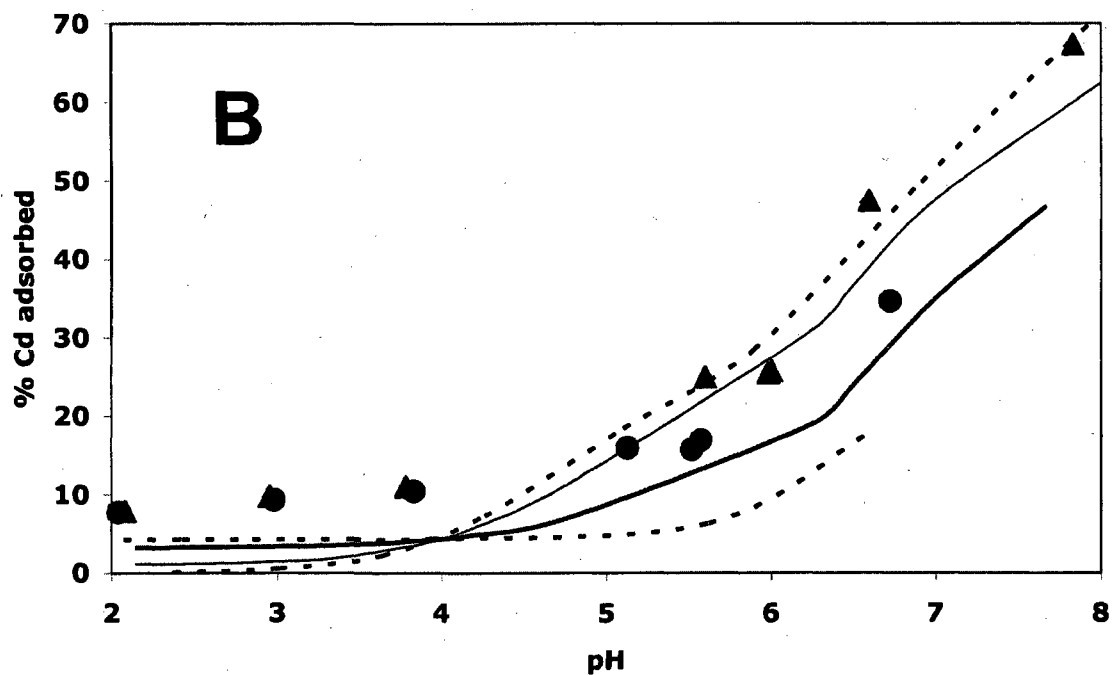
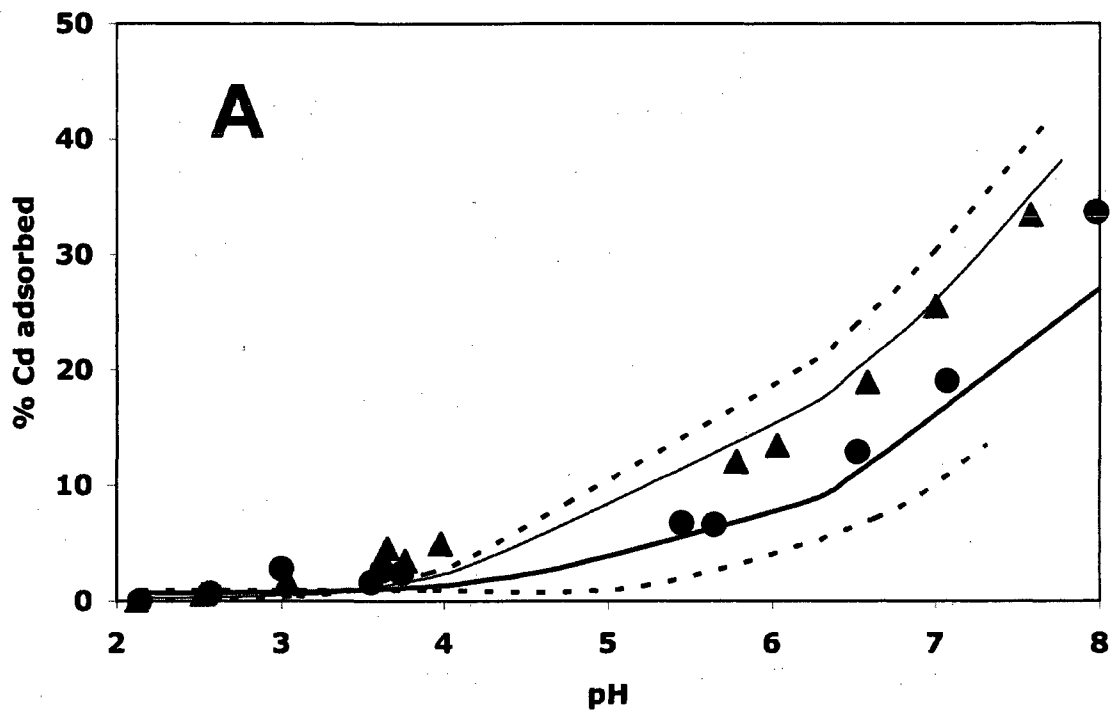


Figure 4.3: Adsorption of (A)  $8.9 \times 10^{-5}$  M Cd(II) and (B)  $8.9 \times 10^{-6}$  M Cd(II) to mixtures of kaolinite and *B. subtilis* cells. Dashed lines represent best-fit models to 1 g l<sup>-1</sup> kaolinite and *B. subtilis* end members from Figure 1. Darkened symbols and lines represent adsorption data and predicted adsorption for two-sorbent mixtures, including 0.75 g l<sup>-1</sup> *B. subtilis* cells + 0.25 g l<sup>-1</sup> kaolinite (▲, thin line), and 0.25 g l<sup>-1</sup> *B. subtilis* cells + 0.25 g l<sup>-1</sup> kaolinite (●, thick line).

Cd adsorption onto mixtures of HFO and kaolinite is depicted in Figure 4.4. A mixture of 75% HFO + 25% kaolinite adsorbs free Cd to a similar extent as the 100% HFO experiments, with only slightly less adsorption above pH 7. The 25% HFO + 75% kaolinite mixture adsorbs substantially more Cd than experiments conducted with 100% kaolinite, but less than those with 100% HFO. These results suggest that HFO dominates the adsorption behavior of Cd in experiments where it is 75% of the total sorbent mass, and strongly influences Cd adsorption even as a minor component of 25% of the sorbent mass. HFO has nearly identical site concentrations as kaolinite, contributing approximately 77% of the surface sites when it is 75% of the mixture, and 27% of the sites when it is 25% of the mixture. The HFO-like adsorption behavior of both mixtures attests to the higher affinity of HFO for adsorption of Cd compared to that of kaolinite and *B. subtilis*. Predictive models of the mixtures containing 10 ppm Cd fit the experimental data well, but the models deviate from the 1 ppm data significantly. This difference can be attributed again to the poor fit of the one-component 1 ppm Cd + HFO model.

Dissolved acetate,  $\text{CH}_3\text{COO}^-$ , is used to determine the effect of aqueous metal-organic complexation on the adsorption of Cd to one- and three-sorbent systems. We conduct these experiments with  $1 \text{ g l}^{-1}$  sorbent in the presence of 0.3 M acetate, as sodium acetate. To predict the effects of aqueous Cd-acetate complexation on the Cd adsorption behavior in one-component systems with acetate, we use the stability constants for the Cd-sorbent complexes that we calculated from our one-component Cd adsorption experiments, along with the acetate acidity constant and Cd-acetate stability constants for the 1:1, 1:2, 1:3, and 1:4 Cd:acetate complexes from the literature (Martell and Smith, 1977). Figure 4.5 compares the measured extents of Cd adsorption in the

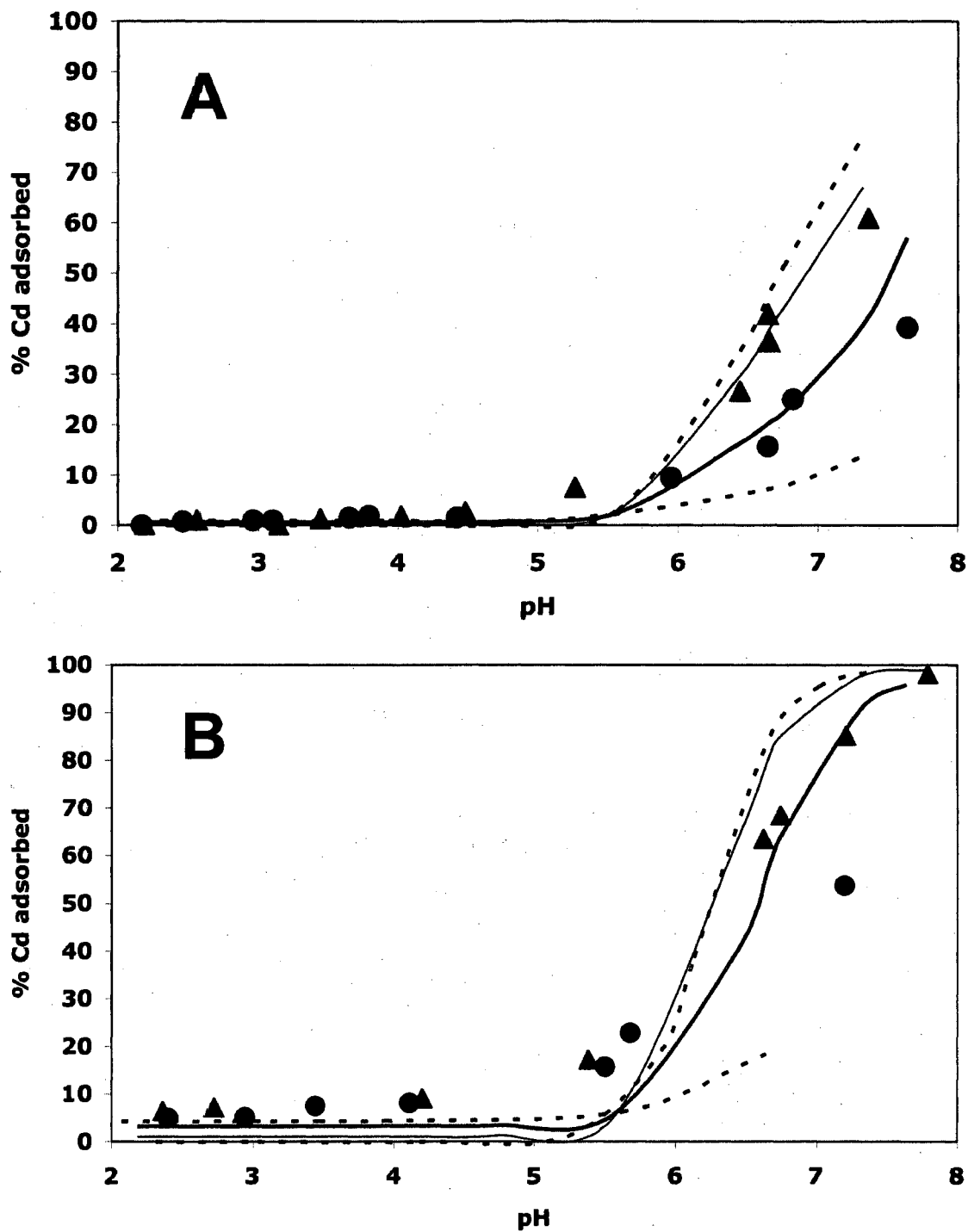
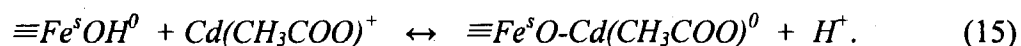


Figure 4.4: Adsorption of (A)  $8.9 \times 10^{-5}$  M Cd(II) and (B)  $8.9 \times 10^{-6}$  M Cd(II) to mixtures of HFO and kaolinite. Dashed lines represent best-fit models to  $1 \text{ g l}^{-1}$  HFO and kaolinite end members from Figure 1. Darkened symbols and lines represent adsorption data and predicted adsorption for two-sorbent mixtures, including  $0.75 \text{ g l}^{-1}$  HFO +  $0.25 \text{ g l}^{-1}$  kaolinite ( $\blacktriangle$ , thin line), and  $0.25 \text{ g l}^{-1}$  HFO +  $0.25 \text{ g l}^{-1}$  kaolinite ( $\bullet$ , thick line).

absence of acetate (solid squares) and in the presence of acetate (open circles). HFO experiments and models at 10 ppm and 1 ppm are depicted in Figures 4.5A and 4.5B, respectively. The predictive models that include Cd-acetate complexation (dashed lines) dramatically underestimate the extent of adsorption observed in the experiments at all pH values between 2 and 8. The misfit at low pH, between 2 and 5.5, is less severe than the misfit of the high pH data, and likely stems from the failure of the basic HFO model to account for Cd adsorption at low pH. Shen et al. (2001) described the adsorption of Pb to soil in an acetate-bearing system by proposing that the aqueous Pb-acetate complex,  $\text{Pb}(\text{CH}_3\text{COO})^+$ , adsorbs to surface sites as a ternary site-Pb-acetate complex. Similarly, in our systems the 1:1 Cd-acetate complex,  $\text{Cd}(\text{CH}_3\text{COO})^+$ , dominates the aqueous Cd speciation. To account for the observed adsorption behavior, we invoke ternary site-Cd-acetate complexation to account for the discrepancy between the predicted extents of adsorption and the higher extents that were observed, according to:



The equilibrium constant,  $K_{15}$ , for the surface-Cd-acetate ternary complex is calculated using the previously-determined Cd-surface constants, and solving for the best-fit ternary surface complex constant. The calculated  $\log K_{15}$  value from this approach is 0.9. The grey lines in Figures 4.5A and 4.5B represent these best-fit models. Adsorption of the Cd-acetate complex improves the fits substantially at high pH, but the models continue to underpredict Cd adsorption below pH 7. This is likely due to the relatively poor fit of the one-component HFO model, and potentially because there are other ternary interactions that must be considered to model the data accurately. Our models suggest that in systems containing HFO and an organic ligand, the CA approach

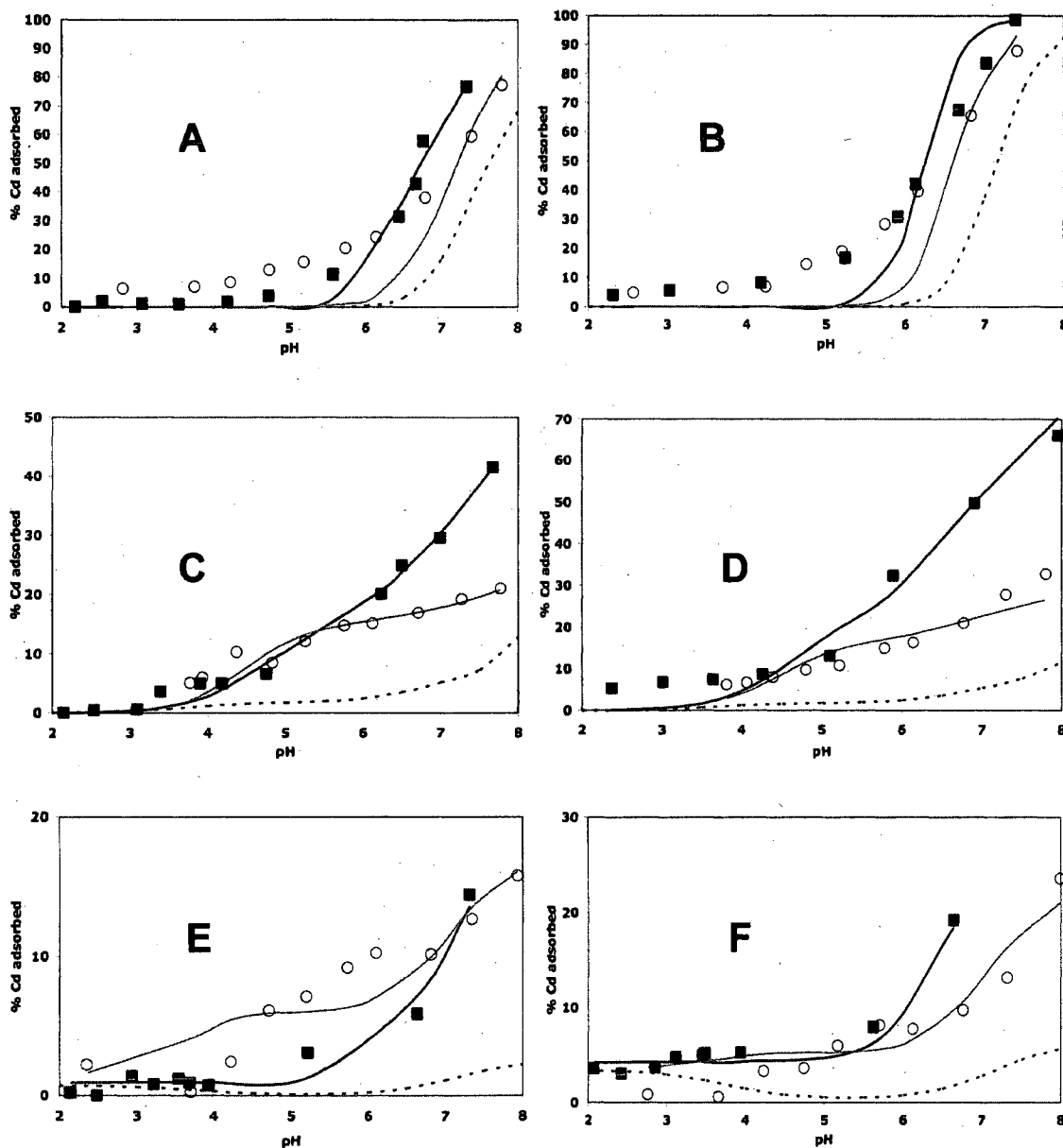


Figure 4.5: Adsorption of  $8.9 \times 10^{-5}$  M Cd to  $1 \text{ g l}^{-1}$  A) HFO, C) *B. subtilis*, and E) kaolinite, and  $8.9 \times 10^{-6}$  M Cd to B) HFO, D) *B. subtilis*, and F) kaolinite. Darkened symbols and lines represent adsorption data and predicted adsorption for mixtures without acetate. Open symbols are adsorption data in the presence of 0.3 M acetate. Dashed line indicates the predicted extent of adsorption in acetate experiments without the adsorption of a Cd-acetate complex, and grey line is the best-fit model including a Cd-acetate ternary surface complex.

may not be sufficient to describe Cd adsorption behavior unless ternary interactions between important aqueous complexes and the HFO surface are considered.

Figures 4.5C and 4.5D depict the adsorption of 10 ppm and 1 ppm Cd to *B. subtilis* cells, respectively. The model predictions of Cd adsorption in the presence of acetate (dashed lines) underestimate the actual extent of adsorption (open circles) across the entire pH range studied here. This result suggests that an aqueous Cd-acetate complex may be adsorbing to the bacterial surface. Models invoking a complexation reaction between the  $\text{Cd}(\text{CH}_3\text{COO})^+$  complex and either Site 2, 3, or 4 yield a better fit to the experimental data, but inclusion of this reaction at Site 2 only (Table 4.3) yields the best-fit (grey line). Models invoking  $\text{Cd}(\text{CH}_3\text{COO})^+$  adsorption at Sites 2 and 3, or Sites 2, 3, and 4 give fits that are equivalent to the Site 2-only model. We use the model invoking only Site 2 for its simplicity.

The adsorption of 10 ppm and 1 ppm Cd in the presence of kaolinite and acetate is displayed in Figures 4.5E and 4.5F, respectively. As with the HFO and *B. subtilis*, the predictive model that does not invoke a ternary complex under-predicts the extent of Cd adsorption across the entire pH range. Poor, but improved fits are obtained when the aqueous  $\text{Cd}(\text{CH}_3\text{COO})^+$  ligand is complexed with either the amphoteric ( $\text{XOH}$ ) or permanent structural ( $\text{YO}^-$ ) sites. The model invoking only the  $\text{XOH}$  site underestimates adsorption below pH 5, and one invoking only the  $\text{YO}^-$  site underestimates adsorption where pH is greater than 5. The best-fit (grey line) is obtained when  $\text{Cd}(\text{CH}_3\text{COO})^+$  adsorbs onto both sites simultaneously (Table 4.3). In the cases of the kaolinite and *B. subtilis* cells, the adsorption of the  $\text{Cd}(\text{CH}_3\text{COO})^+$  complex from solution is sufficient to describe the observed data. Additionally, the stability constants of ternary surface-Cd-acetate complexes calculated for an individual sorbent are similar whether modeling

TABLE 4.3

## TERNARY COMPLEXATION REACTIONS

	Log K values <sup>a</sup>	
	1ppm	10ppm
<b>HFO</b>		
$\equiv Fe^s OH^0 + Cd(CH_3COO)^+ \leftrightarrow \equiv Fe^s O-Cd-CH_3CO_2^0 + H^+$	0.9	0.8
$\equiv Fe^w OH^0 + Cd(CH_3COO)^+ \leftrightarrow \equiv Fe^w O-Cd-CH_3CO_2^0 + H^+$	N/A	-2.9
<b><i>B. subtilis</i> cells</b>		
$R-A_2^- + Cd(CH_3COO)^+ \leftrightarrow R-A_2-Cd-CH_3CO_2^0$	4.8	4.8
<b>Kaolinite</b>		
$XOH + Cd(CH_3COO)^+ \leftrightarrow XO-Cd-CH_3CO_2^0 + H^+$	-1.3	-1.3
$YO^- + Cd(CH_3COO)^+ \leftrightarrow YO-Cd-CH_3CO_2^0$	5.8	6.0

- a. Log K values for each reaction are calculated from best-fit models of 1 ppm and 10 ppm Cd adsorption data.

adsorption data from the 1 ppm or 10 ppm experiments (see Table 4.3). For instance, the log  $K$  values for  $\text{Cd}(\text{CH}_3\text{COO})^+$  complexation at Site 2 of the *B. subtilis* cells is calculated to be 4.8 from both the 1 ppm and 10 ppm data. This provides further evidence that the  $\text{Cd}(\text{CH}_3\text{COO})^+$  complex is adsorbing to each sorbent, that we are using the correct ternary complexation stoichiometries (Table 4.3), and that these reactions are capable of accounting for adsorption over a range of Cd concentrations.

#### 4.3.4 Cd adsorption to three-component mixtures

The adsorption behavior of 1 ppm Cd to three-component mixtures of HFO, *B. subtilis*, and kaolinite is illustrated in Figure 4.6. Four mixtures of the sorbents are investigated, one where each component comprises 33% of the  $1 \text{ g l}^{-1}$  sorbent present (Figure 4.6D), and three sets in which one of the sorbents is 80% of the total mass, and the remaining 2 sorbents represent 10% of the total mass, each. In the mixture where each component contributes 33% of the sorbent mass, the *B. subtilis* cells, HFO, and kaolinite contribute 66%, 18%, and 16% of the reactive sites, respectively. However, as in the two-component experiments containing HFO that are described in Section 3.3, the most Cd adsorption is observed in experiments that contain a greater fraction of HFO. The mixture of 80% HFO + 10% *B. subtilis* cells + 10% kaolinite (Figure 4.6A) adsorbs Cd to a nearly identical extent as the 100% HFO system (see Figure 4.1B). Mixtures containing only 10% HFO and 80% *B. subtilis* or kaolinite (Figures 4.6B, 4.6C, respectively) adsorb Cd to a lesser extent. The lowest extent of Cd adsorption is observed in the single component kaolinite systems (Figure 4.1). Thus, the Cd adsorption behavior in the ternary mixtures of these sorbents is directly related to the extent of adsorption observed in the single-sorbent systems. All 3-component predictive

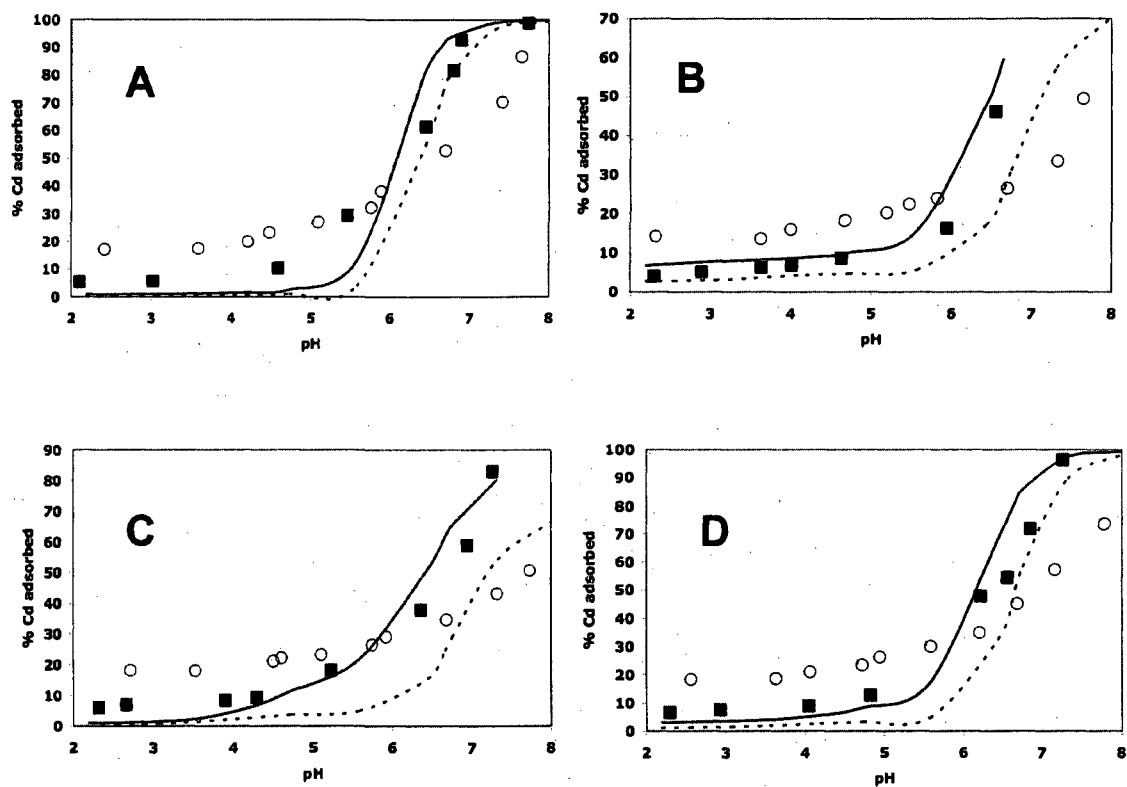


Figure 4.6: Adsorption of  $8.9 \times 10^{-6}$  M Cd to three-component mixtures of HFO, kaolinite, and *B. subtilis*, and in the presence of 0.3 M dissolved acetate. Darkened symbols and lines represent adsorption data and predicted adsorption for mixtures without acetate. Open symbols and dashed lines are adsorption data and predicted adsorption in the presence of 0.3 M acetate, respectively. Sorbent mixtures include A)  $0.8 \text{ g l}^{-1}$  HFO +  $0.1 \text{ g l}^{-1}$  *B. subtilis* +  $0.1 \text{ g l}^{-1}$  kaolinite, B)  $0.1 \text{ g l}^{-1}$  HFO +  $0.8 \text{ g l}^{-1}$  *B. subtilis* +  $0.1 \text{ g l}^{-1}$  kaolinite, C)  $0.1 \text{ g l}^{-1}$  HFO +  $0.1 \text{ g l}^{-1}$  *B. subtilis* +  $0.8 \text{ g l}^{-1}$  kaolinite, D)  $0.33 \text{ g l}^{-1}$  HFO +  $0.33 \text{ g l}^{-1}$  *B. subtilis* +  $0.33 \text{ g l}^{-1}$  kaolinite.

models describe the adsorption data reasonably well. The predicted extent of adsorption in the system containing 80% HFO (Figure 4.6A) shows minor discrepancies due to the fit of the pure HFO end-member. However, in mixtures of HFO, *B. subtilis* cells, and kaolinite, the CA approach is generally successful in predicting Cd adsorption at our experimental conditions.

The results of adsorption experiments conducted with three sorbents in the presence of 0.3 M acetate are depicted in Figure 4.6 (open circles). The dashed lines represent the best-fit Cd adsorption models, including the ternary complexation reactions calculated in this study and listed in Table 4.3. Figure 4.6A depicts Cd adsorption for a mixture of 0.8 g l<sup>-1</sup> HFO + 0.1 g l<sup>-1</sup> *B. subtilis* cells + 0.1 g l<sup>-1</sup> kaolinite in the presence of acetate. Compared to the same mixture in the absence of acetate (solid squares), more adsorption is observed below pH 5, and less above pH 6. Similar trends with pH are observed in the other three-component mixtures, including: 0.1 g l<sup>-1</sup> HFO + 0.8 g l<sup>-1</sup> *B. subtilis* cells + 0.1 g l<sup>-1</sup> kaolinite (Figure 4.6B), 0.1 g l<sup>-1</sup> HFO + 0.1 g l<sup>-1</sup> *B. subtilis* cells + 0.8 g l<sup>-1</sup> kaolinite (Figure 4.6C), and 0.33 g l<sup>-1</sup> HFO + 0.33 g l<sup>-1</sup> *B. subtilis* cells + 0.33 g l<sup>-1</sup> kaolinite (Figure 4.6D). The predictive models of these ternary systems may underestimate Cd adsorption below pH 5 (Figure 4.6) because of poor fit of the basis 1 ppm + HFO data (Figure 4.1B) is carried into these models. At pH greater than 6, all one-sorbent models of HFO, kaolinite, or *B. subtilis* cells in the presence of acetate (Figures 4.5B, 4.5D, 4.5F, respectively) fit the experimental data well. The predictive models of three-sorbent systems with acetate may overestimate adsorption at higher pH due to particle adhesion which causes a decrease in Cd adsorption as reactive sites are blocked. In particular, HFO, which has positively-charged sites under all experimental

conditions, may aggregate with negatively charged kaolinite particles and/or *B. subtilis* cells.

#### 4.4 Conclusions

In this study, we test if the CA approach can account for Cd adsorption to mixtures including *B. subtilis* cells, HFO, kaolinite, and dissolved acetate. We first conduct Cd adsorption experiments onto each sorbent separately at two metal concentrations. Using acidity constants and site concentrations for each sorbent from the literature, we model these adsorption data to calculate Cd stability constants for each sorbent. Using these constants, we predict the extent of Cd adsorption in two- and three-component mixtures of the sorbents at various mass ratios. In the absence of dissolved acetate, the predictive models match experimental data well. However, in the systems that we test that contain dissolved acetate, the models predict a bigger decrease in adsorption than we observed. We account for this enhanced adsorption in the presence of acetate by invoking the adsorption of the  $\text{Cd}(\text{CH}_3\text{COO})^+$  aqueous complex to each sorbent to form a ternary surface-Cd-acetate complex.

The component additivity approach represents a powerful means to extrapolate our understanding of metal adsorption in simple one-sorbent systems to predict metal distributions in complex multi-sorbent settings. Our results indicate that the CA approach is reasonably accurate under some circumstances. However, caution should be used when applying this approach to geologic systems, as site blockage and the formation of ternary complexes can significantly affect the accuracy of the CA predictions.

## CHAPTER 5

### THE EFFECT OF NP(V) INCORPORATION ON THE SOLUBILITY OF SODDYITE

#### 5.1 Introduction

Whereas some properties of materials change rapidly with grain size at the nanoscale (Hochella, 2002; Gilbert et al., 2004), similarly large responses of bulk properties to ppm levels of impurities are uncommon. Solubility in aqueous solutions greatly influences geochemical and environmental systems, yet the extent to which solubility is impacted by low-level impurities is largely unknown. No robust theory exists to explain such influences where they depart from ideal behavior. Here we examine a specific case where ppm-level substitution results in a dramatic reduction of the aqueous solubility of the recipient phase.

A system of particular environmental interest is the substitution of the  $\text{Np(V)O}_2^+$  neptunyl ion for the  $\text{U(VI)O}_2^{2+}$  uranyl ion in a uranyl silicate phase. Commercial spent nuclear fuel consists primarily of the solid phase  $\text{UO}_2$ , but also contains other actinides including  $^{237}\text{Np}$ , a potentially mobile radionuclide under moist oxidizing repository conditions such as those expected at the Yucca Mountain site, Nevada, USA. Under these conditions,  $\text{UO}_2$  is unstable, and rapidly oxidizes to form a range of uranyl  $[\text{U(VI)}]$

phases (Wronkiewicz et al., 1992; Finch and Ewing, 1992; Finn et al., 1996; Finch and Murakami, 1999; Finch et al., 1999; McNamara et al., 2003). Uranyl silicates, including soddyite,  $(\text{UO}_2)_2\text{SiO}_4(\text{H}_2\text{O})_2$ , are among the most important alteration phases to form (McNamara et al., 2003). Np in spent nuclear fuel is present predominantly as Np(IV), but under oxidizing conditions can transform into Np(V), which is present as the neptunyl cation,  $\text{NpO}_2^+$ , in aqueous solutions. Due to the similarities in cation size and coordination geometry, the neptunyl cation can substitute for the uranyl cation,  $\text{U(VI)O}_2^{2+}$ , in soddyite and other alteration phases (Klingensmith and Burns, 2007; Klingensmith et al., 2007), but the effect of its incorporation on the solubility of these phases is unknown.

Cation substitution, or solid-solution, in a crystal structure can either enhance or decrease the solubility of the compound. For example, the incorporation of  $\text{Mg}^{2+}$  into the calcite structure causes an increase in its solubility (Davis et al., 2000), but the incorporation of trace amounts of  $\text{La}^{3+}$  results in crystal growth inhibition and a decrease in mineral solubility (Kamiya et al., 2004). Sass and Rai (1987) co-precipitated amorphous  $\text{Cr}^{3+}$  and  $\text{Fe}^{3+}$  hydroxides, and found these co-precipitates to behave thermodynamically as ideal solid solutions. The closest analog to our study is that of Rai et al. (2004), who determined the effect of  $\text{Np}^{4+}$  incorporation into uraninite ( $\text{UO}_2$ ) across the entire range of solid solution. The authors observed ideal solid solution behavior, or a decrease in the aqueous  $\text{U}^{4+}$  concentration in equilibrium with the solid phase that is equal to the decrease in the mole fraction of  $\text{U}^{4+}$  within the solid phase with increasing extents of  $\text{Np}^{4+}$  substitution. In the cases of Np(V) and U(VI), the approximately linear dioxo cations  $\text{Np(V)O}_2^+$  and  $\text{U(VI)O}_2^{2+}$  dominate both solution and crystal chemistries. The  $\text{Np(V)O}_2^+$  neptunyl ion is geometrically compatible with

$\text{U(VI)O}_2^{2+}$  sites in a crystal (Burns, 2005; Forbes and Burns, 2008), but a charge-balancing co-substitution is needed. Perhaps more importantly, the dominance of cation-cation interactions in  $\text{Np(V)}$  compounds (Forbes and Burns, 2008), and their near-absence in  $\text{U(VI)}$  compounds, is compelling evidence that the bond strengths within the neptunyl and uranyl ions are different. Substitution of the linear  $\text{Np(V)O}_2^+$  ion for the geometrically similar  $\text{U(VI)O}_2^{2+}$  ion may have significant ramifications for the stability of the structure because of the different bonding requirements of the cations and the O atoms. The increased complexity of substitution could lead to non-ideal solid-solution behavior and more complicated solubility effects compared to those observed in uraninite. Here, we test this hypothesis by measuring the solubility effect of  $\text{Np(V)O}_2^+$  substitution for  $\text{U(VI)O}_2^{2+}$  in the uranyl silicate soddyite.

## 5.2 Materials and Methods

Soddyite was synthesized using a mild hydrothermal method similar to that reported by Gorman-Lewis et al. (2007) and Klingensmith and Burns (2007). A  $\text{Np(V)}$  stock solution was prepared from 500 mg of  $\text{NpO}_2$  powder was purchased from Oak Ridge National Laboratory. Approximately 25 mg of the  $\text{NpO}_2$  powder was placed in a 7-mL Teflon cup with a screw top lid. Three mL of concentrated  $\text{HNO}_3$  was added; the cup was tightly sealed and then placed in a 125-mL Teflon-lined Parr acid digestion vessel. Thirty-five mL of ultrapure water was added to the vessel to provide counter-pressure during the heating cycle. The vessel was heated at 150 °C in a Fisher Isotemp oven for 48 hours. After the heating cycle, no  $\text{NpO}_2$  powder was observed and the solution was a dark brownish green color. A UV spectrum of the solution indicated that the neptunium was in both a pentavalent and hexavalent state by the presence of peaks at

980  $\text{cm}^{-1}$  and 1223  $\text{cm}^{-1}$ , respectively. No peaks associated with tetravalent Np were present in the spectrum. A small amount of  $\text{NaNO}_2$  was added to the solution, which resulted in the reduction of Np(VI) into Np(V) as indicated by a color change of the solution from a brownish green to a bright emerald green. The pentavalent Np was precipitated into a relatively insoluble Np hydroxide precipitate using a small amount of a saturated NaOH solution and washed three times with ultrapure water to remove the excess sodium from solution. The precipitate was then re-dissolved in the appropriate amount of 1 M  $\text{HNO}_3$  to create an approximately 1000 ppm stock solution. A UV spectrum of the final stock solution confirmed that no Np(IV) or Np(VI) was present. The actual concentration of the stock solution was measured using LA-ICP-MS.  $\text{Na}^+$  can be incorporated into the Np hydroxide compound and released into solution with the re-dissolution of the precipitate; Therefore, a small amount of  $\text{Na}^+$  is usually present in the final Np(V) stock solution.

An appropriate aliquot of the neptunyl stock solution (1270 ppm Np(V) in 1.0 M  $\text{HNO}_3$ ), was added to each synthesis to achieve the following initial aqueous Np concentrations: 12.7 ppm, 127 ppm, 381 ppm, and 634 ppm. After heating, the resulting precipitate from each synthesis was washed four times with boiling ultrapure 18 M $\Omega$  water to remove adsorbed Np and/or adhered colloidal material. After the powders were washed with boiling water, a small amount of ultrapure water was added to each product to create a slurry mount on a zero-background quartz plate. The powder was air-dried overnight and then covered with a small piece of Kapton® tape to prevent contamination. A X-ray diffraction pattern was collected on a Scintag powder diffractometer from 10-90° 2 $\theta$  with a step size of 0.02 °/sec and scan speed of 10 seconds. The powder pattern matched those of PDF-00-035-0733 and PDF-01-079-1323

for synthetic soddyite. Fourier transform infrared (FTIR) spectroscopy on the dried powders confirmed that no amorphous phases were present. The concentration of Np(V) incorporated into each synthesized solid phase was calculated by the difference between the known initial Np aqueous concentration in the synthesis solution and the Np concentration that remained in the combined synthesis and wash solutions after synthesis. The soddyite phases reported here have 24, 919, 2730, and 6511 ppm Np incorporated into the crystal structure (Table 1).

We used transmission electron microscopy with electron diffraction spectroscopy (TEM-EDS) to obtain images and the chemical composition of individual soddyite crystals from each of the solid phases synthesized in this study. We observed a constant chemical composition for all crystals examined for each Np-incorporated solid phase, and the crystal cores exhibited the same composition as the rims, suggesting that a single phase was present in each sample. TEM electron diffraction patterns from single crystals of each phase indicated that soddyite was the only phase present in each synthesized powder sample.

To begin a solubility experiment, approximately 125 mg of a soddyite powder, 100 mg of silica gel (to buffer aqueous Si concentrations), and 7 ml of 18 MΩ ultrapure water were placed in a teflon-coated centrifuge tube. In order for the systems to reach equilibrium more quickly, the starting solutions were spiked with  $10^{-4.5}$  M  $\text{UO}_2^{2+}$  and  $10^{-3.5}$  M Si, each of which is below the expected equilibrium concentrations for these species. Experiments were conducted at pH 3.4, and the pH was adjusted using small volumes of concentrated  $\text{HNO}_3$  until the pH did not vary. Between sampling intervals, experimental tubes were slowly agitated on a rotary shaker. Aliquots of 400  $\mu\text{L}$  of the experimental solutions were extracted periodically over a period of 24 days. To extract a

TABLE 5.1

PROPERTIES OF NP-INCORPORATED SODDYITES

<b>Np in synthesis solution (ppm)</b>	<b>Np in solid phase (ppm)</b>	<b>Mole Fraction U Soddyite (<math>X_{\text{Soddyite}}</math>)</b>	<b>Mineral Activity Coefficient (<math>\Gamma_{\text{Soddyite}}</math>)</b>
12.7	24	0.9999	1.00
127	919	0.9987	0.95
381	2730	0.9962	0.66
634	6511	0.9908	0.44

sample, the Teflon tubes were centrifuged at 20,000 g for 2.5 minutes. An aliquot of the resulting supernatant was removed, filtered through a 0.20  $\mu\text{m}$  nylon filter, and stored for dilution. Following dilution, these aliquots were analyzed for total aqueous Np, U, and Si concentrations using inductively coupled plasma optical emission spectroscopy (ICP-OES) for U and Si, and inductively coupled plasma mass spectroscopy (ICP-MS) for Np. Samples analyzed for Np were internally standardized with 1 ppb Tl and Bi. Repeat analyses of element internal standards indicated that instrumental uncertainty was  $\pm 3.6\%$ . X-ray diffraction analyses of the solid phase after each experiment did not reveal a change in crystallinity, and confirmed that soddyite was the only crystalline phase present in each solubility experiment.

### 5.3 Results and Discussion

The concentrations of U, Si, and Np increased from undersaturation to reach steady-state within 10 days. As expected, the steady-state aqueous Np concentration increases as a function of the Np concentration in the solid phase (Figure 5.1A). The steady-state aqueous Si concentrations for each experiment are, within analytical uncertainty, independent of the Np concentration in the solid phase used in each experiment (Figure 5.1B). The average steady-state Si concentration value for all experiments is  $10^{-2.66}$  molal, suggesting that Si was successfully buffered in solution by the amorphous silica gel, which has reported solubility values ranging from  $10^{-2.38}$  to  $10^{-2.71}$  molal (Morey et al., 1964; Walther and Helgeson, 1977). However, the steady-state aqueous U concentrations decrease appreciably as the concentration of Np incorporated in the solid phase increases (Figure 5.1B). We average the measured pH and U, Si, and Np concentrations from the final five sampling periods (between days 14

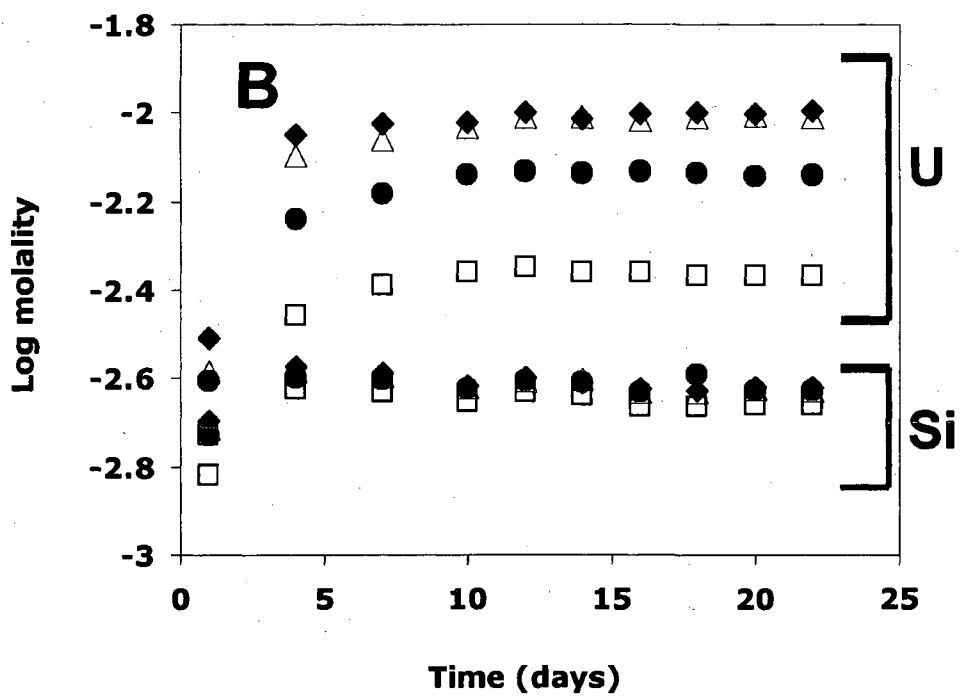
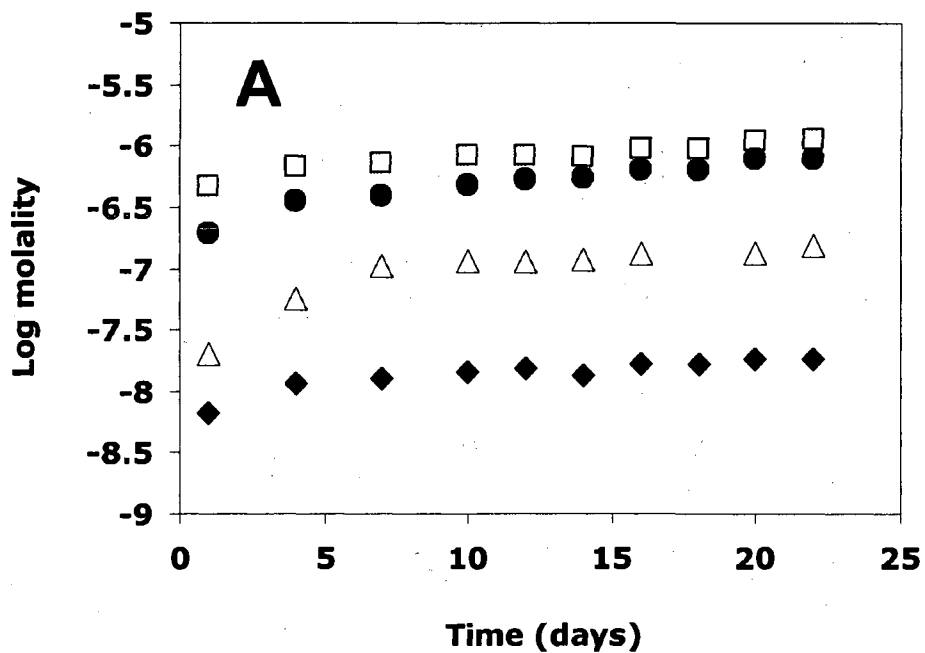


Figure 5.1: Measured aqueous concentrations of Np (A) and U and Si (B) during solubility experiments at pH 3.4. Solid phase Np concentrations are: 24 ppm (◆), 919 ppm (△), 2730 ppm (●), and 6511 ppm (□).

and 22 of the solubility experiments) for use in the thermodynamic calculations. The measured pH and element concentrations for each experiment are given in Table 2.

Using the steady-state measured aqueous Np concentrations and the known Np content of each solid phase, distribution coefficients ( $K_d$ ) were calculated for each phase according to:

$$K_d = \frac{m_{\text{Np},\text{solution}}}{m_{\text{Np},\text{solid}}}, \quad (1)$$

where  $m_{\text{Np},\text{solution}}$  represents the aqueous phase Np molality, and  $m_{\text{Np},\text{solid}}$  represents the solid phase concentration of Np in units of mol kg<sup>-1</sup>. Log  $K_d$  values from experiments involving the 24, 919, 2730, and 6511 ppm Np solid phases are -3.70, -4.46, -4.16, and -4.22, respectively. The high value for the 24 ppm Np solid phase experiment likely has the highest experimental uncertainty; the aqueous Np concentrations in this experiment were near the detection limit for the ICP-MS approach. The other Log  $K_d$  values are relatively close to one another, and do not vary systematically as a function of Np content in the solid phase. The apparent constancy of the  $K_d$  values suggests that aqueous Np concentrations in equilibrium with solid phases with higher Np contents can be estimated using these same  $K_d$  values.

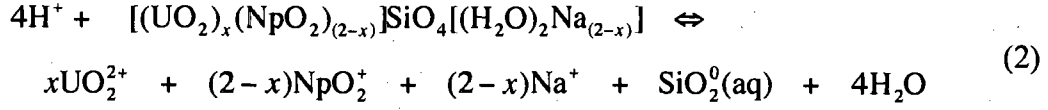
The effect of Np incorporation on the solubility of the solid phase in terms of the release of U into solution is much larger than would be predicted assuming ideal solid-solution behavior for the neptunyl substitution for uranyl. Although the exact structural mechanisms of incorporation have not been determined, because of charge balance considerations, substitution of Np(V)O<sub>2</sub><sup>+</sup> for U(VI)O<sub>2</sub><sup>2+</sup> in the soddyite structure is most likely accompanied by concomitant substitution of Na<sup>+</sup> into a vacant cavity

TABLE 5.2

EQUILIBRIUM SPECIES CONCENTRATIONS AND PH FROM EACH  
SOLUBILITY EXPERIMENT USED FOR THERMODYNAMIC CALCULATIONS,  
REPORTED AS LOG MOLALITIES

Soddyite Phase	Time (days)	pH	Np	U	Si
24 ppm	14	3.38	-7.87	-2.01	-2.61
24 ppm	16	3.42	-7.77	-2.00	-2.63
24 ppm	18	3.42	-7.77	-2.00	-2.63
24 ppm	20	3.40	-7.74	-2.00	-2.62
24 ppm	22	3.40	-7.74	-2.00	-2.62
919 ppm	14	3.40	-6.87	-2.01	-2.60
919 ppm	16	3.42	N/A	-2.02	-2.63
919 ppm	18	3.45	-6.87	-2.01	-2.63
919 ppm	20	3.42	-6.81	-2.01	-2.63
919 ppm	22	3.44	-6.83	-2.01	-2.63
2730 ppm	14	3.42	-6.26	-2.14	-2.62
2730 ppm	16	3.45	-6.20	-2.13	-2.64
2730 ppm	18	3.44	-6.20	-2.14	-2.64
2730 ppm	20	3.43	-6.11	-2.14	-2.64
2730 ppm	22	3.43	-6.10	-2.14	-2.64
6511 ppm	14	3.41	-6.08	-2.36	-2.64
6511 ppm	16	3.44	-6.02	-2.36	-2.66
6511 ppm	18	3.41	-6.02	-2.37	-2.66
6511 ppm	20	3.45	-5.96	-2.37	-2.66
6511 ppm	22	3.45	-5.95	-2.37	-2.66

(Klingensmith and Burns, 2007). Thus, the dissolution reaction for the Np-incorporated soddyite can be expressed as follows:



where  $x$  is the number of uranyl sites in the solid phase occupied by the uranyl cation, and for pure soddyite,  $x = 2$ . The equilibrium constant for reaction (2) is termed the solubility product, and can be expressed as:

$$K_{sp} = \frac{a_{\text{UO}_2^{2+}}^x a_{\text{NpO}_2^+}^{2-x} a_{\text{Na}^+}^{2-x} a_{\text{SiO}_2^0} a_{\text{H}_2\text{O}}^4}{a_{\text{H}^+}^4 a_{\text{Soddyite}}} \quad (3)$$

where  $a$  represents the thermodynamic activity of the subscripted aqueous species or solid phase. The thermodynamic standard state for  $\text{H}_2\text{O}$  is the pure phase at the pressure and temperature of interest. The standard state for aqueous species is a hypothetical one molal solution at the pressure and temperature of interest that behaves as if it were infinitely dilute, and activities are related to molalities by:

$$a_i = \gamma_i \cdot m_i \quad (4)$$

where  $m_i$  is the aqueous molal concentration of species  $i$ , and  $\gamma_i$  is the activity coefficient defined in this study using an extended Debye-Hückel approach (Helgeson et al., 1981):

$$\log \gamma_i = \frac{-Az_i^2\sqrt{I}}{1 + Ba_0\sqrt{I}} + bI. \quad (5)$$

The values of  $A$  and  $B$  are constants, and  $b$  and  $a_0$  are electrolyte-specific constants.  $z_i$  represents the charge of the ion of interest, and  $I$  is the solution ionic strength.

In each experiment with a different Np-incorporated soddyite, we measured the total concentrations of U, Np, and Si, and under the experimental conditions, these concentrations are equal to the concentrations of  $\text{UO}_2^{2+}$ ,  $\text{NpO}_2^+$ , and  $\text{SiO}_2(\text{aq})$ . We

measured pH for each sample, and from the known concentration of base addition to each system, we can calculate the  $\text{Na}^+$  molality. According to equation (3), concentration values for each aqueous species, in conjunction with a value for  $K_{sp}$ , yield a calculated value for the activity of the particular Np-incorporated soddyite used in each experiment. In this study, in order to isolate the effect of Np substitution, we use the 24 ppm Np soddyite solubility measurement to calculate an internally consistent baseline value for  $K_{sp}$  of  $10^{6.56}$ . This value is slightly higher than, but within experimental uncertainty of, the value calculated by Gorman-Lewis et al. (2007).

Because we know the mole fraction of Np in each solid that was studied, we can directly calculate the activity coefficient of each solid phase:

$$a_{\text{Soddyite}} = X_{\text{Soddyite}}^2 \cdot \Gamma_{\text{Soddyite}}^2 \quad (6)$$

where  $X_{\text{Soddyite}}$  is the mole fraction of uranyl soddyite, and  $\Gamma_{\text{Soddyite}}$  is the activity coefficient of the solid. Ideal solid-solution behavior is characterized by a  $\Gamma_{\text{Soddyite}}$  value of 1. Equation 3 is insensitive to the activities of  $\text{NpO}_2^+$  and  $\text{Na}^+$  when values of  $x$  are close to 2, as in these experiments. Therefore, at fixed pH and buffered Si activities, and with increasing Np incorporation in the soddyite, the solid phase would demonstrate ideal solid-solution behavior if the activity of  $\text{UO}_2^{2+}$  decreased by the same amount as  $X_{\text{soddyite}}$ . This behavior was observed for  $\text{Np}^{+4}$  incorporation into  $\text{UO}_2$  by Rai et al. (2004).

We observed an incorporation effect that is dramatically larger than that predicted by ideal solid-solution behavior. For example, the 6511 ppm Np soddyite corresponds to a  $X_{\text{soddyite}}$  value of 0.9908. Ideal solid-solution behavior, then, would correspond to an aqueous  $\text{UO}_2^{+2}$  decrease of only 0.004 log molality units, essentially an unchanged concentration relative to the value measured for the experiments involving

the 24 ppm Np solid. In actuality, the 6511 ppm Np soddyite experiment exhibited a  $\text{UO}_2^{+2}$  molality decrease of 0.36 log molality units (Figure 5.1B), an effect that is approximately two orders of magnitude greater than that expected for ideal solid-solution behavior. Values of  $\Gamma_{\text{Soddyite}}$  increasingly depart from ideal behavior (where  $\Gamma_{\text{Soddyite}} = 1$ ) as  $X_{\text{soddyite}}$  decreases (Figure 5.2). With the limited data available, it is difficult to reliably extrapolate the relationship that is depicted in Figure 5.2 to determine the solubility behavior of solids with higher levels of Np incorporation. However, the effect of Np incorporation into the soddyite structure is dramatic even for the low levels of Np incorporation documented in this study, and Figure 5.2 suggests that the effects are likely to increase with increasing Np incorporation. It is possible that neptunyl forms a complete solid solution with uranyl in the soddyite structure, and our results suggest that these higher Np content solids would be in equilibrium with much lower aqueous uranyl activities than would be expected based on ideal solid-solution behavior.

#### 5.4 Conclusions

The experimental results reported here indicate that neptunyl substitution for uranyl in soddyite is much more complex and exerts a much larger effect on mineral solubilities than the ideal  $\text{Np}^{4+}$  substitution for  $\text{U}^{4+}$  observed by Rai et al. (2004). Several mechanisms may explain the deviation from ideal solid solution behavior observed in soddyites containing Np(V).  $\text{Np(V)O}_2^+$  exhibits markedly different bond strengths than are present within  $\text{U(VI)O}_2^{+2}$ , and due to the charge imbalances that accompany  $\text{NpO}_2^+$  substitution for  $\text{UO}_2^{+2}$ , a co-substitution (most likely with  $\text{Na}^+$ ) must occur. These complicating factors make the substitution of  $\text{NpO}_2^+$  for  $\text{UO}_2^{+2}$  in uranyl phases much more complex than the simple (and ideal) one-for-one incorporation that is possible with

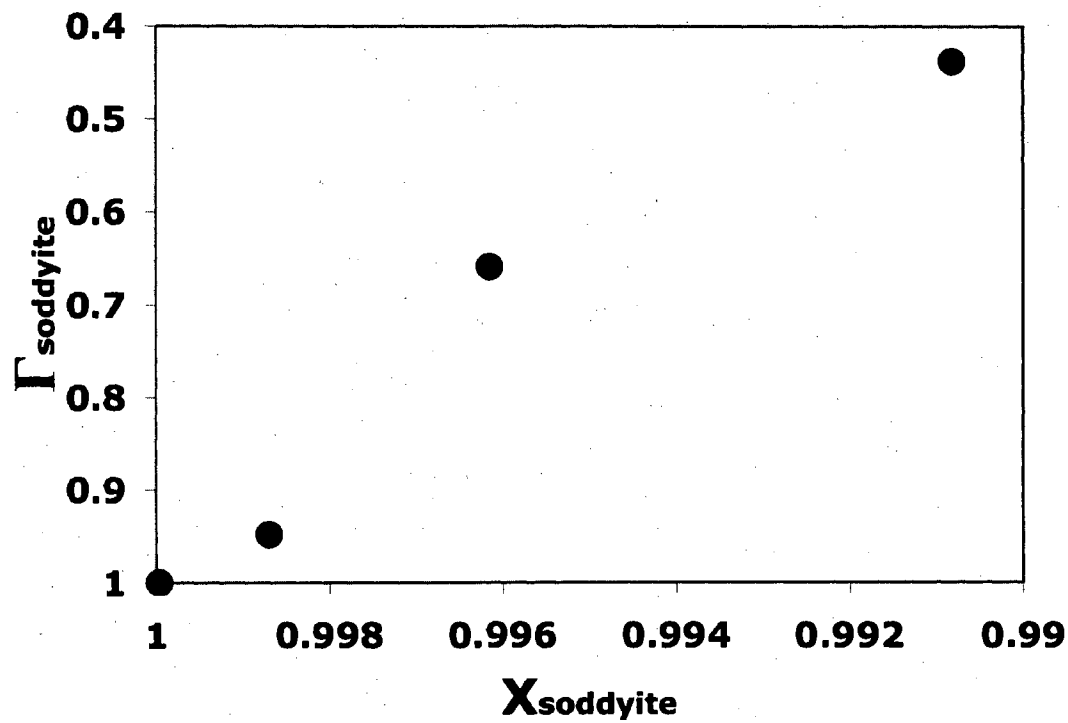


Figure 5.2: The solid phase activity coefficient ( $\Gamma_{\text{soddyite}}$ ) as a function of the mole fraction of uranyl soddyite ( $X_{\text{soddyite}}$ ).

$\text{Np}^{+4}$  substitution for  $\text{U}^{+4}$  in uraninite. The more complex substitution is likely to occur for any  $\text{Np(V)O}_2^+$  substitution for  $\text{U(VI)O}_2^{+2}$  in uranyl compounds in general, so the large  $\text{Np(V)}$  incorporation effect on the solubility of uranyl minerals is likely to significantly affect the solubility of the wide range of uranyl phases that incorporate even fairly low concentrations of  $\text{Np}$ . Our results suggest that incorporation of  $\text{Np(V)}$  into secondary uranyl phases can not only limit and control the mobility of  $\text{Np}$  in repository systems, but may decrease the mobility of  $\text{U}$  as well through non-ideal solid-solution effects.

## CHAPTER 6

### CONCLUSIONS

This dissertation provides new insight into the adsorption of monovalent cations onto bacterial cell walls, the adsorption of cadmium onto mixtures of soil components, the determination of biomass C in soils, and the release of Np and U from a uranyl silicate mineral, soddyite. In Chapter 2, I propose an alternative method to account for the effects of ionic strength on the adsorption of divalent and trivalent metal cations onto bacterial surfaces. The effect of ionic strength on the adsorption of metals has typically been accounted for by varying the extent and strength of the electric field surrounding the bacteria. My results indicate that ionic strength can also be accounted for by calculating equilibrium constants for complexes between monovalent cations in solution and the discrete organic functional groups present on the bacterial surface. In this way, higher-charged metals in solution and monovalent cations compete directly for adsorption to the bacterial surface functional groups. I test this direct competition model by fitting existing data sets of Cd adsorption to *Bacillus subtilis* in the presence of monovalent cation competition. The results show that the apparent equilibrium constants for Cd-surface complexes is higher than was previously calculated when

monovalent cation competition was not included. The non-electrostatic, direct competition approach I develop here is simpler than the electric field approach because it does not entail the use of arbitrary fitting parameters, and is therefore easier to apply to complex geochemical systems.

The universal equilibrium constant I propose for complexes between monovalent metals and Site 2 of *B. subtilis* ( $\log K = 1.9 \pm 0.3$ ) is fairly well constrained by my work. However, to more rigorously test the accuracy of this value, monovalent cation adsorption experiments should be performed at different cation:*B. subtilis* concentration ratios. Experiments containing a lower cation:bacteria ratio are likely to give a greater range of metal uptake than the low percentage (0 – 20%) of metal uptake observed in our experiments. Models of data at different cation:bacteria ratios also may indicate if adsorption is occurring only on Site 2 of the bacteria, as I conclude from experiments in Chapter 2, or if other sites need to be invoked to describe the observed adsorption behavior. Additionally, Yee and Fein (2001) demonstrate that the adsorption behavior of Cd across a wide range of pH values is nearly identical for seven Gram-positive and Gram-negative species. Repeating monovalent cation adsorption experiments using other bacterial species will reveal if the adsorption of these cations is a similarly universal phenomenon.

I test validity of the fumigation-extraction method (Vance et al., 1987; Tate et al., 1988) for determining biomass C in soils in Chapter 3. The method is based on the premise that soils can be exposed to chloroform gas for 24 hours to lyse bacterial cells in the soil, and that the chloroform can be fully recovered by evacuation after that time. I test this assumption by performing the fumigation-extraction process on individual components of soils, including kaolinite, montmorillonite, quartz sand, humic acid, and

bacteria. Chloroform substantially adsorbs to both of the clays, enhancing the carbon pool in extraction solutions of these materials. Since biomass C is measured only as the total organic carbon in the extracts, this adsorbed chloroform that enters into the extraction solutions is likely to be misinterpreted as biomass, causing artificially high biomass C measurements. Thus, in soils containing a significant clay fraction, the fumigation-extraction method may be invalid, or require a correction factor to be usable.

A comprehensive study to determine which types of natural soils adsorb chloroform during the fumigation-extraction process is necessary. Among the factors that may influence chloroform vapor adsorption to a soil are the clay content, as discussed here in Chapter 3, soil moisture (Chen and Dural, 2002), and the presence of adsorbed bacteria and biofilms on clay surfaces. A universal correction factor to adjust experimental data for the adsorption of chloroform to soils is unlikely to be successful because of the complexity and variety of soil compositions found in nature. However, it may be possible to salvage the fumigation-extraction method for an individual soil by determining the fraction of carbon in its extract that is due to bacterial lysis, and the fraction due to chloroform. Methods including gas chromatography – mass spectrometry (GC-MS), or UV-visible spectrometry methods can quantify chloroform in solutions. If the chloroform concentration in extracts is determined using one of these methods, it could be subtracted from the total organic carbon measurement in a sample to give the amount of carbon attributed to the soil sample. In the fumigation-extraction method as currently used, two pools of carbon are determined: that due to cell lysis, which may include chloroform artifacts, and the background carbon in the soil prior to fumigation. Using the correction procedure I propose above, carbon would be divided into three discrete pools: adsorbed chloroform, that due to the lysis of bacteria, and

background carbon extracted from unfumigated soil samples. Thus, a true measure of biomass C may be feasible, despite the adsorption of chloroform vapor.

In Chapter 4, I rigorously test the component additivity (CA) approach in mixtures of *B. subtilis* cells, HFO, kaolinite, and dissolved acetate. Cd is adsorbed to each component individually, and equilibrium constants for Cd-sorbent surface complexes are calculated using existing surface complexation models for each sorbent. I conclude that Cd adsorption to two- and three-component mixtures of the geosorbents is well predicted by combining the constants calculated from the one-component systems. In experiments including dissolved acetate as a representative organic acid, however, the CA approach does not work well even in simple one-sorbent systems. Invoking only aqueous Cd-acetate complexes causes the predictive model to underestimate the observed extent of adsorption at all pH levels. To obtain a better fit, it is necessary to calculate equilibrium constants for the complexation of a cadmium acetate,  $\text{Cd}(\text{CH}_3\text{COO})^+$ , to each sorbent. Accounting for ternary complexation among solid surfaces, metals, and dissolved organic acids is likely important in describing the distribution and transport of heavy metals. Careful consideration of ternary complexation is likely to be important in applying the CA approach to realistic geologic systems, where metal-organic aqueous complexes may be the dominant species adsorbing to soil or aquifer components.

Our data require models that include adsorption of the  $\text{Cd}(\text{CH}_3\text{COO})^+$  complex to each sorbent in order to account for the observed adsorption behaviors. More detailed evidence regarding the types and coordination environments of ternary metal-organic-surface complexes forming in our experiments could be provided by a spectroscopic technique such as extended adsorption x-ray fine structure (EXAFS) or Fourier

transform – infrared spectroscopy (FT-IR). Future studies should determine the impacts of more complex organic ligands on metal adsorption, including fulvic and humic acids that will be present in natural systems. The ultimate application of the CA approach is in predicting metal distribution in soils. The physical components that make up soils can be divided into a few, broadly defined categories, or many detailed categories. The challenge is in defining these component categories well, so that surface complexation modeling provides accurate predictions of metal distributions.

The solubility effect of Np(V) incorporation into the uranyl silicate phase, soddyite, is discussed in Chapter 5. My results show that a relatively minor substitution of less than 1 atomic %  $\text{NpO}_2^+$  for  $\text{UO}_2^{2+}$  in the crystal structure results in a dramatic decrease in phase solubility, approximately 100 times more than would be expected by invoking ideal solid solution chemistry. This non-ideal behavior has important implications for nuclear repositories or Np contaminated groundwaters in oxidizing conditions where soddyite may be present or may form. Specifically, the incorporation of Np(V) into soddyite and the subsequent decrease in phase solubility may dramatically limit the mobility of both Np and U in these systems.

The exact structural mechanisms of Np incorporation into soddyite are not known with certainty. Due to the low concentrations of Np incorporated into the soddyite phases synthesized in my studies, elucidating the coordination of Np(V) in the crystal structure is difficult. If a phase with a higher Np concentration in the solid can be synthesized, EXAFS may reveal more about the binding environment of Np in soddyite. Our studies cover only a small fraction of the theoretical solid solution between uranyl soddyite and a potential end member containing 100% neptunyl cation in the uranyl sites. I propose that the concentration of Np released into solution from Np-soddyite

phases can be predicted by a simple linear distribution coefficient,  $K_d$ , approach at the modest levels of Np incorporation detailed here. However, it is unclear how far into the solid solution this linear relationship extends. The deviation of Np-soddyite from ideal behavior, as quantified by the soddyite activity coefficient  $\Gamma_{\text{soddyite}}$ , is directly related to the mole fraction of uranyl soddyite in a phase. Because of the rapid decrease in  $\Gamma_{\text{soddyite}}$  from pure soddyite, where  $\Gamma_{\text{soddyite}} = 1$ , to 1% Np-incorporated soddyite, where  $\Gamma_{\text{soddyite}} = 0.44$ , this relationship cannot remain linear much further into the solid solution. Another empirical fit, such as a Freundlich or Langmuir isotherm, may substitute for the linear  $K_d$  approach that is valid at low levels of Np incorporation. Additionally, solubility studies on soddyites with more than the 1% Np substitution in my study will provide a better understanding of the observed decrease in solubility. Future work should also include solubility studies of other Np-incorporated uranyl phases, such as uranophane and Na-compregnacite, that may incorporate significant amounts of Np.

The characterization of heavy metal and radionuclide transport in geologic settings requires knowledge of the amount and reactivity of each component in the system. My dissertation contributes to the understanding of these topics by improving existing thermodynamic models for metal adsorption and mineral solubility, and revealing a critical shortcoming in a widely used method of determining biomass in soils. As our understanding of individual mechanisms, such as those described here, increases, we will be able to model more accurately the distribution of metals in geologic systems of increasing complexity.

## REFERENCES

- Ali, M. A., Dzombak, D. A. (1996) Effects of simple organic acids on sorption of  $\text{Cu}^{2+}$  and  $\text{Ca}^{2+}$  on goethite. *Geochim. Cosmochim. Acta* 60:291-304.
- Ams, D. A., Fein, J. B., Dong, H., Maurice, P. A. (2004) Experimental measurements of the adsorption of *Bacillus subtilis* and *Pseudomonas mendocina* onto Fe-oxyhydroxide-coated and uncoated quartz grains. *Geomicrobiol. J.* 21:511-519.
- Baes, C. F., Jr., Mesmer, R. E. (1976) *The Hydrolysis of Cations*. Wiley, New York. 489 p.
- Bakken, L. R. (1985) Separation and Purification of Bacteria from Soil. *Applied and Environmental Microbiology* 49:1482-1487.
- Bethke, C. M. (2007) *Geochemical and Biogeochemical Modeling*. Cambridge University Press, New York, 543 p.
- Bethke, C. M., Brady, P. V. (2000) How the K-d approach undermines ground water cleanup. *Ground Water* 38:435-443.
- Beveridge, T. J., Murray, R. G. E. (1976) Uptake and retention of metals by cell walls of *Bacillus subtilis*. *J. Bacteriol.* 127:1502-1518.
- Beveridge, T. J. (1989) Role of cellular design in bacterial metal accumulation and mineralization. *Annu. Rev. Microbiol.* 43:147-171.
- Bish, D. L. and Post, J. E. (1993) Quantitative mineralogical analysis using the Rietveld full-pattern fitting method. *American Mineralogist* 78:932-940.
- Borrok, D., Fein, J. B., Tischler, M., O'Loughlin, E., Meyer, H., Liss, M., Kemner, K. M. (2004) The effect of acidic solutions and growth conditions on the adsorptive properties of bacterial surfaces. *Chem. Geol.* 209:107-119.
- Borrok, D., Fein, J. B. (2004) Distribution of protons and Cd between bacterial surfaces and dissolved humic substances determined through chemical equilibrium modeling. *Geochim. Cosmochim. Acta* 68:3043-3052.

Borrok, D. M., Turner, B. F., Fein, J. B. (2005) A universal surface complexation framework for modeling proton binding onto bacterial surfaces in geologic settings. *Am. J. Sci.* 308:826-853.

Borrok, D. M., Aumend, K., Fein, J. B. (2007) Significance of ternary bacteria-metal-natural organic matter complexes determined through experimentation and chemical equilibrium modeling. *Chem. Geol.* 238:44-62.

Brindley, G. W. (1984) Quantitative X-ray Mineral Analysis of Clays. In: Brindley, G. W. and Brown, G. (Eds.), *Crystal Structures of Clay Minerals and their X-ray Identification*. Mineralogical Society, London, England, pp. 411-438.

Buerge-Weirich, D., Behra, P., Sigg, L. (2003) Adsorption of copper, nickel, and cadmium on goethite in the presence of organic ligands. *Aquatic Geochemistry* 9:65-85.

Burns, P. C., Ewing, R. C., Miller, M. L. (1997) Incorporation mechanisms of actinide elements into the structures of U<sup>6+</sup> phases formed during the oxidation of spent nuclear fuel. *J. Nucl. Mater.* 245:1-9.

Burns, P. C. (2005) U<sup>6+</sup> minerals and inorganic compounds: Insights into an expanded structural hierarchy of crystal structures. *Can. Mineral.* 43:1839-1894.

Cerato, A.B., Lutenecker, A.J. (2002) Determination of Surface Area of Fine-Grained Soils by the Ethylene Glycol Monoethyl Ether (EGME) Method. *Geotechnical Testing Journal* 25:1-7.

Chen, C. H., (1993) Adsorption of Chlorinated Hydrocarbon Vapors on Soils. M. S. Thesis, University of Missouri-Columbia.

Chen, C.-H., Dural, N. H. (2002) Chloroform Adsorption on Soils. *Journal of Chemical Engineering Data* 47:1110-1115.

Chipera, S.J., Bish, D.L. (2001) Baseline Studies of the Clay Minerals Society Source Clays: Powder X-ray Diffraction Analyses. *Clays and Clay Minerals* 49:398-409.

Covelo, E. F., Vega, F. A., Andrade, M. L. (2007) Competitive sorption and desorption of heavy metals by individual soil components. *J. Hazard. Mater.* 140:308-315.

Cox, J. S., Smith, D. S., Warren, L. A., Ferris, F. G. (1999) Characterizing Heterogeneous Bacterial Surface Functional Groups Using Discrete Affinity Spectra for Proton Binding. *Environ. Sci. Technol.* 33:4514-4521.

Curti, E., (1999) Coprecipitation of radionuclides with calcite: estimation of partition coefficients based on a review of laboratory investigations and geochemical data. *Appl. Geochem.* 14:433-445.

Daughney, C. J., Fein, J. B. (1998) The effect of ionic strength on the adsorption of H<sup>+</sup>, Cd<sup>2+</sup>, Pb<sup>2+</sup>, and Cu<sup>2+</sup> by *Bacillus subtilis* and *Bacillus licheniformis*: A surface complexation model. *J. Colloid Interface Sci.* 198:53-77.

Davis, J. A., James, R. O., Leckie, J. O. (1978) Surface ionization and complexation at the water/oxide interface. I. Computation of electrical double layer properties in simple electrolytes. *J. Colloid Interface Sci.* 63:480-499.

Davis, J. A., Kent, D. B. (1990) Surface complexation modeling in aqueous geochemistry. In: Hochella, M. F. and White, A. F., editors. *Reviews in Mineralogy*, v. 23, Mineral-Water Interface Geochemistry. Mineralogical Society of America, Washington, D. C. pp. 177-260.

Davis, J. A., Coston, J. A., Kent, D. B., Fuller, C. C. (1998) Application of the surface complexation concept to complex mineral assemblages. *Environ. Sci. Technol.* 32:2820-2828.

Davis, K. J., Dove, P. M., DeYoreo, J. J. (2000) The role of Mg<sup>2+</sup> as an impurity in calcite growth. *Science* 290:1134-1137.

Dogan, A. U., Dogan, M., Onal, M., Sarikaya, Y., Aburub, A., Wurster, D. E. (2006) Baseline Studies of the Clay Minerals Society Source Clays: Specific Surface Area by the Brunauer Emmett Teller (BET) Method. *Clays and Clay Minerals* 54:62-66.

Dural, N. H., Peng, D. (1995) Competitive adsorption of chlorinated aliphatic hydrocarbons from aqueous mixtures onto soil. In: *Hazardous and industrial wastes; proceedings of the Twenty-seventh Mid-Atlantic Industrial Waste Conference*. Technomic Publishing Company, Lancaster, PA, pp. 528-537.

Dzombak, D. A., Morel, F. M. M. (1990) *Surface Complexation Modeling: Hydrous Ferric Oxide*. Wiley-Interscience, New York, 393 pp.

Fægri, A., Torsvik, V. L., Goksöyr, J. (1977) Bacterial and Fungal Activities in Soil: Separation of Bacteria and Fungi by a Rapid Fractionated Centrifugation Technique. *Soil Biology & Biochemistry* 9:105-112.

Farrell, J. and Reinhard, M. (1994) Desorption of Halogenated Organics from Model Solids, Sediments, and Soil under Unsaturated Conditions. 1. Isotherms. *Environmental Science & Technology* 28:53-62.

Fein, J. B., Daughney, C. J., Yee, N., Davis, T. A. (1997) A chemical equilibrium model for metal adsorption onto bacterial surfaces. *Geochim. Cosmochim. Acta* 61:3319-3328.

Fein, J. B., Martin, A. M., Wightman, P. G. (2001) Metal adsorption onto bacterial surfaces: Development of a predictive approach. *Geochim. Cosmochim. Acta* 65:4267-4273.

- Fein, J. B. (2002) The effects of ternary surface complexes on the adsorption of metal cations and organic acids onto mineral surfaces. In: *Water-Rock Interactions, Ore Deposits, and Environmental Geochemistry: A Tribute to David A. Crerar* (eds., R. Hellmann and S. A. Wood). Geochemical Society, Special Pub. 7, 462p.
- Fein, J. B., Boily, J. -F., Yee, N., Gorman-Lewis, D., Turner, B. F. (2005) Potentiometric titrations of *Bacillus subtilis* cells to low pH and a comparison of modeling approaches. *Geochim. Cosmochim. Acta* 69:1123-1132.
- Finch, R., Ewing, R. (1992) The Corrosion of Uraninite Under Oxidizing Conditions. *Journal of Nuclear Materials* 190:133-156.
- Finch, R. J., Buck, E. C., Finn, P. A., Bates, J. K. (1999). Oxidative corrosion of spent UO<sub>2</sub> fuel in vapor and dripping groundwater at 90C. Scientific Basis for Nuclear Waste Management XXII, Materials Research Symposium Proceedings.
- Finch, R., Murakami, T. (1999) Systematics and paragenesis of uranium minerals. In: P.C. Burns and R. Finch, Editors, *Reviews in Mineralogy Uranium: Mineralogy, Geochemistry, and the Environment* vol. 38, Mineralogical Society of America, Washington DC, pp. 91-179.
- Fingler, S., Drevenkar, V., Frobe, Z. (2004) Sorption of Chlorophenolates in Soils and Aquifer and Marine Sediments. *Arch. Environ. Contam. Toxicol.* 48:32-39.
- Finn, P. A., Hoh, J. C., Wolf, S. F., Slater, S. A., Bates, J. K. (1996) The release of uranium, plutonium, cesium, strontium, technetium and iodine from spent fuel under unsaturated conditions. *Radiochim. Acta* 74:65-71.
- Forbes, T. Z., Burns, P. C. (2008) Synthesis, structure, and infrared spectroscopy of the first Np<sup>5+</sup> neptunyl silicates, Li-6(NPO<sub>2</sub>)(4)(H<sub>2</sub>Si<sub>2</sub>O<sub>7</sub>)(HSiO<sub>4</sub>)(2)(H<sub>2</sub>O)(4) and K-3(NPO<sub>2</sub>)(3)(Si<sub>2</sub>O<sub>7</sub>). *Inorg. Chem.* 47:705-712.
- Fowle, D. A., Fein, J. B. (1999) Competitive adsorption of metal cations onto two gram positive bacteria: Testing the chemical equilibrium model. *Geochim. Cosmochim. Acta* 63:3059-3067
- Franzluebbers, A. J. (1999) Introduction to Symposium – Microbial Biomass: Measurement and Role in Soil Quality. *Canadian Journal of Soil Science* 79:505-506.
- Gardiner, D. T. and Miller, R. W., 2004. *Soils in Our Environment*, Pearson Education, Inc., Upper Saddle River, New Jersey.
- Gilbert, B., Huang, F., Zhang, H. Z., Waychunas, G. A., Banfield, J. F. (2004) Nanoparticles: Strained and stiff. *Science* 305:651-654.
- Gnanapragasam, E. K. and Lewis, B.-A. G., 1995. Elastic strain energy and the distribution coefficient of radium in solid solutions with calcium salts. *Geochim. Cosmochim. Acta*, 59:5103-5111.

- Gorman-Lewis, D., Elias, P. E., Fein, J. B. (2005) Adsorption of aqueous uranyl complexes onto *Bacillus subtilis* cells. *Environ. Sci. Technol.* 39:4906-4912.
- Gorman-Lewis, D., Mazeina, L., Fein, J. B., Szymanowski, J. E. S., Burns, P. C., Navrotsky, A. (2007) Thermodynamic properties of soddyite from solubility and calorimetry measurements. *J. Chem. Thermodynam.* 39:568-575.
- Gu, X. Y., Evans, L. J. (2008) Surface complexation modelling of Cd(II), Cu(II), Ni(II), Pb(II) and Zn(II) adsorption onto kaolinite. *Geochim. Cosmochim. Acta* 72:267-276.
- Guo, Y., Thibaud-Erkey, C., Akgerman, A. (1998) Gas-Phase Adsorption and Desorption of Single-Component and Binary Mixtures of Volatile Organic Contaminants on Soil. *Environmental Engineering Science* 15, 203-213.
- Haas, J. R., Dichristina, T. J., Wade, R. (2001) Thermodynamics of U(VI) sorption onto *Shewanella putrefaciens*. *Chem. Geol.* 180:33-54.
- Haney, R. L., Franzluebbbers, A. J., Hons, F. M., Zuberer, D. A. (1999) Soil C extracted with water or K<sub>2</sub>SO<sub>4</sub>: pH effect on determination of microbial biomass. *Canadian Journal of Soil Science* 79:529-533.
- Haney, R. L., Franzluebbbers, A. J., Hons, F. M., Hossner, L. R., Zuberer, D. A. (2001) Molar Concentration of K<sub>2</sub>SO<sub>4</sub> and soil pH affect estimation of extractable C with chloroform fumigation-extraction. *Soil Biology & Biochemistry* 33:1501-1507.
- Hayes, K. F., Redden, G., Ela, W. and Leckie, J. O., (1991) Surface complexation models: an evaluation of model parameter estimation using FITEQL and oxide mineral titration data. *J. Colloid Interface Sci.* 142:448-469.
- Helgeson, H. C., Kirkham, D. H., Flowers, G. C. (1981) Theoretical prediction of the thermodynamic behavior of aqueous-electrolytes at high-pressures and temperatures. 4. Calculation of activity-coefficients, osmotic coefficients, and apparent molal and standard and relative partial molal properties to 600-degrees-C and 5 kBar. *Am. J. Sci.* 281:1249-1516.
- Hochella, M. F. (2002) Nanoscience and technology the next revolution in the Earth sciences. *Earth Planet. Sci. Lett.* 203:593-605.
- Jenkinson, D. S. and Powlson, D. S. (1976a) Effects of Biocidal Treatments on Metabolism in Soil – I. Fumigation with Chloroform. *Soil Biology & Biochemistry* 8:167-177.
- Jenkinson, D. S. and Powlson, D. S. (1976b) The effects of biocidal treatments on metabolism in soil – V. A method for measuring soil biomass. *Soil Biology & Biochemistry* 8:209-213.

Johnson, K. J., Szymanowski, J. E. S., Borrok, D., Huynh, T. Q., Fein, J. B. (2007) Proton and metal adsorption onto bacterial consortia: Stability constants for metal-bacteria surface complexes. *Chem. Geol.* 239:13-26.

Kamiya, N., Kagi, H., Tsunomori, F., Tsuno, H., Notsu, K. (2004) Effect of trace lanthanum ion on dissolution and crystal growth of calcium carbonate. *J. Cryst. Gro.* 267:635-645.

Klingensmith, A. L., Deely, K. M., Kinman, W. S., Kelly, V., Burns, P. C. (2007) Neptunium incorporation in sodium-substituted metaschoepite. *Am. Mineral.* 92:662-669.

Klingensmith, A. L., Burns, P. C. (2007) Neptunium substitution in synthetic uranophane and soddyite. *Am. Mineral.* 92:1946-1951.

Koretsky, C. (2000) The significance of surface complexation reactions in hydrologic systems: a geochemist's perspective. *J. Hydrol.* 230:127-171.

Krantz-Rulcker, C., Allard, B., Schnurer, J. (1996) Adsorption of IIB-metals by three common soil fungi-comparison and assessment of importance for metal distribution in natural soil systems. *Soil Biol. Biochem.* 28:967-975.

Kulczycki, E., Fowle, D. A., Fortin, D., Ferris, F. G. (2005) Sorption of cadmium and lead by bacteria-ferrihydrite composites. *Geomicrobiol. J.* 22:299-310.

Ledin, M., Krantz-Rulcker, C., Allard, B. (1999) Microorganisms as metal sorbents: comparison with other soil constituents in multi-compartment systems. *Soil Biol. Biochem.* 31:1639-1648.

Ledin, M., Pedersen, K., Allard, B. (1997) Effects of pH and ionic strength on the adsorption of Cs, Sr, Eu, Zn, Cd and Hg by *Pseudomonas putida*. *Water, Air, and Soil Pollut.* 93:367-381.

Li, X., Coles, B.J., Ramsey, M.H., Thornton, I. (1995) Sequential extraction of soils for multielement analysis by ICP-AES. *Chemical Geology* 124:109-123.

Lindahl, V. and Bakken, L. R. (1995) Evaluation of methods for extraction of bacteria from soil. *FEMS Microbiology Ecology* 16:135-142.

Liu, A., Gonzales, R. D. (1999) Adsorption/Desorption in a system consisting of humic acid, heavy metals, and clay minerals. *J. Coll. Interface Sci.* 218:225-232.

Lower, S. K., Tadanier, C. J., Hochella, M. F. (2001) Dynamics of the mineral-microbe interface: Use of biological force microscopy in biogeochemistry and geomicrobiology. *Geomicrobiol. J.* 18:63-76.

- Lund, T. J., Koretsky, C. M., Landry, C. J., Schaller, M. S., Das, S. (2008) Surface complexation modeling of Cu(II) adsorption on mixtures of hydrous ferric oxide and kaolinite. *Geochem. Transactions* 9:9.
- Madejová, J., Komadel, P. (2001) Baseline Studies of the Clay Minerals Society Source Clays: Infrared Methods. *Clays and Clay Minerals* 49:410-432.
- Malcolm, R.L., MacCarthy, P. (1986) Limitations in the Use of Commercial Humic Acids in Water and Soil Research. *Environmental Science & Technology* 20:904-911.
- Martell A. E., Smith R. M. 1977. *Critical Stability Constants. III: Other Organic Ligands.* Plenum.
- McNamara, B. K., Buck, E. C., Hanson, B. D. (2003) Observation of Studtite and Metastudtite on Spent Fuel. In *Scientific Basis for Nuclear Waste Management XXVI. Materials Research Society Symposium Proceedings, vol. 757, pp. 401-406.* Materials Research Society, Warrendale, PA.
- Meng, X., Letterman, R. D. (1996) Modeling cadmium and sulfate adsorption by Fe(OH)<sub>3</sub>/SiO<sub>2</sub> mixed oxides. *Wat. Res.* 30:2148-2154.
- Mermut, A.R., Cano, A.F. (2001) Baseline Studies of the Clay Minerals Society Source Clays: Chemical Analyses of Major Elements. *Clays and Clay Minerals* 49:381-386.
- Mishra, B., Boyanov, M., Bunker, B. A., Kelly, S. D., Kemner, K. M., Fein, J. B. 2008 (submitted). Integrating bulk adsorption isotherms and EXAFS measurements to constrain the binding mechanisms of Cd to the cell walls of *Bacillus subtilis* and *Shewanella oneidensis*. *Geochim. Cosmochim. Acta.*
- Morey, G. W., Fournier, R. O., Rowe, J. J. (1964) Solubility of amorphous silica at 25 degrees C. *J. Geophys. Res.* 69:1995-2002.
- Ngwenya, B. T., Sutherland, I. W., Kennedy, L. (2003) Comparison of the acid-base behaviour and metal adsorption characteristics of a gram-negative bacterium with other strains. *Appl. Geochem.* 18:527-538.
- Pagnanelli, F., Bornoroni, L., Moscardini, E., Toro, L. (2006) Non-electrostatic surface complexation models for protons and lead(II) sorption onto single minerals and their mixture. *Chemosphere* 63:1063-1073.
- Polgalazova, M. N., Mitskevich, I. N. and Kuzhinovsky, V. A. (1996) A spectrofluorometric method for the determination of total bacterial counts in environmental samples. *Journal of Microbiological Methods* 24:211-218.
- Rai, D., Hess, N. J., Yui, M., Felmy, A. R., Moore, D. A. (2004) Thermodynamics and solubility of (U<sub>x</sub>Np<sub>1-x</sub>)O<sub>2</sub>(am) solid solution in the carbonate system. *Radiochim. Acta*, 92:527-535.

- Sass, B. M., Rai, D. (1987) Solubility of amorphous chromium(III)-iron(III) hydroxide solid-solutions. *Inorg. Chem.* 26:2228-2232.
- Schroth, B. K., Sposito, G. (1997) Surface charge properties of kaolinite. *Clays Clay Miner.* 45:85-91.
- Schroth, B. K., Sposito, G. (1998) Effect of landfill leachate organic acids on trace metal adsorption by kaolinite. *Environ. Sci. Technol.* 32:1404-1408.
- Schroth, M.H., Ahearn, S.J., Selker, J.S., Istok, J.D. (1996) Characterization of Miller-Similar Silica Sands for Laboratory Hydrologic Studies. *Soil Science Society of America Journal* 60, 1331-1339.
- Shen, P., Huang, C., Ganguly, C., Gaboriault-Whitcomb, S., Rabideau, A. J., Van Benschoten, J. E. (2001) Comparison of soluble and immobilized acetate for removing Pb from contaminated soil. *J. Haz. Mat.* B87:59-72.
- Smith, J. L., Halvorson, J. J., Bolton, H. (1995) Determination and use of a corrected control factor in the chloroform fumigation method of estimating soil microbial biomass. *Biology and Fertility of Soils* 19:287-291.
- Steffan, D. G., Akgerman, A. (1998) Single-Component and Binary-Mixture Adsorption of Volatile Organic Contaminants on Silica Gel. *Environmental Engineering Science* 15:191-202.
- Stumm, W., Huang, C. P., Jenkins, S. R. (1970) Specific chemical interactions affecting the stability of dispersed systems. *Croatica Chemica Acta*, v. 24, pp. 223-244.
- Tate, K. R., Ross, D. J., Feltham, C. W. (1988) A direct extraction method to estimate soil microbial C: effects of experimental variables and some different calibration procedures. *Soil Biology & Biochemistry* 19:703-707.
- Tessier, A., Campbell, P.G.C., Bisson, M. (1979) Sequential Extraction Procedure for the Speciation of Particulate Trace Metals. *Analytical Chemistry* 51 :844-851.
- Thibaud-Erkey, C., Campagnolo, J. F., Akgerman, A. (1995) Adsorption of Volatile Organic Contaminants on Soil and Soil Constituents. *Separation and Purification Methods* 24:129-194.
- Vance, E. D., Brookes, P. C., Jenkinson, D. S. (1987) An extraction method for measuring soil microbial biomass C. *Soil Biology & Biochemistry* 19:703-707.
- Voroney, R. P., Brookes, P. C., Beyaert, R. P. (2008) Soil microbial biomass C, N, P, and S. In *Soil Sampling and Methods of Analysis*, 2<sup>nd</sup> ed., M. R. Carter, E. G. Gregorich, eds., CRC, 1264 pp.

Walther, J. V., Helgeson, H. C. (1977) Calculation of the thermodynamic properties of aqueous silica and solubility of quartz and its polymorphs at high-pressures and temperatures. *Am. J. Sci.* 277:1315-1351.

Westall, J. C. (1982) *FITEQL, A computer program for determination of chemical equilibrium constants from experimental data.* Version 2.0. Report 82-02, Dept. of Chemistry, Oregon State Univ., Corvallis, Oregon.

Wightman, P. G., Fein, J. B. (2005) Iron adsorption by *Bacillus subtilis* bacterial cell walls. *Chem. Geol.* 216:177-189.

Wronkiewicz, D. J., Bates, J. K., Gerding, T. J., Veleckis, E., Tani, B. S. (1992) Uranium release and secondary phase formation during unsaturated testing of UO<sub>2</sub> at 90-degrees-C. *J. Nucl. Mater.* 190:107-127.

Wronkiewicz, D. J., Bates, J. K., Wolf, S. F., Buck, E. C. (1996) Ten-year results from unsaturated drip tests with UO<sub>2</sub> at 90 degrees C: Implications for the corrosion of spent nuclear fuel. *J. Nucl. Mater.* 238:78-95.

Yee, N., Fein, J. (2001) Cd adsorption onto bacterial surfaces: A universal adsorption edge? *Geochim. Cosmochim. Acta* 65:2037-2042.

Yee, N., Fein, J. B. (2003) Quantifying metal adsorption onto bacteria mixtures: A test and application of the surface complexation model. *Geomicrobiol. J.* 1:43-60.

Yeo, S.-D., Tuncer, E. and Akgerman, A. (1997) Adsorption of Volatile Organic Compounds on Soil and Prediction of Desorption Breakthroughs. *Separation Science and Technology* 32:2497-2512.

Zachara, J. M., Resch, C. T., Smith, S. C. (1994) Influence of humic substances on Co<sup>2+</sup> sorption by a subsurface mineral separate and its mineralogical components. *Geochim. Cosmochim. Acta* 58:553-566.